Multi-level modeling of dense gas-solid two-phase flows

Promotion committee:

prof.dr.ir. G.F. Versteeg, chairman	University of Twente
prof.dr.ir. J.A.M. Kuipers, promotor	University of Twente
dr.ir. M.A. van der Hoef, assistant promotor	University of Twente
prof.dr O. Simonin	IMFT, France
prof.dr.ir. M.M.C.G. Warmoeskerken	University of Twente
prof.dr. D.Lohse	University of Twente
prof.dr.ir. R.M. Boom	Wageningen Agricultural University
dr. M.A. Gilbertson	Bristol University, UK

Publisher:
Printpartners Ipskamp B.V., P.O. box 333, 7500 AH, Enschede, the Netherlands

Multi-level modeling of dense gas-solid two-phase flows / by Mao Ye. - Enschede: University of Twente, 2005. - Proefschrift.

ISBN 90-365-2190-4

MULTI-LEVEL MODELING OF DENSE GAS-SOLID TWO-PHASE FLOWS

PROEFSCHRIFT

ter verkrijging
van de graad van doctor aan de Universiteit Twente,
op gezag van de Rector Magnificus,
prof.dr. W.H.M. Zijm,
volgens besluit van het College voor Promoties
in het openbaar te verdedigen
op donderdag 14 april, 2005 om 13.15 uur

door

Mao Ye

geboren op 14 februari 1973
te Hubei, China

Dit proefschrift is goedgekeurd door de promotor:

prof.dr.ir. J.A.M. Kuipers

en

assistent-promotor:

dr.ir. M.A. van der Hoef

to my parents
to Jiahua, Dongpei, and Kevin

The work described in this thesis was part of the research program of the Foundation for Fundamental Research on Matter (FOM), and was made possible by financial support from the Dutch Organization for the Advancement of Research (NWO).

Preface

Fluidization is one of the most widely used technologies in chemical engineering. However, accurate predictions of dense gas-solid two-phase flows encountered in fluidization processes remain a major challenge, and a significant barrier against developing more efficient and clean fluidized bed reactors. A major factor that contributes to the complexity of fluidization is the extreme range of scales that arise in a typical gas-solid two-phase flow process. Experiments have provided substantial insights, but measurements in this hostile environment are difficult, expensive, and limited. Theory has also made important contributions, but analysis remains confined to simplified models. Fortunately, computational simulation offers the potential to bridge the gaps between theory and experiments. But the multi-scale nature of dense gas-solid two-phase flows has imposed severe constraints on what can practically be computed. Thus the multi-level modeling approach, where the gas-particle and particle-particle interactions are simulated at different scales, seems to be promising. In the past four years I has been working in this interesting and exciting research direction, which leads to this thesis lying here.

Thus I would like to thank, first of all, my promotor prof. dr. ir. Hans Kuipers for making this expedition possible, and for giving the maximum possible freedom in the research work. I am very grateful for his advices on how to develop into a good researcher. His expertise in fluidization and CFD was very valuable at every stage of the project. Especially, I would like to thank my daily supervisor dr. ir. Martin van der Hoef, whom I rather simply call Martin, and who was never far away if the bears or the mosquitoes became too overwhelming. I greatly admire his deep understanding of physics, sharp analytical skills, and hard-working spirit of a scientist. In spite of his many commitments, the extra effort he took in correcting papers that we submitted or published as well as the chapters of this thesis is greatly appreciated.

I would like to thank all the researchers who inspired me during our cooperations. They gave me confidence in my own ideas, helped me broaden my knowledge, and were simply nice people to work with. In order of appearance: Gerard Finnie, Niels Kruyt, Christiaan Zeilstra, Biljana Potic, Sascha Kersten, Prof. Wim van Swaaij, Gregor Czok, and Prof. Joachim Werther. Furthermore, I would like to thank Gregor Czok and Prof. Joachim Werther for their hospitality when I visited Technical University Hamburg-Harburg. Jie Li, Jeroen Link, and Christiaan Zeilstra were involved in discussions of the discrete particle model at different stages of this research. I appreciate their help. I would also thank Niels Deen for his spontaneous

suggestion concerning the application of the soft-sphere DPM code to simulate the bubbling fluidization in an external electrical field.

I would also express my gratitude to a number of people who had offered their friendship and kindness during my stay in Twente. Nicole Haitjema and Ria Hofs-Winkelman are appreciated for their administrative support which makes my life in Enschede easy and smoothly. I would thank Liesbeth Kuipers for her effort on organizing the unforgettable FAP parties. Special gratitude also goes to all other colleagues in FAP group. They make the atmosphere very friendly and offer a sharp insight into different cultures. I also own a lot to the Chinese community in Twente for all kinds of assistances and enjoyment.

Finally, there is my family to thank. I am deeply indebted to my parents. I would like to thank my sisters and mother-in-law for their support and understanding. My wife Jiahua and my two kids Dongpei and Kevin have become so invaluable that I could fill a thesis on them alone. I love you all very much, and I hope that you will continue to join me on the hiking trips that are yet to come.

Mao Ye
Enschede, March 2005

Contents

1 Introduction **1**
- 1.1 Fluidization . . . 2
- 1.2 Cohesive forces between particles . . . 7
- 1.3 Multi-level modeling for dense solid-gas two-phase flows . . . 9
- 1.4 Outline of the thesis . . . 11
- References . . . 11

2 Numerical models **15**
- 2.1 Introduction . . . 16
- 2.2 Numerical models for gas-solid two-phase flows . . . 16
- 2.3 Euler-Lagrange model . . . 21
- 2.4 Euler-Euler model . . . 41
- References . . . 47

3 2D DPM simulation **51**
- 3.1 Introduction . . . 52
- 3.2 Model description . . . 53
- 3.3 Numerical simulation . . . 54
- 3.4 Results and discussion . . . 56
- 3.5 Conclusions . . . 70
- References . . . 72

4 A full 3D simulation of Geldart A particles **75**
- 4.1 Introduction . . . 76
- 4.2 Discrete particle model . . . 77
- 4.3 Simulation procedures . . . 79
- 4.4 Simulation results . . . 82
- 4.5 Conclusions and discussions . . . 91
- References . . . 93

5 Test of kinetic theory of granular flows **97**
5.1 Introduction . . . 98
5.2 Kinetic theory of granular flows . . . 99
5.3 Discrete particle model . . . 101
5.4 Particle pressure Measurement . . . 104
5.5 Simulation procedure . . . 106
5.6 Results . . . 107
5.7 Conclusion and discussions . . . 116
References . . . 119

6 Two-fluid modeling of Geldert A particles **121**
6.1 Introduction . . . 122
6.2 The Two-fluid model . . . 123
6.3 Simulation conditions . . . 128
6.4 Simulation results . . . 128
6.5 Discussion and conclusions . . . 133
References . . . 135

Summary **139**

Samenvatting **143**

List of Publications **147**

About the author **149**

1

Introduction

ABSTRACT

In this chapter a brief introduction to gas fluidization, with emphasis on Geldart A particles, is presented. Unlike other groups of particles, Geldart A particles can display an interval of homogeneous fluidization, where no obvious bubbles are observed. The mechanism underlying this homogeneous fluidization is still a matter of debate, since two schools of viewpoints exist. One school attributes the origin of homogeneous fluidization to hydrodynamical factors whereas the other school postulates cohesive particle-particle interaction as the relevant phenomenon. The poor understanding of the mechanism underlying homogenous fluidization leads to considerable difficulties in modeling fluidized beds of Geldart A particles. A multi-level modeling approach is thus introduced to study the fluidization behavior of Geldart A particles. With information of gas-particle interaction obtained from lattice Boltzmann simulations and particle-particle interaction from discrete particle simulations, a continuum description of the dense solid-gas two-phase flows based on the classical two-fluid model and kinetic theory of granular flows is expected to become available. The cohesive forces between particles are also discussed and the van der Waals force is considered as the primary cohesive interaction between Geldart A particles, which will be considered in this thesis. Finally the outline of this thesis is presented.

1.1 Fluidization

Fluidization refers to the suspension or transport of granular materials by a continuous fluid (gas or liquid), and is encountered frequently in industry in gas-fluidized beds. A fluidized bed is typically a container of solid particles through the bottom of which an upward fluid flow passes. If operated with well-matched fluid and particle parameters, fluidized beds can provide many advantages such as uniform temperature distribution, high mass transfer rates between fluid and solids phases, continuous operation, and relative simplicity in geometric configuration [1]. In history, the use of fluidization technology dates back to as early as the 16th century. The major development of modern fluidized beds came with the Bergus-Pier process for coal liquefaction and the Winkler process for coal gasification in the mid 1920s [2]. Since then, fluidized beds have been widely applied in the petroleum, metallurgical, chemical, energy, environmental, and food industries.

However, the design and scale up of fluidized bed reactors still remains a considerable challenge for engineers. This is mostly due to the poor understanding of the hydrodynamics of the complex particulate two-phase flows in fluidized beds. To develop a new fluidized bed under optimal conditions, a small or a pilot-scale reactor, instead of the real one, is always used in the preliminary tests. Even with well defined measurement techniques and pilot-scale models, the optimal operation parameters obtained in these tests may still differ significantly from those required for the real large-scale reactors. The development of computational fluid dynamics (CFD) techniques in recent years provides an efficient and promising tool to support the design and scale up of fluidized bed reactors [3]. However, the establishment of a general mathematical model, if not impossible, is quite difficult, since for different operation conditions a number of distinctly different fluidization regimes can be encountered.

1.1.1 Fluidization regimes

When a gas is fed through a bed of particles, it will exert a drag force upon the particles which results in a pressure drop across the bed. With increasing superficial gas velocity U_0, the gravity force acting on the particles can be partially or completely compensated by the drag force, which transforms the system gradually from the solid-like state to a fluid-like state. In Figure 1.1 the typical (fluidization) regimes observed in fluidized beds are shown. At a low flow rate, gas merely percolates through the bed, and the particles stay in a packed state due to the action of gravity. This is a fixed bed. With increasing flow rate, the drag force becomes sufficient to support the weight of the particles in the bed, the bed is said to be fluidized. The minimum fluid velocity at which the weight of the solids is just balanced by the drag force is called the minimum fluidization velocity U_{mf}. At an even higher flow rate, different fluidization behaviors will be found for liquid- and gas-fluidization systems. In a liquid-fluidized bed, a smooth, progressive expansion of the bed can be observed, in which no big bubbles or other void structures appear. A bed such as this is called a particulate fluidized bed or a homogeneous fluidized

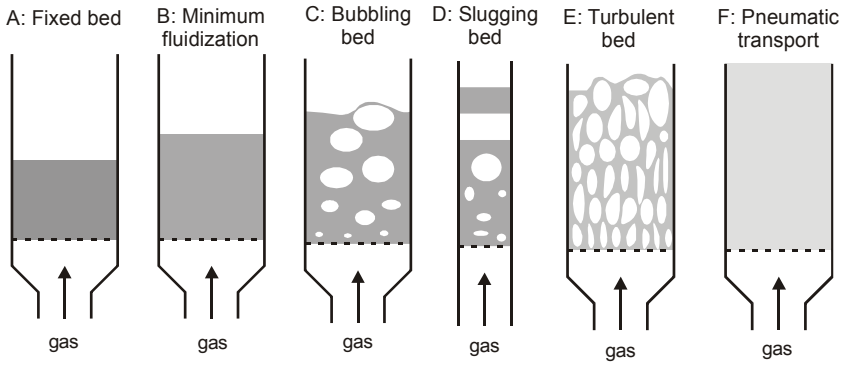

Figure 1.1: *The fluidization regimes encountered in industrial fluidized beds (from C. Dechsiri, Ph.D thesis, University of Groningen, 2004 [4]).*

bed. On the contrary a gas-fluidized bed has the appearance of boiling liquid. The homogeneous expansion is only found for small and light particles in a very narrow interval of superficial velocities. In most gas-fluidized beds the bubbles will grow and burst. If the dimension of the bed is small the bubbles will develop into slugs. At very high flow rate the gas-fluidized bed might display turbulence-like structures, which is called turbulent fluidization. Turbulent fluidization is often found in the riser or downer in a circulating fluidized bed. For extremely high flow rates the terminal velocity of the solids will be exceeded. In this case the particles in both liquid- and gas-fluidized beds can be carried out with the fluid stream and the upper surface of the bed does not exist anymore. This is the so-called pneumatic conveying regime of solids.

Practically all important industrial applications of fluidization involve gas-fluidized bed systems. Because of this, we shall deal primarily with gas-fluidized bed systems in this work.

1.1.2 Types of gas fluidization

As discussed above, the flow patterns in gas fluidization are far more complicated than that in liquid fluidization. However, not all types of particles can be fluidized in a gas-fluidized bed. Even if fluidized, not all particles will experience all fluidization regimes shown in Figure 1.1. The fluidization behavior of a gas-fluidized bed depends strongly on the particle and gas properties. Based on experimental observations, Geldart [5] proposed a classification diagram for gas fluidization, In this famous diagram (as shown in Figure 1.2), particles were categorized into four groups according to their typical characteristics exhibited in gas fluidization. Geldart A particles are defined as *aeratable* particles, which normally have a small particle size ($d_p < 130$ μm) and low particle density (< 1400 kg/m^3). This kind of particles can be easily fluidized at ambient conditions. The most important feature of Geldart A particles is the interval of homogeneous fluidization when the gas veloc-

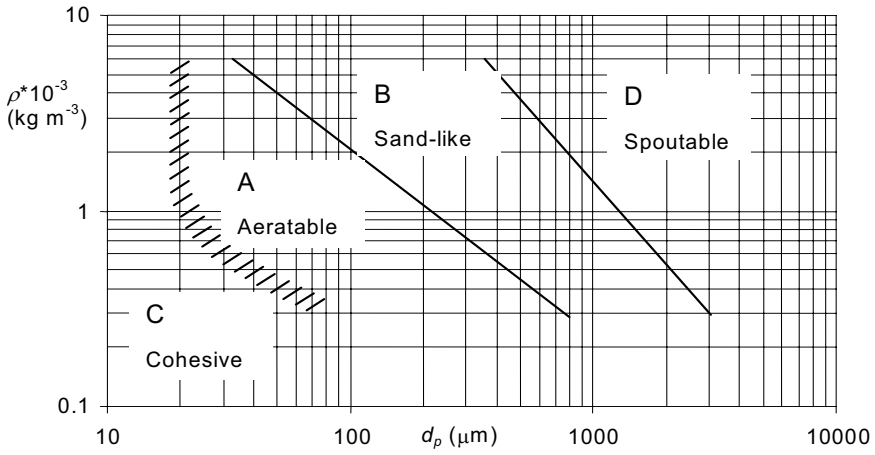

Figure 1.2: *The classification of gas fluidization. Here ρ^* is the difference of the density between particles and gas phase (based on D. Geldart, Powder Technol., 1973 [5]).*

ity exceeds the minimum fluidization velocity U_{mf}. In the homogeneous fluidization regime the particles are mobile and macroscopic circulations patterns can be observed. This differs significantly from the fixed bed regime as in the later case particles are essentially static. A bed of Geldart A particles will not bubble until the so-called minimum bubbling velocity U_{mb} is reached. Fluid cracking catalysts (FCC) particles typically are in this category.

Geldart B particles are called *sandlike* particles or *bubbly* particles. Most particles of this group have a size of 150 to 500 μm and a density from 1400 to 4000 kg/m^3. For these particles, once the minimum fluidization velocity is exceeded, the excess gas appears in the form of bubbles. The size of bubbles in a bed of Geldart B particles can be as large as the dimension of the bed. Glass beads and sand are belonging to this group.

Geldart C particles are *cohesive* particles with a mean size usually less than 30 μm. These particles are extremely difficult to fluidize because the interparticle attractive van der Waals forces are relatively large. In small diameter fluidized beds, this kind of particle easily gives rise to channeling. Examples of Geldart C materials are talc, flour and starch.

Geldart D particles are called *spoutable*, and the materials are either very large or very dense. They are also very difficult to fluidize in deep beds. As the gas velocity increases, a jet can be formed in the bed and the particles may then be blown out with the jet in a spouting motion. If the gas distribution is uneven, spouting behavior and severe channeling can be expected. Lead shot and some roasted metal ores are examples of Geldart D materials.

Although the Geldart's classification is based on purely experimental observations, it proves to be an easy and useful tool for estimating the type of fluidization at ambient conditions and for U_0 less than about $10U_{mf}$. For any solid of a known

density ρ_p and mean particle size d_p this diagram provides a good prediction of the actually observed fluidization regimes.

However, the physics behind this diagram is still unclear. In most of the industrial applications Geldart A and B particles are employed. Unlike Geldart B particles, Geldart A particles can display an interval of homogeneous fluidization that is only found in liquid-fluidization systems. This interval of homogeneous fluidization is particularly important for the Fluid Catalytic Cracking (FCC) fluidized bed reactor, which is currently a standard component in the production of gasoline and other fuels from heavy oil components in an oil refinery. Compared to Geldart B particles, however, less is known concerning the mechanism of the fluidization of Geldart A particles. The CFD techniques developed so far are still unsuccessful to predict the two-phase flows in large-scale fluidized beds of Geldart A particles.

1.1.3 The mechanism of fluidization of Geldart A particles

Despite many detailed phenomenological investigations [5–8], the mechanism behind the fluidization of Geldart A particles, however, has not yet been fully understood.

In the 1940s, Wilhelm and Kwauk [9] tried to explain the difference between homogeneous fluidization and heterogeneous fluidization. Based on a careful investigation of both liquid- and gas-fluidized beds, they proposed the dimensionless Froude number Fr to define the transition point. They found that the homogeneous expansion will mostly occur if $Fr \ll 1.0$ [9]. This criterion, however, has been found to be inaccurate in later studies.

From the theoretical viewpoint, homogeneous fluidization is closely related to the stability of continuum field conservation equations that govern the solid-gas two-phase flow inside a fluidized bed [10]. Jackson and his co-workers [11, 12] were among the pioneers who tried to analyze this stability. They found that in addition to the inertia and drag force, a new term similar to the gas pressure is required to describe the motion of the particulate phase, otherwise the bed would always be unstable [12]. This new term, which was found to be a function of the porosity [13], has been considered as the particulate pressure. Unlike the pressure of a liquid or a gas, the particulate pressure is somewhat artificial since it has no clear physical meaning. However, the physical origin of the particulate pressure actually reflects the mechanism of the homogeneous fluidization in gas-fluidized beds.

Foscolo and Gibilaro [14], in the spirit of Verloop and Heertjes [15], suggested that a shock wave due to the change of porosity (i.e. when porosity wave rises faster than the velocity of the so-called equilibrium disturbance) is the dominant factor that causes the instability of the homogeneous fluidization regime. They related the origin of the particulate pressure to the propagation of some kind of elasticity wave and defined an elasticity modulus to account for the stability of the bed. Although Foscolo and Gibilaro were able to predict the minimum bubbling points in many cases, not all phenomenon associated with homogeneous fluidization in a gas-fluidized bed [16] could be explained. On the other hand, Rietema and his co-workers [8, 17] proposed that the interparticle forces should be responsible for

the homogeneous fluidization behavior of small particles, rejecting Foscolo and Gibilaro's purely hydrodynamic analysis. Rietema and his co-workers argued that the concept of an effective elastic modulus could be related to some kind of mechanical structure induced by the interparticle van der Waals forces. Although the viewpoint of Rietema and his co-workers [8, 17] has a clear physical basis, it proves difficult to find a quantitative relation between the interparticle van der Waals forces and the macroscopic physical quantities of the bed. The reasons are twofold: Firstly, up to date there is no technique that can measure the detailed microscopic structure inside a gas-fluidized bed; Secondly, the interparticle van der Waals forces are short-range forces and strongly depend on the shape and surface properties of particles.

The mechanism underlying the homogeneous fluidization has since then been a matter of debate between researchers. Experimental results by Tsinontides and Jackson [18] and Menon and Durian [19] suggest that the state of homogeneous fluidization is actually solid-like where the enduring contacts make particles stay at rest, which supports the assumption that interparticle forces play a crucial role in homogeneous fluidization regime. By contrast, in another set of experiments Cody et al. [20, 21] showed a pronounced increase in the particle velocity fluctuations during the transition from Geldart B to Geldart A fluidization behavior, which means that the bed of particles displays a fluid-like behavior. In a recent experiment, Valverde et al. [22] fluidized very fine particles ($d_p \sim 8.53\mu$m) by adding some nano-seed flow conditioners, which can greatly reduce the cohesive force between particles. They observed a relatively long interval of homogeneous fluidization, and found that even during homogeneous fluidization both the solid-like and fluid-like behavior can be distinguished. This finding bridges the gap between the experimental results by Tsinontides and Jackson [18] and Menon and Durian [19] and Cody et al. [20, 21]. However, since Valverde et al. [22] used Geldart C particles, it is unclear yet as to whether the solid-like or the fluid-like behavior is dominant for true Geldart A particles in gas-fluidized beds as well.

A theoretical approach was initiated by Koch and Sangani [23], who derived a very detailed kinetic theory taking into account the fluid-particle interaction and particle-particle collisions. From a stability analysis based on their theory, Koch and Sangani [23] showed that the homogeneous fluidization is not stable, unless other non-hydrodynamical factors such as interparticle forces are considered. Buyevich and his co-workers [24, 25] also developed a similar kinetic theory based on the random fluctuation of particles induced by hydrodynamics. Based on this theory, very recently Sergeev et al. [26] found that the apparent stability of uniform fluidization can also be explained without taking into account interparticle forces. Clearly, so far no consensus has been reached on the precise mechanism underlying homogeneous fluidization.

1.2 Cohesive forces between particles

In many industries which deal with particulate materials, cohesion plays a crucial role. Cohesion between particles can arise from a variety of sources including van der Waals forces, electrostatic forces, liquid bridging (i.e. capillary forces), sintering, and so on. These interparticle forces become increasingly important as particle size decreases. Although all these forces may be encountered in fluidized beds, the van der Waals forces are generally accepted as the key force with respect to the influence on the fluidization behaviors of fine particles (Geldart A and C particles). Normally the cohesive forces can lead to a substantial change of the behavior of particulate flows, as particles tend to aggregate so that the flow behavior is mostly determined by the clusters of solids, instead of the individual particles.

1.2.1 Van der Waals forces

The van der Waals force is present between any two molecules (polar or non-polar) and therefore the force is usually connected with the intermolecular interactions. At the molecular level, the van der Waals force follows from the fluctuating dipole-dipole interactions. According to London's theory, the intermolecular potential can be expressed as

$$\phi \sim S^{-6}, \tag{1.1}$$

where S is the distance between two molecules. We assume:
(1) *No repulsive interaction exists*;
(2) *Interparticle potential can be just related to the sum of intermolecular potentials between two particles*;
(3) *The shapes of particles under consideration are spherical.*

The interparticle van der Waals potential can thus be obtained by integrating the London potential between macroscopic spherical particles [27, 28]. The resulting force is given by

$$F_{vdw,ab}(S) = \frac{A}{3} \cdot \frac{2R_aR_b(S+R_a+R_b)}{\left[S(S+2R_a+2R_b)\right]^2} \left[\frac{S(S+2R_a+2R_b)}{(S+R_a+R_b)^2-(R_a-R_b)^2} - 1 \right]^2, \tag{1.2}$$

where R is the sphere radius, A is the Hamaker constant and S is the intersurface distance, which takes a minimum value of the order of the inter-molecular spacing. Eq.(1.2) can be approximately reduced to

$$F_{vdw,ab}(S) = \frac{AR}{12S^2}, \tag{1.3}$$

if $R_a = R_b = R$.

1.2.2 Liquid bridge

Due to capillary condensation, at relative humidities below 100% water may form liquid bridges at contact points between solid bodies. The shape of the liquid

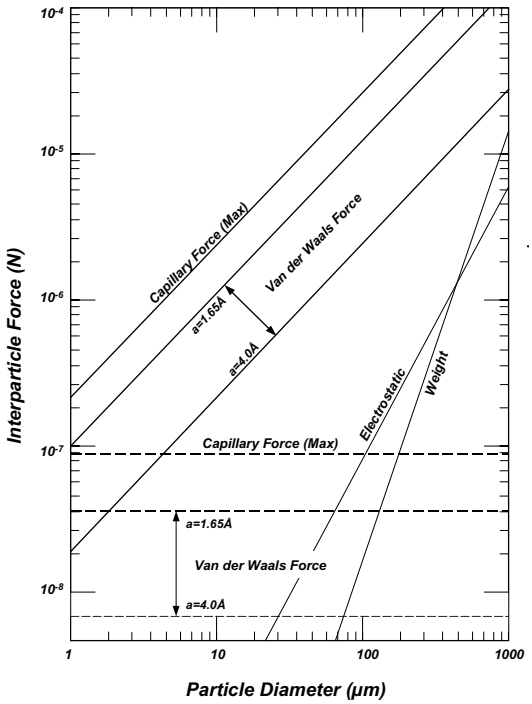

Figure 1.3: *The cohesive forces between two spheres. Dashed lines: the asperity-to-plane contact. Liquid bridge force calculated from a quartz/water system (from J. Seville, Powder Technol., 2001 [29]).*

bridge is determined by the Laplace-Young equation (mechanical equilibrium), which is related to the humidity via the Kelvin equation (physico-chemical equilibrium). The extent of liquid bridge formation depends on the amount of free liquid, the surface tension and the liquid viscosity. Normally the liquid bridge force includes both dynamic and static parts and is of dissipative nature [29]. The static force depends mainly on the shape of the gas-liquid interface while the dynamical part depends mainly on the fluid motion near the point of closest contact. Usually, the maximum static liquid bridge force occurs at close contact and is approximately given by

$$F_{ls,max} = 2\pi\, R\gamma, \tag{1.4}$$

with γ the surface tension of water. The exact calculation of the dynamical part is difficult. A first approximation is normally given by Reynolds' lubrication equation,

$$F_{ld} = 6\pi\mu_l\, R^2 v_r/r, \tag{1.5}$$

where μ_l is liquid viscosity, v_r is the relative velocity between two particles, and r is the interparticle distance.

1.2.3 Relative importance of cohesion

The relative importance of cohesive forces in a gravitational system can be reflected by the Bond number Bo, which is defined as the ratio of particle weight to cohesive force. In fact for real particles both the van der Waals force and liquid bridge force strongly depend on the surface properties. In many cases one would assume a particle surface roughness and use this to determine the curvature. The radius R is then taken as the local curvature instead of the gross radius of the spheres.

The typical results of the van der Waals force and liquid bridge force for different parameters are shown in Figure 1.3 [29]. The dashed lines stand for the results with a local curvature instead of the gross radius of the particles. It is shown that for spherical particles of diameter around 100 μm the Bond number should equal unity. If the gross particle radius is directly used, the particle diameter will be 1 mm when the Bond number Bo reaches 1.0. However, in a real system, particles of 100 μm are commonly found adhering to surfaces while 1 mm particles are not.

In fact the exact determination of local curvature is considerably more involved. In this study we only consider the van der Waals force between smooth spheres. To adjust the magnitude of the cohesive forces, we prefer to change the Hamaker constant, rather than search for a suitable local curvature when using Eq.(1.2).

1.3 Multi-level modeling for dense solid-gas two-phase flows

Computational fluid mechanics (CFD) constitutes a powerful and emerging tool to understand hydrodynamics of gas-particle flows in fluidized beds. However, being a complex system, gas-fluidized beds can display quite different flow patterns on both spatial and temporal scales. On one hand, for the same fluidized bed, if operated at a different conditions, several fluidization regimes might be experienced. On the other hand, even operated at the same conditions, flow structures at different length scales will be present: the largest flow structures such as bubbles can be of the order of meters; while the fine structures such as grain clusters, which are formed by the microscopic particle-particle interactions, take place on the scale of millimeters or less. The large separation of scales presents the prime challenge for modeling gas-fluidized beds [31]. Development of CFD in recent years, on the other hand, makes it possible to simulate the flow behavior at microscopic, mesoscopic and macroscopic scales of solid-gas two-phase systems respectively. Due to the limitation of computer resources, the microscopic- and mesoscopic-scale models are difficult, if not impossible, to be extended to engineering application (macroscopic-scale simulation) in the foreseeable future. However, they can help us to gain a better insight into the gas-particle, particle-particle, and particle-wall interaction in dense particle-gas flows. The results from microscopic and mesoscopic-scale simulations therefore can be used to improve the currently available macroscopic models. Along this line, a multi-level CFD modeling approach is utilized in this study.

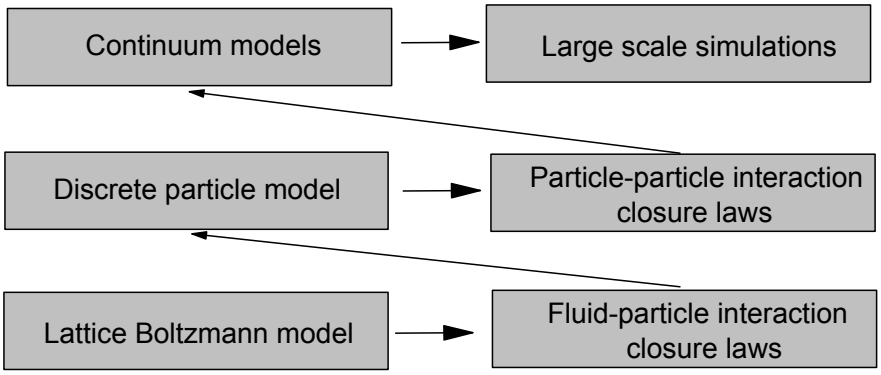

Figure 1.4: *The multi-level modeling concept for dense gas-solid two-phase flows (based on B.P.B. Hoomans, Ph.D thesis, University of Twente, 2004 [30]).*

The schematic representation of the multi-level approach is shown in Figure 1.4. The microscopic, mesoscopic and macroscopic level models consist of the lattice Boltzmann model (LBM), discrete particle model (DPM) and kinetic theory of granular flow (KTGF) based two-fluid model (TFM) respectively.

At the most fundamental level, the gas flow field is modeled at scales smaller than the size of the particles. The interaction of the gas phase with the particles is considered by imposing suitable boundary conditions at the surface of the solids. The flow field between the spheres can be solved by the lattice Boltzmann method (LBM) [32, 33]. The detailed gas-particle interaction (in the form of drag force) obtained from this microscopic level LBM simulation will be applied to higher level models instead of the conventional empirical correlations, which are only valid for spatially homogeneous flows.

At the mesoscopic level, the flow field is modeled at a scale much larger than the size of the particles, and the fluid velocity and pressure are obtained by solving the volume-averaged Navier-Stokes equations. The particle-particle interactions (particle-wall as well) are formulated with the so-called discrete particle models (DPM), which are based on the schemes that are traditionally used in molecular dynamics simulations, modified such as to take dissipation of energy and friction into account, which are absent in a molecular system [34–36].

At the macroscopic scale, a two-fluid model (TFM) is used where the continuum description is employed for both the particle phase and the fluid phase [37, 38]. The information obtained in the two lower-level models is then included in the continuum models via the kinetic theory of granular flow (KTGF). The advantage of this model is that it can predict the flow behavior of gas-solid flows at life-size scales, and these models are therefore widely used in commercial fluid flow simulators of industrial scale equipment.

1.4 Outline of the thesis

This book considers the multi-leveling approach for Geldart A particles in gas-fluidized beds, by staring with a general introduction of the background in this Chapter.

In ***chapter 2*** the numerical modeling approaches for dense gas-solid two-phase flows are described, with the emphasis on the mesoscopic-scale soft-sphere discrete particle model and macroscopic-scale two-fluid model.

Chapter 3 reports on a 2D numerical study of fluidization behavior of Geldart A particles by use of the soft-sphere discrete particle model, where some typical features encountered in fluidization of Geldart A particles are displayed, and the mechanism underlying the homogeneous fluidization, based on an analysis of the velocity fluctuation of particles, is discussed.

In ***chapter 4*** we present a 3D discrete particle simulation by alternating different gas and particle properties, which aims at the comparison of the simulation results and the classical empirical correlations by Abrahamsen and Geldart [7].

Chapter 5 describes a test of the kinetic theory of granular flows (KTGF) with Geldart A particles. In this chapter, we first compare the results of discrete particle model for cohesiveless particles, and then study the effect of the cohesive forces on KTGF closures.

The two-fluid modeling of Geldart A particles is discussed in ***chapter 6***. Based on the information obtained in chapter 5, the impact of cohesion between particles bed expansion dynamics is studied. Also the particle-fluid interaction, in the form of drag force, is considered.

References

[1] Kunii D., and Levenspiel O., 1991. *Fluid Engineering*. Butterworth Heinemann, Boston, USA.

[2] Fan L.-S., and Knowlton T.M., 1998. *Fluidization IX*. Engineering Foundation, New York, USA.

[3] Kuipers J.A.M., and van Swaaij W.P.M., 1998. Computational fluid dynamics applied to chemical reaction engineering. *Adv. Chem. Engng.*, **24**: 227.

[4] Dechsiri C., 2004. *Particle transport in fluidized beds: experiments and stochastic models*. Ph.D thesis, University of Groningen, Groningen, the Netherlands.

[5] Geldart D., 1973. Types of gas fluidization. *Powder Technol.*, **7**: 285.

[6] de Jong J.A.H., and Nomden J.F., 1974. Homogeneous gas–solid fluidization. *Powder Technol.*, **9**: 91.

[7] Abrahamsen A.R., and Geldart D., 1980. Behaviour of gas-fluidized beds of fine powders. Part I: Homogeneous expension. *Powder Technol.*, **26**: 35.

[8] Rietema K., and Piepers H.W., 1990. The effect of interparticle forces on the stability of gas-fluidized beds–I. Experimental evidence. *Chem. Engng. Sci.*, **45**: 1627.

[9] Wilhelm R.H., and Kwauk M., 1948. Fluidization of solid particles. *Chem. Engng. Progress.*, **44**: 201.

[10] Homsy G.M., 1998. Nonlinear waves and the origin of bubbles in fluidized beds. *Appl. Sci. Res.*, **58**: 251.

[11] Jackson R., 1963. The mechanics of fluidized beds: I. The stability of the state of uniform fluidization. *Trans Inst. Chem. Engng.*, **41**: 13.

[12] Anderson T.B., and Jackson R., 1968. Fluid mechanical description of fluidized beds. Stability of the state of uniform fluidization. *Ind. Engng. Chem. Fundam.*, **8**: 137.

[13] Grag S.K., and Pritchett J.W., 1975. Dynamics of gas fluidized beds. *J. Appl. Phys.*, **46**: 4493.

[14] Foscolo P.U., and Gibilaro L.G., 1984. A fully predictive criterion for the transition between particulate and aggregate fluidization. *Chem. Engng. Sci.*, **39**: 1667.

[15] Verloop J., and Heertjes P.M., 1970. Shock waves as a criterion for the transition from homogeneous to heterogeneous fluidization. *Chem. Engng. Sci.*, **25**: 825.

[16] Lettieri P., Brandam S., Yates J.G., and Newton D., 2001. A generalization of the Foscolo and Gibilaro particle-bed model to predict the fluid bed stability of some fresh FCC catalysts at elevated temperatures. *Chem. Engng. Sci.*, **56**: 5401.

[17] Rietema K., Cottaar E.J.E., and Piepers H.W., 1993. The effects of interparticle forces on the stability of gas-fluidized beds–II. Theoretical derivation of bed elasticity on the basis of van der Waals forces between powder particles. *Chem. Engng. Sci.*, **48**: 1687.

[18] Tsinontides S.C., and Jackson R., 1993. The mechanics of gas fluidized beds with an interval of stable fluidization. *J. Fluid Mech.*, **225**: 237.

[19] Menon N., and Durian D.J., 1997. Particle motions in a gas-fluidized bed of sand. *Phys. Rev. Lett.*, **79**: 3407.

[20] Cody G.D., Goldfarb D.J., Storch G.V., and Norris A.N., 1996. Particle granular temperature in gas fluidized beds. *Powder Technol.*. **87**: 211.

[21] Cody G.D., Kapbasov S.K., and Buyevich Y.A., 1999. Particulate fluctuation velocity in gas fluidized beds—fundamental models compared to recent experimental data. *AIChE Symp. Ser.*, **95**: 7.

[22] Valverde J.M., Castellanos A., and Quintanilla M.A.S., 2001. Self-diffusion in a gas-fluidized bed of fine powder. *Phys. Rev. Lett.*, **86**: 3020.

[23] Koch D.L., and Sangani A.S., 1999. Particle pressure and marginal stability limits for a homogeneous monodisperse gas-fluidized bed: kinetic theory and numerical simulations. *J. Fluid Mech.*, **400**: 229.

[24] Buyevich Y.A., 1999. Particulate stresses in dense disperse flow. *Ind. Eng. Chem. Res.*, **38**: 731.

[25] Buyevich Y.A., and Kapbasov S.K., 1999. Particulate pressure in disperse flow. *Int. J. Fluid Mech.*, **26**: 72.

[26] Sergeev Y.A., Swailes D.C., and Petrie C.J.S., 2004. Stability of uniform fluidization revisited. *Physica A*, **335**: 9.

[27] Chu B., 1967. *Molecular forces.* John Wiley & Sons, New York, USA.

[28] Israelachvili J., 1991. *Intermolecular & surface forces.* Academic Press, London, UK.

[29] Seville J.P.K., Willett C.D., and Knight P.C., 2000. Interparticle forces in fluidization: a review. *Powder Technol.*, **113**: 261.

[30] Hoomans B.P.B., 2004. *Granular dynamics of gas-solid two-phse flows.* Ph.D. thesis, University of Twente, Enschede, the Netherlands.

[31] van der Hoef M.A., van Sint Annaland M., and Kuipers J.A.M., 2004. Computational fluid dynamics for dense gas-solid fluidized beds: a multi-scale modeling strategy. *Chem. Engng. Sci.*, **56**: 5157.

[32] Ladd A.J.C., 1993. Lattice-Boltzmann simulations of particle fluid suspensions. *J. Fluid Mech.*, **271**: 285.

[33] Ladd A.J.C., and Verberg R., 2001. Lattice-Boltzmann simulations of particle fluid suspensions. *J. Stats. Phys.*, **104**: 1191.

[34] Tsuji Y., Kawaguchi T., and Tanaka T., 1993. Discrete particle simulation of two-dimensional fluidized bed. *Powder Technol.*, **77**: 79.

[35] Hoomans B.P.B., Kuipers J.A.M., Briels W.J., and van Swaaij W.P.M., 1996. Discrete particle simulation of bubble and slug formation in a two-dimensional gas-fluidized bed a hard sphere approach. *Chem. Engng. Sci.*, **51**: 99.

[36] Xu B.H., and Yu A.B., 1997. Numerical simulation of the gas-solid flow in a fluidized bed by combining discrete particle method with computational fluid dynamics. *Chem. Engng. Sci.*, **52**: 2785.

[37] Kuipers J.A.M., van Duin K.J., van Beckum F.P.H., and van Swaaij W.P.M., 1992. A numerical model of gas-fluidized beds. *Chem. Engng. Sci.*, **47**: 1913.

[38] Gidaspow D., 1994. *Multiphase Flow and Fluidization Continuum and Kinetic Theory Descriptions.* Academic Press, Boston, USA.

2

Numerical Modeling for Dense Gas-solid Two-phase Flows

ABSTRACT

In this chapter the numerical modeling approaches for dense gas-solid two-phase flows are described. For the gas phase, continuum models are used, although at very small scales, also discrete models are used (see section 2.21). For the solid phase, both continuum models and discrete models can be applied, where the most suitable choice strongly depends on the length scale of interest. The combination of these models, together with a suitable coupling technique, can be used to model gas-solid two-phase flows. Based on this concept, a multi-level modeling approach is introduced. In this research, we focus on the meso- and marco-scale models of Geldart A particles. On the meso-scale, a soft-sphere discrete particle model is used, from which we can investigate the effects of the particle-particle interactions in detail. The gas is treated as a continuum where the volume-averaged Navier-Stokes equations are used to compute the flow field. Apart from the collision forces, also the cohesive forces are considered in the discrete particle model. On the macro-scale, the two-fluid model based on the kinetic theory of granular flows is applied. The information obtained from the meso-scale simulations will be further used to improve the closures of the solid phase stress tensor, which is essential for developing a two-fluid model for Geldart A particles with predictive capability. In this chapter, we first give a general overview of the discrete particle model and the two-fluid model, after which the details of these models are presented.

Based on: M. Ye, C. Zeilstra, M. A. van der Hoef and J. A. M. Kuipers, 2005. Discrete particle model for gas-solid two-phase flows. In preparing for publication.

2.1 Introduction

Granular materials are frequently encountered in various natural processes and their man-made counterparts [1]. They represent the most common form of raw material in industry world-wide. In weight, it is estimated that at least 75% of the raw material and 50% of the products in the chemical industry are handled as granular material [2]. Thus it is not surprising that the understanding of granular flows is playing a crucial role in designing and scaling up of a wide variety of industrial processes. Short of a general theory and efficient experimental techniques, the challenge therefore is to find computational models that are on one hand accurate enough to allow reliable predictions, but where on the other hand the computing efficiency is sufficiently high to permit a simulation of large scale granular systems.

Although the granular dynamics has attracted considerable interests from researchers [3], it is not possible to accurately simulate the large scale industrial granular flows at present. A flow of granular materials is typically a two-phase process since the void spaces between particles are filled with air. The flow behavior of the granular material is not only determined by the interactions between particles, but is also affected by the interstitial air. Meanwhile, the flow of the interstitial air can also be modified due to the presence of particles. In most industrial applications, the granular materials are encountered in the form of dense gas-solid two-phase flows. In this research we will concentrate on the flow behavior of these systems, especially those encountered in gas-fluidized bed reactors of Geldart A particles.

2.2 Numerical models for gas-solid two-phase flows

2.2.1 Gas phase

The description of a gas flow has already been well established from the micro- to macro- scales. The length scale of a gas flow can be characterized by the local Knudsen number, which is defined as

$$Kn = \frac{\lambda}{L}, \tag{2.1}$$

where λ is the mean free path of the molecules, and L is the characteristic length scale of the flow. In Figure 2.1 the models for a gas flow are schematically shown. For large scale systems with $Kn < 0.01$, the gas flow can be described by ordinary fluid dynamics where the macroscopic fields (such as density and velocity) are formulated by Navier-Stokes equations in a three-dimensional coordinate space, together with no-slip boundary conditions. A number of well-developed numerical algorithms and meshing techniques in computational fluid dynamics (CFD) can be used to handle very complex geometries [4]. If the system becomes smaller, say $0.01 < Kn < 0.1$, the Navier-Stokes equations still hold but caution must be given to the boundary conditions since partial slip might exist between the gas-solid interfaces. For a rarefied gas where $Kn > 0.1$, the continuum assumption

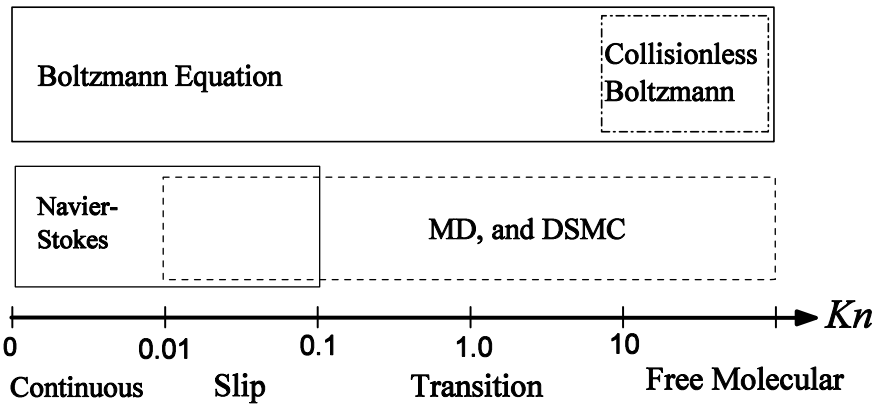

Figure 2.1: *The scheme of multi-level modeling for gas flows.*

breaks down, and the so-called kinetic theory of (dense) molecular gases should be applied. Kinetic theory differs from the ordinary fluid dynamics as there is just one field (the density of molecules) in the phase space. The basic equation in kinetic theory, in the simplest form, is the Boltzmann equation which describes the evolution of the density function f in a six dimensional space (three coordinates and three velocity components) [5]. At this scale, computational techniques such as Molecular Dynamics (MD) [6] and Direct Simulation Monte Carlo (DSMC) approach [7] can be very efficient. In these techniques the motion of molecules is traced on an individual basis. Gas pressure and other transport coefficients including gas viscosity and thermal conductivity are obtained from a statistical mechanics approach [5]. Molecules can be treated either as hard-spheres or points with certain interaction potentials, depending on their physical properties. In the extreme case where the mean free path is very large compared to the system sizes (i.e, > 10), the molecules move freely, and just collide with the walls. This is the limit of *free molecular flow* where the gas can be simply assumed as an ideal gas.

Clearly there are two quite different types of models for a gas flow: the continuum models and the molecular models. Although the molecular models can, in principle, be used to any length scale, it has been widely applied at the micro-scale because of the limitation of computing capacity at present. The continuum models present the main stream of engineering applications and are more flexible when applying to different macro-scale gas flows, however, they are not suited for micro-scale flows. The gap between the continuum and molecular models can be bridged by the kinetic theory which is based on the Boltzmann equation.

2.2.2 Solid phase

The methods used for modeling pure granular flows are essentially borrowed from that of a molecular gas. Similarly there are two main types of models: the continu-

ous (Eulerian) models [8] and discrete particle (Lagrangian) models [3, 9, 10]. The continuum models are developed for large-scale simulations, where the controlling equations resemble the Navier-Stokes equations for a ordinary gas flow. The discrete particle models are typically used in small scale simulations or in the investigation of the detailed physics of granular flows. A kinetic theory of granular flows has also been proposed to connect the micro-scale picture of granular flows to the macro-scale description [11, 12].

However, a granular flow differs significantly from a molecular gas flow. The collisions between molecules are elastic, and the kinetic energy is conserved in isothermal systems. For the molecular gas an equilibrium state can be easily established in the absence of any external energy sources, and we can define a thermal temperature based on the internal kinetic energy. The interaction between macroscopic particles, however, is far more complicated. The collision between two macroscopic particles will come with surface friction and elastic-plastic deformation, which leads to the dissipation of kinetic energy. This inelasticity forms the primary feature of granular flow that differentiates it from molecular gas [13]. Clearly, without any external energy sources, a granular system will continuously "cool down", and an equilibrium state can never be reached.

In modeling a granular system, the discrete particle models play an important role and assume that the particle motion can be well-described by the Newtonian equations. However, in order to establish a continuum description, a number of serious difficulties are encountered when one tries to describe the fields in phase space. First, a source term and a dissipative term should be included in the Boltzmann equations, which complicates the (approximate) solution. Also, even for the same type of materials, particle sizes may show a certain distribution. It is well-known that a difference in particle sizes will result in the segregation of granular materials (e.g. the Brazil nut effect). Furthermore, in most granular flows the effect of gravity cannot be ignored, which introduces an anisotropy in the velocity fluctuation of particles. Clearly the definitions of particle phase pressure and other transport coefficients are not straightforward because a homogeneous equilibrium state normally does not exist. This keeps the establishment of a hydrodynamical model for granular flows a great challenge for both scientists and engineers [14].

2.2.3 The interphase coupling

The interphase coupling deals with the effects of gas flow on the solids motion and vice versa. Elgobashi [15] proposed a classification for gas-solid suspensions based on the solid volume fraction ε_p, which is shown in Figure 2.2. When the solid volume fraction is very low, say $\varepsilon_p < 10^{-6}$, the presence of particles has negligible effect on the gas flow, but their motion is influenced by the gas flow for sufficiently small inertia. This is called "one-way coupling". In this case, the gas flow is treated as a pure fluid and the motion of particle phase is mainly controlled by the hydrodynamical forces (e.g. drag force, buoyancy force, and so on), while the particle-particle interaction is assumed to be irrelevant. With increasing solid volume fraction up to $\varepsilon_p < 10^{-3}$, the effects of the particle phase on the gas phase

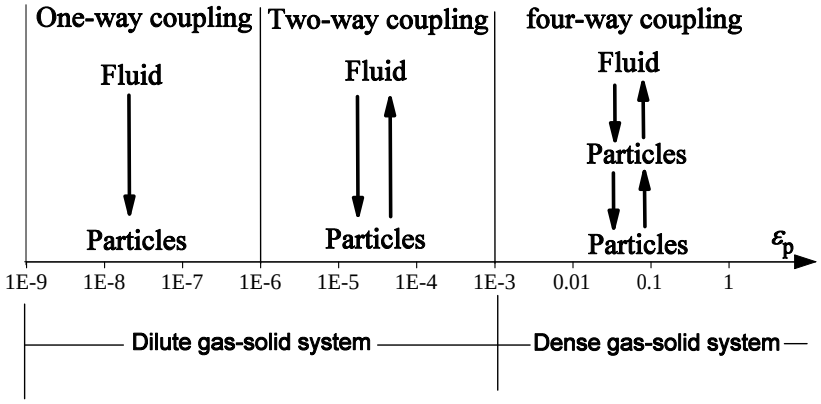

Figure 2.2: *Interphase coupling. (based on Elgobashi, Applied Sci. Res., 1991. [15])*

flow pattern will become important. In this region, turbulent structures encountered in gas flows can be modified by the presence of particles. So the gas phase and particle phase can interact with each other. It is commonly accepted that the particle-particle interaction still does not play a dominant role in this regime, which we normally refer to as "two-way coupling". For even higher solid volume fraction $\varepsilon_p > 10^{-3}$, the momentum of particles will be transported not only by the free flight mechanism, but also by the collisions between particles and particles and the confining walls. In this connection, the particle-particle interaction will be very important and "four-way coupling" should be taken into account.

2.2.4 The multi-level modeling approach for gas-solid two-phase flows

As shown above, for both the gas and particle phase, the continuum-(Eulerian) and discrete- (Lagrangian) type of models can be applied, depending on the length scales. In fact, to model gas-solid two-phase flows, one can make use of the combinations of these models provided that they are linked with a suitable coupling method. In this thesis, a multi-level modeling approach is used to study the gas-solid two-phase flow in gas-fluidized beds, with focus on systems with Geldart A particles [16]. In Figure 2.3 we show the concept of the multi-level modeling approaches for gas-solid two-phase flows, which can be divided into three groups, i.e, Lagrange-Lagrange, Euler-Lagrange, and Euler-Euler models.

At the most fundamental level, the idea of Lagrange-Lagrange models are employed. However, as a macro-scale gas volume is composed of a huge number of molecules, the direct use of molecule-grain approach is, although in principle possible, not feasible with present day computers. One can introduce some approximations by treating the gas phase as discrete "particles" on a scale much larger

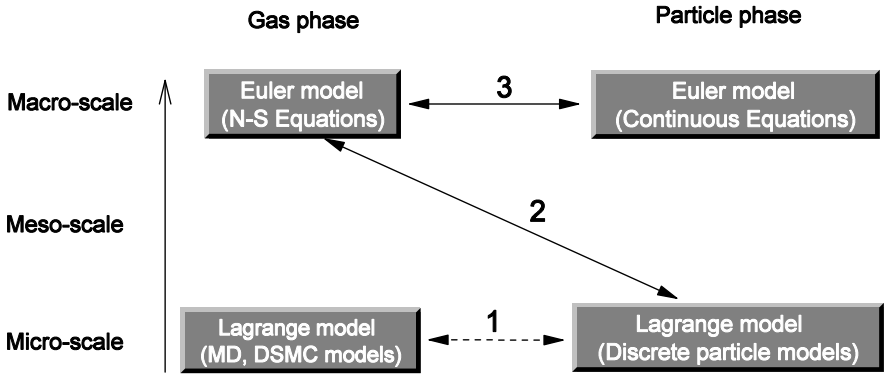

Figure 2.3: *The scheme of multi-level modeling for gas-solid two-phase flows.*

than that of a single molecule, but still smaller than the size of macro-scale particles. These gas "particles" obey the Boltzmann equations and transport the momentum in a lattice. A carefully chosen no-slip boundary conditions is required at gas-solid interfaces. This is the so-called lattice Boltzmann method (LBM) [17, 18]. The results obtained in LBM simulations will be applied to obtain the detailed gas-particle interaction (in the form of drag force), which can be used in higher level models instead of the conventional empirical correlations. This idea has been adopted in a project parallel to this one. The details of LBM will not be described in this thesis .

The starting point of this study is the meso-scale Euler-Lagrange model. In this model the particle-particle and particle-wall interactions will be taken into account by use of a soft-sphere discrete particle approach. The gas phase dynamics is calculated by solving the volume-averaged Navier-Stokes equations in the domain of interest. In principle four-way coupling is required, however, the interactions between particles are coupled in a natural way in the discrete particle model. Consequently, the essential part is the two-way coupling between gas and particle phases, which are realized in the form of the drag force that presents the most important gas-particle interaction in a gas-fluidized bed. This meso-scale Euler-Lagrange model can help us to gain necessary information of particle-particle interactions of Geldart A particles, which is required to develop and improve the kinetic theory of granular flows. A reliable kinetic theory of granular flows specialized to Geldart A particles has not been established so far, and even the applicability of the standard theory has not been verified. The latter is very essential for developing the closure laws for a macroscopic-scale Euler-Euler model. The Euler-Euler model in this research is typically a two-fluid model (TFM) [19] based on the modified kinetic theory of granular flows. By use of well-developed computational fluid dynamics (CFD) techniques, this model is expected to be directly applied to the engineering scale equipments.

2.3 Euler-Lagrange model

2.3.1 Discrete particle model

Discrete particle models offer a viable tool to study the macroscopic behavior of assemblies of particles, and originated from molecular dynamics (MD) methods. Initiated in the 1950s [20], MD has been extensively developed, with thousands of papers published in the open literature. A thorough discussion of MD techniques was given by Allen and Tildesley [6], where the details of both numerical algorithms and computational tricks have been presented. Also Frenkel and Smit [21] provided a comprehensive introduction to the "recipes" of classical molecular dynamics and also explained the physics underlying these methods. Nearly all techniques developed for MD can be directly applied to discrete particles models, except the formulation of particle-particle interactions. Based on the mechanism of particle-particle interaction a granular system may be described either as "hard-spheres" or as "soft-spheres".

Hard-sphere model

In a hard-sphere system the trajectories of particles are determined by momentum-conserving binary collisions. The interactions between particles are assumed to be pair-wise and instantaneous. In the simulation, the collisions are processed one by one according to the order in which the events occur. For not too dense systems, the hard-sphere models are considerably faster than the soft-sphere models. Note that the occurrence of multiple collisions at the same instant cannot be taken into account.

Campbell and Brennen [22] reported the first hard-sphere discrete particle simulation used to study granular systems. Subsequently, the hard-sphere models have been applied to a wide variety of simulations, for studying the basic physics of complex granular systems.

Hoomans et al. [23] used the hard-sphere model, in combination with a CFD approach for the gas phase conservation equations, to study gas-solid two-phase flows in gas-fluidized beds. By using this model, they studied the effect of particle-particle interaction on bubble formation [23] and the segregation induced by particle size differences and density differences [24]. This model has been further used in connection with the kinetic theory of granular dynamics by Goldschmidt et al. [25], high pressure fluidization by Li and Kuipers [26], and circulating fluidized beds by Hoomans et al. [43].

Similar simulations have been carried out by other groups. Ouyang and Li [27] developed a slightly different version of this model. Helland et al. [28] recently developed a discrete particle model in which the hard-sphere collisions are assumed, but where a time-driven scheme (typically found in the soft-sphere model) was used to locate the collisional particle pair. Effect of the gas turbulence has also been taken into account in some hard-sphere models by Helland et al. [29], Lun [30] and Zhou et al. [31].

At high densities or low coefficients of restitution e, the collisions will lead to a dramatical decrease in kinetic energy. This is the so-called inelastic collapse [32], in which regime the collision frequencies diverge as relative velocities vanish. Clearly in that case, the hard-sphere method becomes useless.

Soft-sphere model

In more complex situations, the particles may interact via short or long range forces, and the trajectories are determined by integrating Newtonian equations of motion. The soft-sphere method originally developed by Cundall and Strack [33] was the first granular dynamics simulation technique published in the open literature. In soft-sphere models the particles are allowed to overlap slightly, and the contact forces are subsequently calculated from the deformation history of the contact using a contact force scheme. The soft-sphere models allow for multiple particle overlap although the net contact force is obtained from the addition of all pair-wise interactions. The soft-sphere models are essentially time-driven where the time step should however be carefully chosen in calculating the contact force. Normally soft-particle models differ from each other with respect to the contact force scheme that is used. A review of various popular schemes for repulsive inter-particle forces is presented by Schäfer et al. [34]. Walton and Braun [35] developed a model which uses two different spring constants to model the energy dissipation in the normal and tangential direction respectively. In the force scheme proposed by Langston et al. [36], a continuous potential of an exponential form containing two unknown parameters, i.e. the stiffness of the interaction and an interaction constant, has been used.

A 2D soft-sphere approach was first applied to gas-fluidized beds by Tsuji et al. [37], where the linear-spring/dashpot model similar to the one presented by Cundall and Strack [33] was employed. Xu and Yu [38] independently developed a two-dimensional model of a gas-fluidized bed. However in their simulations a collision detection algorithm that is normally found in hard-sphere simulations was used to determine the first instant of contact precisely. Based on the model developed by Tsuji et al. [37], Iwadate and Horio [39] incorporated van der Waals forces forces to simulate cohesive particle fluidization. Kafui et al. [40] developed a discrete particle model based on the theoretical contact mechanics, thereby enabling the collision of the particles to be directly specified in terms of material properties such as friction, elasticity, elasto-plasticity and auto-adhesion.

It is also interesting to note that soft sphere models have also been applied to other applications such as gas-particle heat transfer by Li and Mason [41] and coal combustion by Zhou et al. [42]. Clearly these methods open a new way to study difficult problems in fluidized bed reactors.

Comparison between hard- and soft-sphere models

Although both hard- and soft-sphere models have been used in the simulation of granular flows, each of them has own charateristics which make them very effi-

Table 2.1: *Comparison between hard- and soft-sphere models.*

	hard-sphere	soft-sphere
Computing efficiency	++	+
Multiple contacts	-	++
Lower coefficient of restitution	-	++
Incorporation of cohesive force	+	++
Energy conservation during collisions	++	+
Multiple particle sizes	++	+

++: good
+ : normal
- : fail

cient in some cases while inefficient in other cases. In Table 2.1 these two types of models have been compared. Hard-sphere models use an event driven scheme because the interaction times are (assumed to be) small compared to the free flight time of particles, where the progression in physical time depends on the number of collisions that occur. On the other hand, in the soft-sphere models a time step that is significantly smaller than the contact time should be used. Clearly the contact time is much shorter than the free flight time, which indicates the computing efficiency is accordingly much lower than the hard-sphere models. In the soft-sphere models a slight deformation of particles is allowed, so the multiple contacts between several pairs of particles are possible, which never happen in the event-driven models. As mentioned above, a lower coefficient of restitution may lead to the inelastic collapse in hard-sphere simulations, which, however, has not been found in soft-sphere simulations. Incorporation of cohesive forces, especially the pair-wise forces, is quite straightforward in soft-sphere models. This is because the collisional processes in soft-sphere models is described via the Newtonian equations of motion of individual particles, that is, in terms of forces. In the hard-sphere system, the update is not via forces (they are either zero or infinite), and thus forces and collisions are separately treated. Since the cohesive forces are essentially short-range forces, the incorporation of cohesive forces is quite involved. If there exists particles with different sizes, the soft-sphere model may suffer some difficulties. In a soft-sphere system using a linear-spring/dashpot scheme, the spring stiffness is dependent on the particle size. This means that in principle different spring stiffness should be used for calculating the contact forces between particles with different sizes. Otherwise the computing efficiency will drop substantially.

In this research, we will focus on the fluidization of Geldart A particles. This type of particles are normally operated in a very dense (homogeneous expansion) regime, and multiple contacts are expected. Furthermore, the cohesive interaction between this type of particles is also believed to be important. Therefore, the soft-sphere model will be used in this work.

2.3.2 The scheme of soft-sphere model

The equations of motion

The motion of a single spherical particle a with mass m_a and moment of inertia I_a can be described by Newtonian equations:

$$m_a \frac{d^2\mathbf{r}_a}{dt^2} = \mathbf{F}_{contact,a} + \mathbf{F}_{coh,a} + \mathbf{F}_{ext,a} \tag{2.2}$$

$$I_a \frac{d^2\Theta_a}{dt^2} = \mathbf{T}_a \tag{2.3}$$

where $\mathbf{r}_a$ is the position, $\mathbf{F}_{contact,a}$ the sum of all interparticle contact forces, $\mathbf{F}_{coh,a}$ the sum of cohesive forces, $\mathbf{F}_{ext,a}$ the sum of all other external forces, $\mathbf{T}_a$ the torque, and Θ_a the angular displacement. The external forces $\mathbf{F}_{ext,a}$ include, for example, the drag force, the gravitational force, and the buoyancy force. The calculation of the external forces and cohesive forces will be described in the following sections. $\mathbf{F}_{contact,a}$ is computed as the sum of all contact forces exerted by all particles being in contact with the particle of interest, which are naturally divided into a normal and a tangential component,

$$\mathbf{F}_{contatc,a} = \sum_{b \in contactlist} (\mathbf{F}_{ab,n} + \mathbf{F}_{ab,t}) \tag{2.4}$$

The cohesive force is considered to be the interparticle van der Waals force. The torque $\mathbf{T}_a$ equals

$$\mathbf{T}_a = \sum_{b \in contactlist} (R_a \mathbf{n}_{ab} \times \mathbf{F}_{ab,t}) \tag{2.5}$$

Contact force

The calculation of the contact force between two particles is actually quite involved. A detailed model for accurately computing contact forces involves complicated contact mechanics [44], the implementation of which is extremely cumbersome. Many simplified models have therefore been proposed, which use an approximate formulation of the interparticle contact force. The simplest one is originally proposed by Cundall and Strack [33], where a linear-spring and dashpot model is employed to calculate the contact forces. The scheme of this linear-spring /dashpot soft-sphere model is shown in Figure 2.4. In this model, the normal component of the contact force between two particles a and b can be calculated by

$$\mathbf{F}_{ab,n} = -k_n \delta_n \mathbf{n}_{ab} - \eta_n \mathbf{v}_{ab,n}, \tag{2.6}$$

where k_n is the normal spring stiffness, $\mathbf{n}_{ab}$ the normal unit vector, η_n the normal damping coefficient, and $\mathbf{v}_{ab,n}$ the normal relative velocity. The overlap δ_n is given by

$$\delta_n = (R_a + R_b) - |\mathbf{r}_a - \mathbf{r}_b|, \tag{2.7}$$

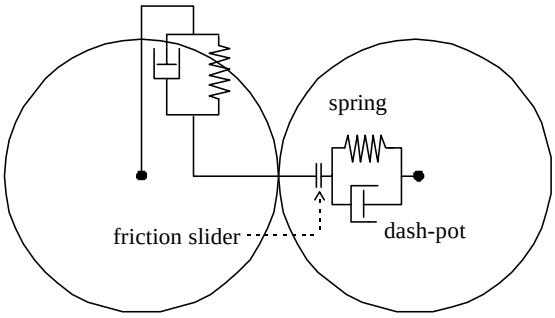

Figure 2.4: *The scheme of linear-spring/dashpot soft-sphere model. (from Hoomans, Ph.D. thesis, University of Twente, 2000. [43])*

with R_a and R_b denoting the radii of the particles. The normal unit vector is defined as

$$\mathbf{n}_{ab} = \frac{\mathbf{r}_b - \mathbf{r}_a}{|\mathbf{r}_b - \mathbf{r}_a|}. \tag{2.8}$$

The relative velocity of particles a and b is

$$\mathbf{v}_{ab} = (\mathbf{v}_a - \mathbf{v}_b) + (R_a\omega_a + R_b\omega_b) \times \mathbf{n}_{ab}, \tag{2.9}$$

where $\mathbf{v}_a$ and $\mathbf{v}_b$ are particle velocities, and ω_a and ω_b the angular velocities. The normal component of the relative velocity between particle a and b is

$$\mathbf{v}_{ab,n} = (\mathbf{v}_{ab} \cdot \mathbf{n}_{ab})\mathbf{n}_{ab}. \tag{2.10}$$

The tangential component of the contact force is given out by equation (2.11), where the Coulomb-type friction law is taking into account.

$$\mathbf{F}_{ab,t} = \begin{cases} -k_t\delta_t - \eta_t\mathbf{v}_{ab,t} & \text{for } |\mathbf{F}_{ab,t}| \leq \mu_f|\mathbf{F}_{ab,n}| \\ -\mu_f|\mathbf{F}_{ab,n}|\mathbf{t}_{ab} & \text{for } |\mathbf{F}_{ab,t}| > \mu_f|\mathbf{F}_{ab,n}| \end{cases} \tag{2.11}$$

Note that k_t is the tangential spring stiffness, δ_t the tangential displacement, η_t the tangential damping coefficient, $\mathbf{v}_{ab,t}$ the tangential relative velocity, μ_f the friction coefficient, and $\mathbf{t}_{ab}$ the tangential unit vector. The calculation of the tangential displacement δ_t is quite important and will be addresses in a separate section. The tangential relative velocity is

$$\mathbf{v}_{ab,t} = \mathbf{v}_{ab} - \mathbf{v}_{ab,t}. \tag{2.12}$$

And the tangential unit vector $\mathbf{t}_{ab}$ is defined as

$$\mathbf{t}_{ab} = \frac{\mathbf{v}_{ab,t}}{|\mathbf{v}_{ab,t}|}. \tag{2.13}$$

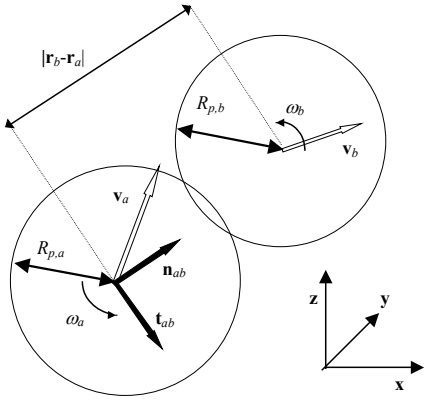

Figure 2.5: *The coordinate system used in the soft-sphere model.*

Tangential displacement

Suppose at a given instant t_0 the tangential displacement is δ_{t_0}, after an interval $dt = t - t_0$ the new tangential displacement will be [43]

$$\delta_t = \delta_{t_0} + \int_{t_0}^{t} \mathbf{v}_{ab,t}\, d\,t \tag{2.14}$$

This expression, however, is only justified for 2D systems. In a 2D system, the particles are represented essentially by circles or disks, which are confined in a single plane and the particle-particle contact occurs along a line, as shown in Figure 2.6. So the tangential component of the relative velocity is always in the same plane and no coordinate transformation is required. Eq.(2.14) is, in principle, only suitable for the 2D situation.

In a 3D system, however, it becomes more complicated. The particle-particle contact now occurs in a plane. The tangential component of the relative velocity is always in this plane and vertical to the normal unit vector (according to the definition). Since the normal unit vector is not necessarily situated in the same plane at any time, it is desired to transfer the old tangential displacement to the new contact plane before we calculate the new tangential displacement. To this end, a 3D rotation of the old tangential displacement is desired. As the tangential velocity vector is always vertical to the normal unit vector, the 3D rotation can be done around the vector determined by $\mathbf{n}_{ab} \times \mathbf{n}_{0,ab}$, as shown in Figure 2.7. So in a 3D situation, the tangential displacement is determined by

$$\delta_t = \delta_{t_0}\mathbf{H} + \int_{t_0}^{t} \mathbf{v}_{ab,t}\, d\,t \tag{2.15}$$

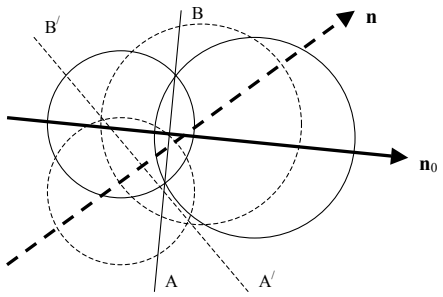

Figure 2.6: *The rotation of the contact plane during particle-particle collisions.*

where the rotation matrix is

$$\mathbf{H} = \begin{pmatrix} qh_x^2 + c & qh_xh_y - sh_z & qh_xh_z + sh_y \\ qh_xh_y + sh_z & qh_y^2 + c & qh_yh_z - sh_x \\ qh_xh_z - sh_y & qh_yh_z + sh_x & qh_z^2 + c \end{pmatrix}. \tag{2.16}$$

Note that vector $\mathbf{h}$ is given by

$$\mathbf{h} = \frac{\mathbf{n}_{ab} \times \mathbf{n}_{0,ab}}{|\mathbf{n}_{ab} \times \mathbf{n}_{0,ab}|}$$

and q, s and c are obtained through following expressions

$$c = \cos\varphi$$

$$s = \sin\varphi$$

$$q = 1 - c$$

$$\varphi = \arcsin(|\mathbf{n}_{ab} \times \mathbf{n}_{0,ab}|)$$

Are Eqs.(2.15) and (2.16) sufficient to describe the tangential displacement during particle-particle contact? In the absence of friction the answer is yes. When we consider friction during particle-particle contact, as pointed out by Brendel and Dippel [45], the use of Eqs.(2.15) and (2.16), may give rise to a unphysical behavior in dense granular system. This is due to the allowance of an arbitrarily large tangential displacement in Eqs.(2.15) and (2.16). In a dilute system, this is not a big problem since the multiple-particle contacts do not happen frequently. In this case, if the contacts finish the tangential displacements will be set to zero. In a dense system, however, the multiple-particle contacts are very common and the contact history for a specific particle could be very long. The long contact history causes a relatively large tangential displacement, which means that an extra friction force should be taken into account. So to make our 3D code suitable for simulating very dense systems, it is essential to seek for an improved approach to account for the tangential displacement. Brendel and Dippel [45] proposed a so-

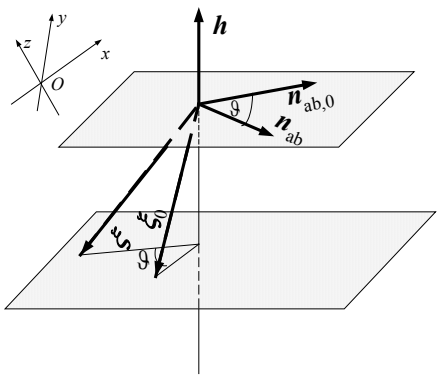

Figure 2.7: *The transformation of tangential displacement vector.*

lution for this problem. In this method, the tangential displacement during the friction is calculated by

$$\delta_t = \mu_f |\mathbf{F}_{ab,n}| \mathbf{t}_{ab} / k_t$$

Therefore the tangential displacement in the current soft-sphere model is given by:

$$\delta_t = \begin{cases} \delta_{t_0}\mathbf{H} + \int_{t_0}^{t} \mathbf{v}_{ab,t}\, d\,t & \text{for } |\mathbf{F}_{ab,t}| \leq \mu_f |\mathbf{F}_{ab,n}| \\ \mu_f |\mathbf{F}_{ab,n}| \mathbf{t}_{ab} / k_t & \text{for } |\mathbf{F}_{ab,t}| > \mu_f |\mathbf{F}_{ab,n}| \end{cases} \tag{2.17}$$

Collision parameters

To solve the Eqs.(2.2) and (2.3), we still need to know five parameters: normal and tangential spring stiffness k_n and k_t, normal and tangential damping coefficient η_n and η_t, and the friction coefficient μ_f. To get a better understanding, we return to Eq.(2.6) written in another form

$$m_{eff} \frac{d\delta_n^2}{dt^2} = -k_n \delta_n - \eta_n \frac{d\delta_n}{dt} \tag{2.18}$$

where m_{eff} is the reduced mass of the normal linear spring-dashpot system. This is the well-known differential equation of the damped harmonic oscillator. Suppose that v_0 is the initial relative velocity, we can write down the solution of Eq.(2.18) as

$$\delta_n(t) = (v_0/\Omega) \exp(-\Psi\, t) \sin(\Omega\, t). \tag{2.19}$$

So the relative velocity is

$$\dot{\delta}_n(t) = (v_0/\Omega) \exp(-\Psi\, t)(-\Psi \sin(\Omega\, t) + \Omega \cos(\Omega\, t)). \tag{2.20}$$

where

$$\Omega = \sqrt{\Omega_0^2 - \Psi^2},$$

$$\Omega_0 = \sqrt{k_n/m_{eff}},$$
$$\Psi = \eta_n/(2m_{eff}).$$

The duration of a contact can be determined by $\delta_n(t_{contact,n}) = 0$, which leads to

$$t_{contact,n} = \pi/\Omega.$$

So the relative velocity just after a contact is

$$\dot{\delta}_n(t_{contact,n}) = -v_0 \exp(-\Psi\, t_{contact,n})$$

According to the definition, the coefficient of restitution is given by

$$e_n = -\frac{\dot{\delta}_n(t_{contact,n})}{\dot{\delta}_n(0)} = \exp(-\pi\Psi/\Omega) \tag{2.21}$$

Thus we can calculate the normal damping coefficient via

$$\eta_n = \frac{-2\ln\, e_n\sqrt{m_{eff}\, k_n}}{\sqrt{\pi^2 + \ln^2\, e_n}} \quad (e_n \neq 0) \tag{2.22}$$

In case of $e_n = 0$, according to equation (2.21), we find that

$$\Omega = 0,$$

which determines the damping coefficient by

$$\eta_n = 2\sqrt{k_n m_{eff}} \tag{2.23}$$

We can follow a similar procedure for the tangential spring-dashpot system. So the tangential damping coefficient is determined by

$$\eta_t = \frac{-2\ln\, e_t\sqrt{m'_{eff}\, k_t}}{\sqrt{\pi^2 + \ln^2\, e_t}} \quad (e_t \neq 0) \tag{2.24}$$

where m'_{eff} is the reduced mass for the tangential spring-dashpot system. It is argued that in a tangential direction both the rotational and translational momentum must be considered and the reduced mass m'_{eff} is different from that in normal direction. The definitions of these two reduced mass are as follows:

$$m_{eff} = \frac{m_a m_b}{m_a + m_b} \tag{2.25}$$

$$m'_{eff} = \frac{2}{7}\left(\frac{m_a m_b}{m_a + m_b}\right) \tag{2.26}$$

In the case of particle-wall contact, we shall simply treat particle b as a big particle that has an infinite radius, so we have

$$m_{eff} = m_a \tag{2.27}$$

$$m'_{eff} = \frac{2}{7} m_a \tag{2.28}$$

In order to calculate the contact force between two particles, we now need five parameters: normal and tangential spring stiffness k_n and k_t, normal and tangential coefficient of restitution e_n and e_t, and the friction coefficient μ_f. In should be added here, however, that k_n and k_t in principle are related to the Young modulus and Possion ratio of the solid material, so we are left with the specification of three collision parameters e_n, e_t, and μ_f.

Integrating the equations of motion

Mathematically the equations of particle motion represent a set of initial value differential equations. The evolution of particle positions and velocities can be traced by using any kind of method for ordinary differential equations. The simple first-order integrating scheme is widely used, which gives

$$\mathbf{v}_a = \mathbf{v}_a^{(0)} + \mathbf{a}_a \Delta t \tag{2.29}$$

$$\mathbf{r}_a = \mathbf{r}_a^{(0)} + \mathbf{v}_a \Delta t \tag{2.30}$$

$$\theta_a = \theta_a^{(0)} + \omega_a \Delta t \tag{2.31}$$

where $\mathbf{a}_a$ is the acceleration, ω_a the rotational velocity of particle a. The superscript (0) denotes the initial time. The first-order integration scheme, however, induces errors for energy calculation. From Eq.(2.29), we have

$$(\mathbf{v}_a - \mathbf{a}_a \Delta t)^2 = (\mathbf{v}_a)^2 + (\mathbf{a}_a \Delta t)^2 - (2\mathbf{v}_a \cdot \mathbf{a}_a \Delta t) = (\mathbf{v}_a^{(0)})^2 \tag{2.32}$$

So

$$\frac{1}{2}(\mathbf{v}_a)^2 - (\mathbf{v}_a \cdot \mathbf{a}_a \Delta t) + O(\Delta t^2) = \frac{1}{2}(\mathbf{v}_a^{(0)})^2 \tag{2.33}$$

The first term on the left of Eq.(2.33) is the reduced kinetic energy of the particle, the second term is the work due to all kinds of external forces, and the first term in the right is the initial kinetic energy. Obviously, the extra energy of $O(\Delta t^2)$ is always positive, and will be introduced to the system for each time step solely due to the numerical method.

In the past decades, a lot of methods have been devised to achieve better energy conservation, for example, the Gear family of algorithms and the family of Verlet algorithms [21]. In our 3D code, we have incorporated another type of integrating method. This method was developed by Beeman and is possibly the most accurate of the Verlet family of algorithms [21]. In this method, the position and velocity of particle is calculated via

$$\mathbf{r}_a = \mathbf{r}_a^{(0)} + \mathbf{v}_a^{(0)} \Delta t + (\frac{2}{3}\mathbf{a}_a^{(0)} - \frac{1}{6}\mathbf{a}_a^{(-1)})(\Delta t)^2 \tag{2.34}$$

$$\mathbf{v}_a = \mathbf{v}_a^{(0)} + \frac{1}{3}\mathbf{a}_a \Delta t + (\frac{5}{6}\mathbf{a}_a^{(0)} - \frac{1}{6}\mathbf{a}_a^{(-1)})(\Delta t) \tag{2.35}$$

$$\theta_a = \theta_a^{(0)} + \frac{1}{3}\theta_a \Delta t + (\frac{5}{6}\theta_a^{(0)} - \frac{1}{6}\theta_a^{(-1)})(\Delta t) \tag{2.36}$$

where the superscript (-1) denotes the initial time in the previous time step. Note that the Beeman-Verlet algorithm is not self starting. It requires the storage of the old value of the acceleration $\mathbf{a}^{(-1)}$. But this second-order integrating scheme leads to an improved calculation of velocities and better energy conservation, compared to the first order methods.

Time step

The time step Δt depends on the duration of a contact. Since there are two different spring-dashpot systems in our current model, it is essential to assume

$$t_{contact,n} = t_{contact,t} \tag{2.37}$$

So we have

$$\sqrt{\frac{\pi^2 + (\ln\, e_n)^2}{k_n/m_{eff}}} = \sqrt{\frac{\pi^2 + (\ln\, e_t)^2}{k_t/m'_{eff}}} \tag{2.38}$$

If we further assume that $e_n = e_t$, then the relation between the normal and tangential spring stiffness is

$$\frac{k_t}{k_n} = \frac{m_{eff}}{m'_{eff}} = \frac{2}{7} \tag{2.39}$$

Based on the discussion in previous sections, we can calculate the time step by

$$\Delta t = \frac{1}{K_N} t_{contact,n} = \frac{1}{K_N}\sqrt{\frac{\pi^2 + (\ln\, e_n)^2}{k_n/m_{eff}}} \tag{2.40}$$

where K_N is the minimum number of steps during one contact. Our experience is that K_N must not be less than 5, and is normally in the range 15$\sim$50. From Eq.(2.19) we can calculate the maximum overlap

$$\delta_{max} = (v_0/\Omega_0)\exp[(-\Psi/\Omega)\arcsin(\Omega/\Omega_0)], \tag{2.41}$$

which occurs at

$$\frac{d\delta_n(t)}{dt} = 0.$$

To get a reasonable time step, we also need to check the maximum overlap which should in general be less than 1% of the particle diameter.

Neighbor list and cell list

To perform simulations of relatively large systems for relatively long times it is essential to optimize the computational strategy of discrete particle simulations. The *tricks of the trade* originally developed in Molecular Dynamics can be applied to

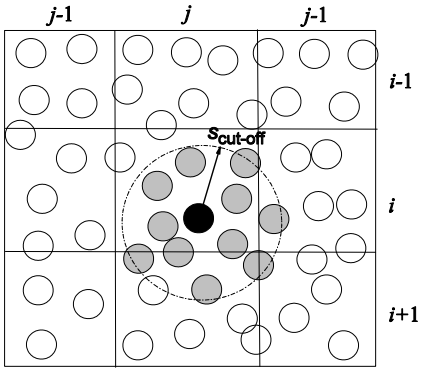

Figure 2.8: *The scheme of neighbor list and cell list. The black is the particle of interest; the grey are particles within the neighbor list cut-off.*

discrete particle simulations to speed up the simulation. Hoomans [43] employed the techniques including neighbor list and cell list in his discrete particle model.

The neighbor list contains a list of all particles within the cut-off sphere of a particular particle, so that the separations do not need to be calculated at each step, which is shown in Figure 2.8. The neighbor list cut-off $s_{cut-off}$ should be defined with care. A too small cut-off value may lead some neighboring particles to be excluded from the list; On the other hand, however, a big cut-off value will greatly reduce the computational efficiency.

To speed up the searching for neighbors, the particles in each fluid cell in this research are put into a corresponding list. All neighbors of a particle will then be found either in the cell containing the particle or an immediately adjacent cell, so that the search for possible collision partners is a rapid process.

Interparticle van der Waals froce

The van der Waals force acting on particle a, $\mathbf{F}_{vdw,a}$, is given by

$$\mathbf{F}_{vdw,a} = \sum_{b \in Neighbourlist} F_{vaw,ab}\mathbf{n}_{ab}. \tag{2.42}$$

To calculate the interparticle van der Waals forces, we adopt the Hamaker scheme [46] given by:

$$F_{vdw,ab}(S) = \frac{A}{3} \cdot \frac{2r_a r_b(S + r_a + r_b)}{[S(S + 2r_a + 2r_b)]^2} \left[\frac{S(S + 2r_a + 2r_b)}{(S + r_a + r_b)^2 - (r_a - r_b)^2} - 1 \right]^2 \tag{2.43}$$

where S is the intersurface distance between two spheres, A the Hamaker constant, and r_a and r_b the radii of the two spheres respectively. However, Eq.(2.43) exhibits

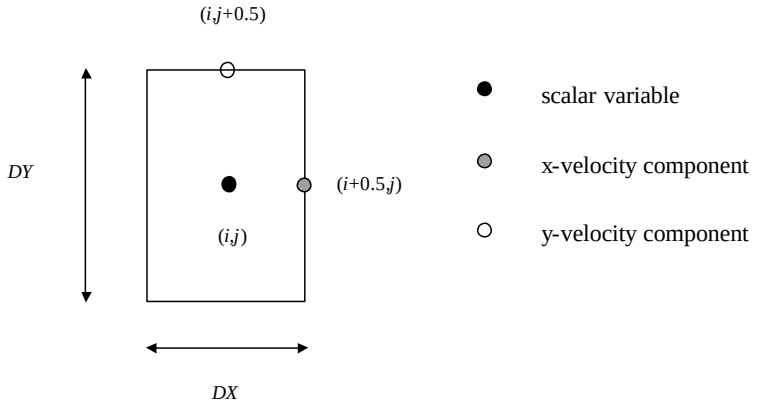

Figure 2.9: *Lay-out of the staggered grid.*

an apparent numerical singularity that the van der Waals interaction diverges if the distance between two particles approaches zero. In reality such a situation will never occur, because of the short-range repulsion between particles. In the present model, we have not included such a repulsion, however, we can avoid the numerical singularity by defining a cut-off (maximal) value of the van der Waals force between two spheres. In practice it is more convenient to use the equivalent cut-off value for the intersurface distance, S_0, instead of the interparticle force.

2.3.3 Gas dynamics

Governing equations

The gas phase is treated as a continuum phase, the dynamics of which can be described by a set of volume-averaged Navier-Stokes equations [19]. From mass conservation, we have

$$\frac{\partial(\varepsilon\rho_g)}{\partial t} + \nabla\cdot(\varepsilon\rho_g\mathbf{u}) = 0 \tag{2.44}$$

where ρ_g is the gas density, ε the local porosity, and $\mathbf{u}$ the gas velocity. Momentum conservation gives that

$$\frac{\partial(\varepsilon\rho_g\mathbf{u})}{\partial t} + \nabla\cdot(\varepsilon\rho_g\mathbf{uu}) = -\varepsilon\nabla p - \mathbf{S}_P - \nabla\cdot(\varepsilon\overline{\boldsymbol{\tau}}) + \varepsilon\rho_g\mathbf{g} \tag{2.45}$$

where p is the gas phase pressure, $\mathbf{S}_P$ the source term, and $\mathbf{g}$ the gravitational acceleration. The source term $\mathbf{S}_P$ is defined as

$$\mathbf{S}_P = \frac{1}{V}\int\sum_{a=0}^{Npart}\frac{\beta V_a}{1-\varepsilon}(\mathbf{u}-\mathbf{v}_a)\delta(\mathbf{r}-\mathbf{r}_a)\,dV \tag{2.46}$$

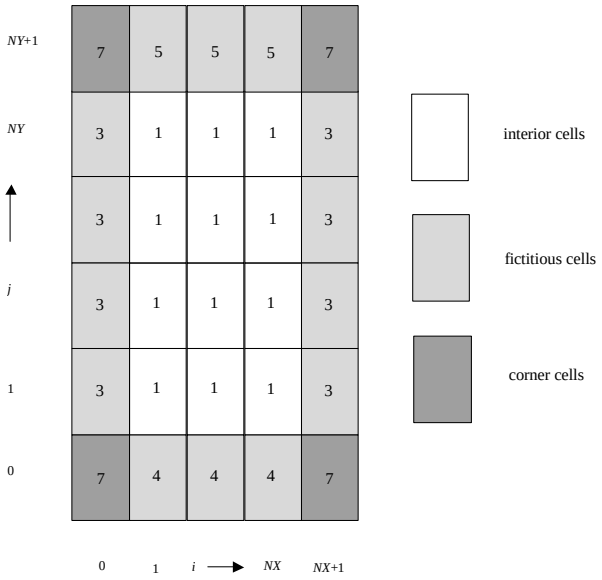

Figure 2.10: *The typical set of boundary conditions used in 2D simulations.*

Here V represents the local volume of a computational cell and V_a the volume of a particle. The δ-function ensures that the drag force acts as a point force at the (central) position of this particle. β is the momentum transfer coefficient.

Constitutive equations

The gas phase density ρ_g is calculated via the equation of state of an ideal gas law:

$$\rho_g = \frac{pM_g}{RT} \tag{2.47}$$

where R is the universal gas constant (8.314 J/(mol·K)), T the temperature, and M_g the molecular mass of the gas. The equation of state of the ideal gas can be applied for most gases at ambient temperature and pressure. The viscous stress tensor $\overline{\tau}$ is assumed to depend only on the gas motion. The general form for a Newtonian fluid [47] is used in our model:

$$\overline{\tau} = -(\lambda_g - \frac{2}{3}\mu_g)(\nabla \cdot \mathbf{u})\mathbf{I} + \mu_g(\nabla \mathbf{u} + (\nabla \mathbf{u}^T)) \tag{2.48}$$

with λ_g the gas phase bulk viscosity, μ_g the gas phase shear viscosity, and $\mathbf{I}$ the unit tensor. In the simulations the bulk viscosity of the gas phase is set equal to zero which is allowed for gases [47].

Note that no turbulence modelling was taken into account. For dense gas-solid fluidization this can be justified since the turbulence is completely suppressed in the particle bed due to the very high solids volume fraction.

Table 2.2: *Comparison between hard- and soft-sphere models.*

$fl(i,j,k)$	the type of cell
1	Interior cell, no boundary conditions have to be specified
2	Impermeable wall, free slip boundaries
3	Impermeable wall, no slip boundaries
4	Influx cell, velocities have to be specified
5	Prescribed pressure cell, free slip boundaries
6	Continuous outflow cell, free slip boundaries
7	Corner cell, no boundary conditions have to be specified

Numerical solution

The numerical solution follows the lines of Kuipers et al. [19] and will not be discussed in detail here. A finite difference technique, employing a staggered grid to ensure numerical stability, is used to solve the gas-phase conservation equations. The scalar variables (p and ε) are defined at the cell center, and the velocity components are defined at the cell faces as is shown in Figure 2.9.

A pressure correction technique was employed to solve the discretised set of partial differential equations. The solution method can easily be extended to three dimensions and will therefore not be discussed here.

Boundary conditions

The boundary conditions are taken into account by utilizing the flag matrix concept, which allows different boundary conditions to be applied for each single cell. A variety of boundary conditions can be applied by specification of the value of the cell flag $fl(i,j,k)$, which defines the relevant boundary condition for the corresponding cell (i,j,k). A typical set of boundary conditions used in a 2D simulation is shown in Figure 2.10.

In Table 2.2 we explain the meaning of each type of boundary condition. Normally the bottom distributor is defined as influx cells formulated by $fl(i,j,k) = 4$, where the void fraction is set to a constant value of 0.4.

2.3.4 Interphase coupling

For dense gas-solid two-phase flows, a four-way coupling is normally required. However, the coupling between particles is managed in a natural way in discrete particle models. The task is therefore to find a two-way coupling that satisfies Newton's third law. This technique involves the calculation of the void fraction and the incorporation of fluid-particle interaction in the momentum conservation equation for the gas-phase.

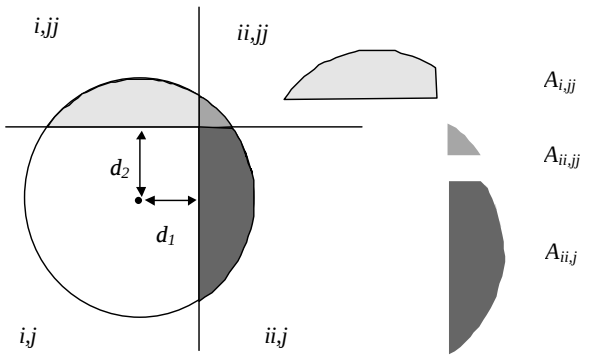

Figure 2.11: *The multiple cell overlap of a single particle. (from Hoomans, Ph.D. thesis, 2000, University of Twente)*

Void fraction calculation

From the position of each particle, we can calculate its contribution to the local solid volume fraction ε_p in any specified fluid cell. This local void fraction $\varepsilon = 1.0 - \varepsilon_p$, is one of the key parameters that controls the momentum exchange between the phases. Thus the calculation of the void fraction is essential in the interphase coupling.

For a 2D situation, the void fraction $\varepsilon(i,j)$ can be calculated based on the area occupied by the particles in the cell of interest. A particle can be present in multiple cells, however, as shown in Figure 2.11. Hoomans [24] developed a method to account for the multiple cell overlap. The area of $A_{ii,jj}$ is given by

$$A_{ii,jj} = \delta_1\delta_2 - \frac{1}{2}R_p\left[C_1 + C_2 - R_p\left(\operatorname{acos}\frac{\delta_1}{R_p} - \operatorname{asin}\frac{\delta_2}{R_p}\right)\right], \tag{2.49}$$

and area $A_{i,jj}$ by

$$A_{ii,jj} = \frac{1}{2}\pi R_p^2 - \delta_1\delta_2 + \frac{1}{2}R_p\left[C_1 - C_2 - R_p\left(\operatorname{acos}\frac{\delta_1}{R_p} - \operatorname{acos}\frac{\delta_2}{R_p}\right)\right]. \tag{2.50}$$

The area $A_{ii,j}$ can be calculated following Eq.(2.50). Note that the two constants are defined as

$$C_1 = \delta_1\sqrt{1 - \left(\frac{\delta_1}{R_p}\right)^2},$$

and

$$C_2 = \delta_2\sqrt{1 - \left(\frac{\delta_2}{R_p}\right)^2}.$$

However, the void fraction calculated in this way is based on a two-dimensional distribution of (circles) disks that is inconsistent with the applied empiricism in the

calculation of the drag force exerted on a particle. To correct for this inconsistency the void fraction calculated on the basis of area (ε_{2D}) is transformed into a three-dimensional void fraction (ε_{3D}) using the following equation:

$$\varepsilon_{3D} = 1 - \frac{2}{\sqrt{\pi\sqrt{3}}(1-\varepsilon_{2D})^{3/2}}. \tag{2.51}$$

In a true 3D situation, we can calculate the void fraction based on the real volume of particles. However, no analytical expression is available for volume $V_{ii,jj}$. Hoomans [24] introduced an approximation to calculate this 3D volume. Suppose a particle overlaps with two cells, the volume of a spherical cap can be calculated exactly by

$$V_{cap} = \frac{\pi(R_p - \delta_1)^2}{3}(2R_p + \delta_1), \tag{2.52}$$

with δ_1 the distance from the center of the particle to the cell boundary. $V_{ii,jj}$ can thus be approximated by

$$V_{ii,jj} \approx \frac{V_{jj}}{V_p}\frac{V_{ii}}{V_p}V_p. \tag{2.53}$$

Note that

$$V_{jj} = V_{ii,jj} + V_{i,jj}, \tag{2.54}$$

and

$$V_{ii} = V_{ii,jj} + V_{ii,j}, \tag{2.55}$$

Fluid-particle interaction

The fluid-particle interaction can be divided into two parts in this research: the drag force and the pressure gradient.

Drag force We start by introducing a more general form of the drag force,

$$\mathbf{F}_d = 3\pi\mu_g\varepsilon^2\, d_p\,(\mathbf{u}-\mathbf{v})\, f(\varepsilon)$$

where μ_g is the viscosity of the gas phase, ε the porosity, d_p the diameter of particle, u the local gas velocity, and $f(\varepsilon)$ is defined as the porosity function. The common-used drag model in the simulation of gas-fluidized beds is the Ergun-Wen-Yu model [48, 49], the porosity function of which is given by

$$f(\varepsilon) = \frac{150(1-\varepsilon)}{18\varepsilon^3} + \frac{1.75}{18}\frac{Re_p}{\varepsilon^3}$$

for $\varepsilon < 0.8$ [48] and

$$f(\varepsilon) = \frac{C_d}{24}Re_p\varepsilon^{-4.65}$$

for $\varepsilon \geq 0.8$ [49]. The drag coefficient C_d is a function of the particle Reynolds number and given by (in the case of $Re_p < 1000$):

$$C_d = \frac{24}{Re_p}(1 + 0.15Re_p^{0.687})$$

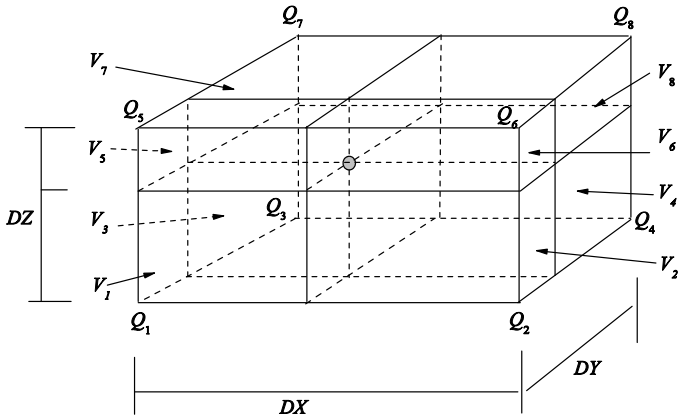

Figure 2.12: *The scheme of volume weight average.*

The validity of this model for low Reynolds number Re_p has been questioned in recent years. Note that the typical Re_p of Geldart A particles for a fluidized bed is typically less than $O(1)$. Recent results derived from lattice Boltzmann simulations show that a more accurate drag model, for example the model introduced by Koch and Sagani [50], should be used. In this model, the porosity function is given by

$$f(\varepsilon) = \frac{10(1-\varepsilon)}{\varepsilon^3} + 0.7$$

for $\varepsilon < 0.6$ and

$$f(\varepsilon) = \frac{1 + 3\sqrt{0.5(1-\varepsilon)} + (135/64)(1-\varepsilon)\ln(1-\varepsilon) + 17.14(1-\varepsilon)}{1 + 0.681(1-\varepsilon) - 8.48(1-\varepsilon)^2 + 8.16(1-\varepsilon)^3}$$

for $\varepsilon \geq 0.6$.

Pressure gradient The pressure gradient in the first term on the right hand side of Eq.(2.45) is calculated by using a second order approximation. The local value is obtained from an volume-weighted averaging technique using the values of the pressure gradients at the eight surrounding grid nodes. This technique is also used to obtain local gas velocities and local void fractions at the position of the center of the particle. The volume-weighted averaging technique used to obtain the local averaged value $\bar{Q}$ of a quantity Q_{ijk} from the eight surrounding computational nodes is shown in Figure 2.12. The local averaged value is calculated as follows:

$$\bar{Q} = \frac{Q_1 V_8 + Q_2 V_7 + Q_3 V_6 + Q_4 V_5 + Q_5 V_4 + Q_6 V_3 + Q_7 V_2 + Q_8 V_1}{DX \cdot DY \cdot DZ} \tag{2.56}$$

where:

$$V_1 = \delta_x \delta_y \delta_z$$
$$V_2 = (DX - \delta_x)\delta_y \delta_z$$
$$V_3 = \delta_x (DY - \delta_y)\delta_z$$
$$V_4 = (DX - \delta_x)(DY - \delta_y)\delta_z$$
$$V_5 = \delta_x \delta_y (DZ - \delta_z)$$
$$V_6 = (DX - \delta_x)\delta_y (DZ - \delta_z)$$
$$V_7 = \delta_x (DY - \delta_y)(DZ - \delta_z)$$
$$V_8 = (DX - \delta_x)(DY - \delta_y)(DZ - \delta_z)$$

The distances δ_x, ϵ_y and δ_z, necessary in this averaging technique, are calculated from the position of the particle in the staggered grid.

2.3.5 Energy budget

To relate our current work to the kinetic theory of granular flows, it is very useful to analyze the detailed information of the energy evolution in the system. The total energy balance of the system is obtained by calculating all relevant forms of energy as well as the work performed due to the action of external forces.

- Potential energy

$$E_p = -\sum_{a=0}^{N_{part}} m_a(\mathbf{g} \cdot \mathbf{r}_a). \tag{2.57}$$

- Kinetic energy

$$E_k = \frac{1}{2}\sum_{a=0}^{N_{part}} m_a(\mathbf{v}_a \cdot \mathbf{v}_a). \tag{2.58}$$

- Rotational kinetic energy

$$E_r = \frac{1}{2}\sum_{a=0}^{N_{part}} I_a(\boldsymbol{\theta}_a \cdot \boldsymbol{\theta}_a). \tag{2.59}$$

- Potential energy of the normal spring

$$E_{sn} = \frac{1}{2}\sum_{a=0}^{N_{part}} \sum_{b} k_n \delta_{ab,n}^2. \tag{2.60}$$

  where $b > a$ and $b \in$ the contactlist of a, $\delta_{ab,n}$ the overlap between particle a and b.

- Potential energy of the tangential spring

$$E_{st} = \frac{1}{2} \sum_{a=0}^{N_{part}} \sum_{b} k_t(\boldsymbol{\delta}_{ab,t} \cdot \boldsymbol{\delta}_{ab,t}). \tag{2.61}$$

  where $b > a$ and $b \in$ the contactlist of a, $\boldsymbol{\delta}_{ab,t}$ the relative tangential displacement between particle a and b.

The work due to the action of external forces has to be considered as well, and can be calculated as follows:

- Work due to the drag force

$$W_d = \int \sum_{a=0}^{N_{part}} (\frac{\beta V_a}{(1-\varepsilon)}(\mathbf{u} - \mathbf{v}_a) - V_a \nabla p) \cdot \mathbf{v}_a dt. \tag{2.62}$$

- Work due to the van der Waals forces

$$W_v = \int \sum_{a=0}^{N_{part}} (\mathbf{F}_{vdw} \cdot \mathbf{v}_a)\, dt. \tag{2.63}$$

Finally the energy dissipated during the particle-particle contact process has to be considered and is determined by:

- Energy dissipated by the normal spring

$$E_{dn} = \int \sum_{a=0}^{N_{part}} \sum_{b} \eta_n(\mathbf{v}_{ab,n} \cdot \mathbf{v}_{ab,n}) dt. \tag{2.64}$$

- Energy dissipated by the tangential spring

$$E_{dt} = \int \sum_{a=0}^{N_{part}} \sum_{b} \eta_t(\mathbf{v}_{ab,t} \cdot \mathbf{v}_{ab,t}) dt. \tag{2.65}$$

- Energy dissipated by the friction between particles

$$E_{df} = \int \sum_{a=0}^{N_{part}} \sum_{b} (\mu_f |\mathbf{F}_{ab,n}| \mathbf{t}_{ab} \cdot \mathbf{v}_{ab,t}) dt. \tag{2.66}$$

  where $b > a$ and $b \in$ the contactlist of a.

Finally we give the expression for the (total) energy balance of the system:

$$E_t = E_p + E_k + E_r + E_{sn} + E_{st} - W_d - W_v + E_{dn} + E_{dt} + E_{df}. \tag{2.67}$$

2.4 Euler-Euler model

2.4.1 Two fluid model

In the Euler-Euler models, i.e. the two-fluid models, it is assumed that both the gas and the solid phase are interpenetrating continua. This continuous approach is especially useful and computationally cost effective when the volume fractions of the phases are comparable, or when the interaction within and between the phases plays a significant role in determining the hydrodynamcis of the system. As discussed before, it is not difficult to numerically solve the governing equations for the gas phase utilizing well-established CFD techniques. The challenge is to establish a complete hydrodynamics description of the particulate phase.

Anderson and Jackson [51–53] and Ishii [54] have separately derived the governing equations for two-fluid models from first principles. Although the inherent assumptions used in deriving these governing equations are different, it has been shown that they give essentially similar predictions at an engineering scale. The two-fluid models differ significantly from each other as different closures for the solids stress tensor are used.

Classification of two-fluid models

There are basically three types of approaches to define the solid stress tensor. In the early hydrodynamic models the particulate phase parameters, especially the viscosity, is defined empirically as a constant. Examples are the work done by Jackson and his co-workers [51, 55], Kuipers et al., [19], and Tsuo and Gidaspow [56]. The advantage of this model is its simplicity, but it does not take into account the underlying characteristics of this quantity.

In another type of models pioneered by Elghobashi and Abou-Arab [57] and Chen [58], a particle turbulent viscosity, derived by extending the concept of turbulence from the gas phase to the solid phase, has been used. This is the so-called $k-\epsilon$ model, where the k corresponds to the granular temperature equation and ϵ is a dissipation parameter for which another conservation law is required. By coupling with the gas phase $k-\varepsilon$ turbulence model, Zhou and Huang [59] developed a $k-\varepsilon$ model for turbulent gas-particle flows. The $k-\epsilon$ models do not include the effect of particle-particle collisions, so these models are restricted to dilute gas-particle flows.

Significant contributions to the modeling of gas-solid flows have been made by Gidaspow and co-workers [60], who combined the kinetic theory for the granular phase with continuum representations for the particle phase. There are a number of other studies using this approach. Sinclair and Jackson [61] predicted the core-annular regime for steady developed flow in a riser. Ding et al. [62] simulated a bubbling fluidized bed. Transient simulations and comparisons to data were done by Samuelsberg and Hjertager [63]. Nieuwland et al. [64] investigated a circulating fluidized bed using the kinetic theory of granular flows. Detamore et al [65] have performed an analysis of scale-up of circulating fluidized beds using kinetic theory.

One of the strengths of the kinetic theory of granular flows, although still under development, is that it can offer a very clear physical picture with respect to the key parameters (e.g. particle pressure, particle viscosity and other transport coefficients) that are used in the two-fluid models. The two-fluid models based on KTGF requires less ad-hoc adjustment than other two types of models. Therefore, it is the most promising framework for modeling engineering scale fluidized beds.

Two-fluid model for Geldart A particles

In the past decades, the two-fluid models based on the kinetic theory of granular flows (KTGF) saw the rapid development and wide applications in different solid-gas two-phase flows. However, most of the studies have focused on systems with either large particles (Geldart B or D particles) or dilute systems (circulating fluidized beds). Very few studies have been performed for dense systems of fine particles, especially Geldart A particles. The standard two-fluid model has so far failed to predict even the bubbling fluidization of Geldart group A particles. Several researchers tried to predict the bed expansion of FCC particles using two-fluid CFD models. Ferschneider and Mege [66] found a major over-prediction of bed expansion in a bubbling bed of FCC particles and Bayle et al. [67] obtained the same results in a turbulent bed of FCC particles. Recently McKeen and Pugsley [68] used the two-fluid CFD code MFIX to simulate a freely bubbling bed of FCC catalyst for $U_0 = 0.05 - 0.2$ m/s and compared their simulation results with ECT data. In accordance with findings of Ferschneider and Mege [66], McKeen and Pugsley [68] also found that the standard CFD model greatly over-predicted bed expansion without any modifications of the drag closures. By using a scale factor of 0.25 for the common-used gas-solids drag laws, they found that their simulation results are in accordance with experimental observations. They argued that this is due to the formation of clusters with a size smaller than the CFD grid size. Such small scale clusters have not been reported before, in particular for particles with a size of 75 μm. Although the van der Waals force can play a role in the fluidization of Geldart A particles, it is not clear how this force affects the gas-solid drag. The influence of the cohesion on the KTGF has not been carefully checked so far. The KTGF was originally developed based on the kinetic theory of dense gases by taking into account the inelasticity during particle-particle collisions [12]. Recently Kim and Arastoopour [69] tried to extend the kinetic theory to cohesive particles, however, their final expression for the particular phase stress is very complex.

In the chapter 5 of this thesis, we will investigate the effect of cohesive forces on the KTGF closures by use of the soft-sphere discrete particle model, which proved to be a powerful and useful tool to study the effect of detailed particle-particle interaction models.

2.4.2 Governing equations

In the two-fluid model, both the gas and particulate phase are considered as a continuum. The continuity and momentum equations for the gas phase are given by

$$\frac{\partial(\varepsilon\rho_g)}{\partial t} + (\nabla\cdot\varepsilon\rho_g\mathbf{u}) = 0 \tag{2.68}$$

$$\frac{\partial(\varepsilon\rho_g\mathbf{u})}{\partial t} + (\nabla\cdot\varepsilon\rho_g\mathbf{uu}) = -\varepsilon\nabla p - \beta(\mathbf{u}-\mathbf{v}) - \nabla\cdot(\varepsilon\overline{\tau}) + \varepsilon\rho_g\mathbf{g} \tag{2.69}$$

whereas the continuity and momentum equations for particle phase are given by

$$\frac{\partial(\varepsilon_s\rho_s)}{\partial t} + (\nabla\cdot\varepsilon_s\rho_s\mathbf{u}) = 0 \tag{2.70}$$

$$\frac{\partial(\varepsilon_s\rho_s\mathbf{u})}{\partial t} + (\nabla\cdot\varepsilon_s\rho_s\mathbf{uu}) = -\varepsilon_s\nabla p + \beta(\mathbf{u}-\mathbf{v}) - \nabla p_s - \nabla\cdot(\varepsilon_s\overline{\tau}) + \varepsilon_s\rho_s\mathbf{g} \tag{2.71}$$

where $\varepsilon_s = 1-\varepsilon$.

2.4.3 Kinetic theory of granular flows

The kinetic theory of elastic particles has been well documented by Chapman and Cowling in their classical textbook [5]. The kinetic theories of granular flows, which have appeared in the literature, differ only slightly from that of the elastic particles. For a system of smooth hard spheres of mass m and radius r_p, the evolution of the one-particle distribution function $f^{(1)}(\mathbf{r},\mathbf{v},t)$ can be described by the Boltzmann equation

$$\frac{\partial f^{(1)}(\mathbf{r},\mathbf{v},t)}{\partial t} + v\cdot\nabla f^{(1)}(\mathbf{r},\mathbf{v},t) = J[\mathbf{r},\mathbf{v}|f(t)] \tag{2.72}$$

where $f^{(1)}(\mathbf{r},\mathbf{v},t)d\mathbf{r}d\mathbf{v}$ represents the probable number of particles in a volume $d\mathbf{v}$ at the position $\mathbf{r}$ with the velocity ranging from $\mathbf{v}$ to $\mathbf{v}+d\mathbf{v}$ at time t. J is the Boltzmann collision operator,

$$J[\mathbf{r},\mathbf{v_1}|f(t)] = r_p^2\int d\mathbf{v_2}\int A\Theta(\hat{\mathbf{k}}\cdot\mathbf{v}_{12})(\hat{\mathbf{k}}\cdot\mathbf{v}_{12})\,d\hat{\mathbf{k}} \tag{2.73}$$

with

$$A = e^{-2}f^{(1)}(\mathbf{r},\mathbf{v_1'},t)f^{(1)}(\mathbf{r},\mathbf{v_2'},t) - f^{(1)}(\mathbf{r},\mathbf{v_1},t)f^{(1)}(\mathbf{r},\mathbf{v_2},t).$$

where $\hat{\mathbf{k}}$ is the unit vector alone the line connecting the center of particle 2 to particle 1, $\mathbf{v}_{12} = \mathbf{v}_1 - \mathbf{v}_2$ is the relative velocity, Θ is the Heaviside step function. The velocities $\mathbf{v}_1'$ and $\mathbf{v}_2'$ are the velocities of particles just before collision, and $\mathbf{v}_1$ and $\mathbf{v}_2$ are post-collisional velocities.

The hydrodynamic quantities such as the number density, average velocity, and granular temperature, can be defined as the moments of the single-particle distribution function:

$$n(\mathbf{r},t) = \int f^{(1)}(\mathbf{r},\mathbf{v},t)d\mathbf{v} \tag{2.74}$$

$$\mathbf{u}(\mathbf{r},t) = \frac{1}{n(\mathbf{r},t)} \int f^{(1)}(\mathbf{r},\mathbf{v},t)\mathbf{v}d\mathbf{v} \tag{2.75}$$

$$T(\mathbf{r},t) = \frac{2}{3n(\mathbf{r},t)k_B} \int f^{(1)}(\mathbf{r},\mathbf{v},t)\frac{1}{2}m(\mathbf{v}-\mathbf{u})^2 d\mathbf{v} \tag{2.76}$$

where k_B is the Boltzmann constant. Kinetic theory gives the connection to the continuum equations for mass, momentum, and kinetic energy, which take the following forms:

$$\frac{\partial n}{\partial t} + \nabla \cdot (n\mathbf{u}) = 0, \tag{2.77}$$

$$\frac{\partial \mathbf{u}}{\partial t} + \mathbf{u} \cdot \nabla \mathbf{u} = \mathbf{f_b} - \frac{1}{mn}\nabla \cdot \mathbf{p}, \tag{2.78}$$

$$\frac{\partial T}{\partial t} + \mathbf{u} \cdot \nabla T = -\frac{2}{3nk_B}(\nabla \cdot \mathbf{q} + \mathbf{p} : \nabla \mathbf{u}) - \gamma. \tag{2.79}$$

Note that $\mathbf{f_b}$ is the body force per unit mass, and $\gamma = -\chi(\frac{1}{2}mv^2)$ is the rate of dissipation per unit volume. In Eqs.(2.78) and (2.79), the pressure tensor $\mathbf{p}$ and heat flux $\mathbf{q}$ are given by

$$\mathbf{p}(\mathbf{r},t) = \int f^{(1)}(\mathbf{r},\mathbf{v},t)m(\mathbf{v}-\mathbf{u})(\mathbf{v}-\mathbf{u})d\mathbf{v}$$

$$\mathbf{q}(\mathbf{r},t) = \int f^{(1)}(\mathbf{r},\mathbf{v},t)\frac{m|\mathbf{v}-\mathbf{u}|^2}{2}(\mathbf{v}-\mathbf{u})d\mathbf{v}$$

Normally the evolution of $f^{(1)}(\mathbf{r},\mathbf{v},t)$ depends on the joint probability distribution, $f^{(2)}(\mathbf{r_1},\mathbf{v_1};\mathbf{r_2},\mathbf{v_2};t)$, which is given in the following expression:

$$f^{(2)}(\mathbf{r_1},\mathbf{v_1};\mathbf{r_2},\mathbf{v_2};t) = g(r_p,\varepsilon_s)f^{(1)}(\mathbf{r_2} - r_p\hat{\mathbf{k}},\mathbf{v_1},t)f^{(1)}(\mathbf{r_2},\mathbf{v_2},t) \tag{2.80}$$

where $g(r_p,\nu)$ is the radial distribution function, ε_s the fraction of solid particles. Instead of the full radial distribution function $g(r_p,\varepsilon_s)$, it is often sufficient to use the value at $r = r_p$, i.e., we define a new function $\chi(\varepsilon_s)$:

$$\chi(\varepsilon_s) = \varepsilon_s\, g(r_p,\varepsilon_s).$$

Note that for very dilute system, $g(r_p,\varepsilon_s)$ should equal 1.

Eqs.(2.77-2.79) can only describe granular flows when the pressure tensor, the heat flux, and the rate of dissipation are expressed in terms of the macroscopic fields ("closures"). For the pressure tensor, it is assumed that

$$\mathbf{p} = p - (\lambda - \frac{2}{3}\mu)\mathrm{Tr}(\mathbf{E})\mathbf{I} - 2\mu\mathbf{E}.$$

where $\mathbf{I}$ is the unit tensor, and Tr denotes trace, whereas the components of $\mathbf{E}$ are given by:

$$E_{ij} = \frac{1}{2}(\frac{\partial v_j}{\partial x_i} + \frac{\partial v_i}{\partial x_j}).$$

For the heat flux $\mathbf{q}$ we assume that Fourier's law is valid,

$$\mathbf{q} = -\kappa \nabla T$$

By using these expressions, the Eqs.(2.77-2.79) becomes a closed set, and can be solved for ρ, $\mathbf{u}$, and T. The parameters which are introduced by closing the expressions are transport coefficients: κ, λ, μ, γ, and p. The main challenge of kinetic theory is to find reliable expressions for these transport coefficients. In the next section we will summarize the most widely used results.

2.4.4 Closure relations

Elastic particles

Elastic particles have been studied intensively in the past century. A classical textbook on this subject was written by Chapman and Cowling in 1939 [5].
Dilute system For sufficient low density, we can use the well-known ideal gas law:

$$p_0 = n k_B T. \tag{2.81}$$

The shear viscosity μ_0 can be obtained by

$$\mu_0 = \frac{5}{64 r_p^2} \sqrt{\frac{k_B m T}{\pi}}. \tag{2.82}$$

The thermal conductivity κ_0 is given by

$$\kappa_0 = \frac{5}{2} c_v \mu_0,$$

where the specific heat at constant volume is defined as

$$c_v = \frac{3 k_B}{2m}.$$

Thus we have

$$\kappa_0 = \frac{75 m k_B}{256 r_p^2} \sqrt{\frac{m k_B T}{\pi}}. \tag{2.83}$$

Dense system For dense system, the transfer of momentum and energy occurs not only via the movement of the particles, but also via the collisions. Enskog first studied the effect of collisions for rigid elastic spheres. Based on the standard Enskog theory (SET), the equation of state is written as [5]

$$p_1 = n k_B T (1 + \chi \, b\rho.) \tag{2.84}$$

with $b\rho = 16 n \pi \, r_p^3/3 = 4\varepsilon_s$. The shear viscosity and the thermal conductivity are given by

$$\mu_1 = \mu_0 \left(\frac{1}{\chi \, b\rho} + \frac{4}{5} + 0.7614 \chi \, b\rho \right) b\rho. \tag{2.85}$$

and

$$\kappa_1 = \kappa_0 \left(\frac{1}{\chi\, b\rho} + \frac{6}{5} + 0.7574\chi\, b\rho \right) b\rho. \tag{2.86}$$

respectively.

The term $\chi\, b\rho$ has been replaced by the excess compressibility y, through which the equations take the following form:

$$p_1 = p_0(1+y), \tag{2.87}$$

$$\mu_1 = 4\mu_0\varepsilon_s(\frac{1}{y} + \frac{4}{5} + 0.7614y), \tag{2.88}$$

and

$$\kappa_1 = 4\kappa_0\varepsilon_s(\frac{1}{y} + \frac{6}{5} + 0.7574y). \tag{2.89}$$

Inelastic particles

For the inelastic particles, there is a general agreement on the form of the particle pressure in the literature, given by Lun et al. [12] as

$$p_3 = nk_BT(1 + 2(1+e)\varepsilon_s\,\chi). \tag{2.90}$$

As can be seen, in the case of $e = 1$ Eq.(2.90) will reduce to (2.84). We rewrite Eq.(2.90) as follows:

$$p_3 = nk_BT(1 + 4\varepsilon_s\,\chi + 2(e-1)\varepsilon_s\,\chi) = p_0(1 + y + 2(e-1)y). \tag{2.91}$$

If we replace $y + 2(e-1)y$ by a new term y_3, we get

$$p_3 = p_0(1+y_3). \tag{2.92}$$

Then the equations for the shear viscosity and thermal conductivity are found to take the same form as those for the elastic particles [60]

$$\mu_3 = 4\mu_0\varepsilon_s(\frac{1}{y_3} + \frac{4}{5} + 0.771y_3),$$

$$\kappa_3 = 4\kappa_0\varepsilon_s(\frac{1}{y_3} + \frac{6}{5} + 0.767y_3),$$

or with slightly different prefactors [64]

$$\mu_3 = 4.064\mu_0\varepsilon_s(\frac{1}{y_3} + \frac{4}{5} + 0.761y_3),$$

$$\kappa_3 = 4.10052\kappa_0\varepsilon_s(\frac{1}{y_3} + \frac{6}{5} + 0.748y_3),$$

References

[1] Jaeger H.M., Nagel S.R. and Behringer R.P., 1996. Granular solids, liquids and gases. *Rev. Mod. Phys.*, **68**: 1259-1273.

[2] Nedderman R.M., 1992. *Statics and kinematics of granular materials*. Cambridge University Press, Cambridge, UK.

[3] Herrmann H.J., and Luding S., 1998. Modeling granular media on the computer. *Contin. Mech. Thermodyn.*, **10**: 189.

[4] Anderson J.D., 1995. *Computational fluid dynamcis: the basic with applications*. McGraw-Hill, New York, USA.

[5] Chapman S., and Cowling T.G., 1970. *The Mathematical theory of theory of non-uniform gases*. Cambridge University Press, Cambridge, UK.

[6] Allen M. P., and Tildesley D.J., 1990. *Computer simulations of liquids*. Oxford Science Publications, Oxford, UK.

[7] Bird G.A., 1976. *Molecular gas dynamics and direct simulation of gas flows*. Oxford University Press, Oxford, UK.

[8] Dufty J.W., 2000. Statistical mechanics, kinetic theory, and hydrodynamics for rapid granular flow. *J. Phys.: Condens. Matter*. **12**: 47.

[9] Walton O.R., 2004. Numerical simulation of inelastic frictional particleparticle interaction. In: M.C. Roco (Eds.), *Particulate Two-Phase Flow*, Butterworth-Heineman, Boston, USA. pp.884, Chpt.25..

[10] Luding S., 1998. Collisions & Contacts between two particles. In: H.J. Herrmann, J.P. Hovi, and S. Luding (Eds.), *Physics of dry granular Media*, Kluwer Academic Publishers, Dordrecht, pp.1-19, Chpt.5.

[11] Jenkins J.T., and Savage S.B, 1983. A theory for the rapid flow of identical, smooth, nearly elastic, spherical particles. *J. Fluid Mech.*, **130**: 187.

[12] Lun C.K.K., Savage S.B., Jeffrey D.J., and Chepurniy N., 1984. Kinetic theories for granular flow: inelastic particles in Couette flow and slightly inelastic particles in a general flowfield. *J. Fluid Mech.*, **140**: 223.

[13] Campbell C.S., 1990. Rapid granular flows. *Ann. Rev. Fluid Mech.*, **22**: 57.

[14] Goldhirsch I., 1999. Scales and kinetics of granular flows. *Chaos*. **9**:659.

[15] Elgobashi S., 1991. Particle-laden turbulent flows: Direct numerical simulation and closure models. *Appl. Sci. Res.*, **48**:301-304.

[16] Geldart D., 1973. Types of gas fluidization. *Powder Technol.* **7**:285.

[17] Ladd A.J.C., 1993. Lattice-Boltzmann simulations of particle fluid suspensions. *J. Fluid Mech.*, **271**: 285.

[18] Ladd A.J.C., and Verberg R., 2001. Lattice-Boltzmann simulations of particle fluid suspensions. *J. Stats. Phys.*, **104**: 1191.

[19] Kuipers J.A.M., van Duin K.J., van Beckum F.P.H., and van Swaaij W.P.M., 1992.

A numerical model of gas-fluidized beds. *Chem. Engng. Sci.*, **47**: 1913.

[20] Alder B.J., and Wainwright T.E., 1957. Phase transition for a hard-sphere system. *J. Chem. Phys.*, **27**: 1208.

[21] Frenkel D., and Smit B., 1996. *Understanding molecular simulation: from algorithms to applications*. Academic Press, San Diego, USA.

[22] Campbell C.S., and Brennen C.E., 1985. Computer simulations of granular shear flows. *J. Fluid. Mech.*, **151**: 167.

[23] Hoomans B.P.B., Kuipers J.A.M., Briels W.J., and van Swaaij W.P.M., 1996. Discrete particle simulation of bubble and slug formation in a two-dimensional gas-fluidized bed: a hard sphere approach. *Chem. Engng. Sci.*, **51**: 99.

[24] Hoomans B.P.B., Kuipers J.A.M., and van Swaaij W.P.M., 2000. Granular dynamics simulation of segregation phenomena in bubbling gas-fluidised beds. *Powder Technol.*, **109**: 41.

[25] Goldschmidt M.J.V., Kuipers J.A.M., and van Swaaij W.P.M., 2001. Hydrodynamic modeling of dense gas-fluidised beds using the kinetic theory of granular flow: effect of coefficient of restitution on bed dynamics. *Chem. Engng. Sci.*, **56**: 571.

[26] Li J., and Kuipers J.A.M., 2002. Effect of pressure on gasCsolid flow behavior in dense gas-fluidized beds: a discrete particle simulation study. *Powder Technol.*, **127**: 173.

[27] Ouyang J., and Li J., 1999. Particle-motion-resolved discrete model for simulating gas-solid fluidization. *Chem. Engng. Sci.*, **54**: 2077.

[28] Helland E., Occelli R., and Tadrist L., 1999. Numerical study of cohesive powders in a dense fluidized bed. *CR Acad. Sci. II B*, **327**: 1397.

[29] Helland E., Occelli R., and Tadrist L., 2000. Numerical study of cluster formation in a gas-particle circulating fluidized bed. *Powder Technol.*, **110**: 210.

[30] Lun C.C.K., 2000. Numerical simulation of dilute turbulent gas-solid flows. *Int. J. Multiphase flow*, **26**: 1707.

[31] Zhou H., Flamant G., Gauthier D., and Lu J., 2004. Numerical simulation of the turbulent gas-particle flow in a fluidized bed by an LES-DPM model. *Chem. Engng. Res. Design*, **82**: 918.

[32] McNamara S., and Young W.R., 1992. Inelastic collapse and clumping in a one-dimensional granular medium. *Phys. Fluids*, **4**: 496.

[33] Cundall P.A., and Strack O.D.L., 1979. A discrete numerical model for granular assemblies. *Gáotechnique*, **29**: 47.

[34] Schfer J., Dippel S. and Wolf D.E., 1996. Force schemes in simulations of granular materials. *J. Phys. I France*, **6**: 5.

[35] Walton O.R., and Braun R.L., 1986. Viscosity and temperature calculations for assemblies of inelastic frictional disks. *J. Rheol.*, **30**: 949.

[36] Langston P.A., Tüzün U., and Heyes D.M., 1994. Continuous potential discrete particle simulations of stress and velocity fields in hoppers transition from fluid to granular flow, *Chem. Engng. Sci.*, **49**: 1259.

[37] Tsuji Y., Kawaguchi T., and Tanaka T., 1993. Discrete particle simulation of two-dimensional fluidized bed. *Powder Technol.*, **77**: 79.

[38] Xu B.H., and Yu A.B., 1997. Numerical simulation of the gas-solid flow in a fluidized bed by combining discrete particle method with computational fluid dynamics. *Chem. Engng. Sci.*, **52**: 2785.

[39] Iwadate M., and Horio, M., 1998. Agglomerating fluidization of wet powders and group c powders: a numerical analysis. In: L.S. Fan, and T. Knowlton Eds., *Fluidization IX*, Engineering Foundation, Durango, USA. p.293.

[40] Kafui K.D., Thornton C., and Adams M.J., 2002. Discrete particle-continuum fluid modelling of gas-solid fluidised beds. *Chem. Engng. Sci.*, **57**: 2395.

[41] Li J., and Mason D.J., 2000 A computational investigation of transient heat transfer in pneumatic transport of granular particles. *Powder Technol.*, **112**: 273.

[42] Zhou H., Flamant G., Gauthier D., and Flitris Y., 2003. Simulation of coal combustion in a bubbling fluidized bed by distinct element method. *Chem. Engng. Res. Design.* **81**: 1144.

[43] Hoomans B.P.B., 2000. *Granular dynamics in gas-solids two-phase flows*. Ph.D. dissertation, University of Twente, Enschede, the Netherlands.

[44] Johnson K.L, 1985. *Contact Mechanics*. Cambridge University Press, Cambridge, UK.

[45] Brendel L, and Dippel S., 1998. Lasting Contacts in MD Simulations. In: H.J. Herrmann, J.P. Hovi, and S. Luding (Eds.), *Physics of dry granular Media*, Kluwer Academic Publishers, Dordrecht, pp.313-318.

[46] Israelachvili J., 1991. *Intermolecular & surface forces*. Academic Press, London, UK.

[47] Bird R.B., Stewart W.E., and Lightfood E.N., 1960. *Transport Phenomana*. John Wiley & Sons., New York, USA.

[48] Ergun S., 1952. Fluid flow through packed columns. *Chem. Engng. Progs.*, **48**: 89.

[49] Wen C.Y., and Yu Y.H., 1966. Mechanics of fluidization. *Chem. Engng. Prog. Symp. Ser.*, **62**: 100.

[50] Hill R.J., Koch D.L., and Ladd J.C., 2001. Moderate-Reynolds-numbers flows in ordered and random arrays of spheres. *J. Fluid. Mech.*, **448**: 315.

[51] Anderson T.B., and Jackson R., 1967. Fluid mechanical description of fluidized beds: Equations of motion. *Ind. Engng. Chem. Fund.*, **6**: 527.

[52] Anderson T.B., and Jackson R., 1968. Fluid mechanical description of fluidized beds: Stability of the state of uniform Fluidization. *Ind. Engng. Chem. Fund.*, **7**:

12.

[53] Anderson T.B., and Jackson R., 1969 Fluid mechanical description of fluidized beds: Comparison of theory and experiment. *Ind. Engng. Chem. Fund.*, **8**: 137.

[54] Ishii M., 1975. *Thermo-fluid dynamic theory of two-phase flow*. Eyrolles, Paris, France.

[55] Anderson K., Sundaresan S., and Jackson R., 1995. Instabilities and the formation of bubbles in fluidized beds. *J. Fluid Mech.*, **303**: 327.

[56] Tsuo Y.P., and Gidaspow D., 1990. Computations of flow patterns in circulating fluidized beds. *AIChE J.*, **36**: 885.

[57] Elghobashi S.E., and Abou-Arab T.W., 1983. A two-equation turbulence model for two-phase flows. *Phys. Fluids*, **26**: 931.

[58] Chen C.P., 1985. *Studies in two-phase turbulence closure modeling*. Ph.D. Thesis, Michigan State University, USA.

[59] Zhou L.X., and Huang X.Q., 1990. Prediction of confined turbulent gas-particle jet by an energy equation model of particle turbulence. *Science in China*, **33**: 428.

[60] Gidaspow D., 1994. *Multiphase flow and fluidization: continuum and kinetic theory descriptions*. Academic Press, New York, USA.

[61] Sinclair J.L., and Jackson R., 1989. Gas-particle flow in a vertical pipe with particle-particle interactions. *AIChE J.*, **35**: 1473.

[62] Ding J., and Gidaspow D., 1990. A bubbling fluidization model using kinetic theory of granular flow. *AIChE J.*, **36**: 523.

[63] Samuelsberg A., and Hjertager B.H., 1996. Computational modeling of gas/particle flow in a riser. *AIChE J.*, **42**: 1536.

[64] Nieuwland J.J., van Sint Annaland M., Kuipers J.A.M., and van Swaaij W.P.M., 1996. Hydrodynamic modeling of gas/particle flows in riser reactors. *AIChE J.*, **42**: 1569.

[65] Detamore M.S., Swanson M.A., Frender K.R., and Hrenya C.M., 2001. A kinetic-theory analysis of the scale-up of circulating fluidized beds. *Powder Technol.*, **116**: 190.

[66] Ferschneider G., and Mege P., 1996. Eulerian simulation of dense phase fluidized bed. *Revue de l' Institut français du pétrole*, **51**: 301.

[67] Bayle J., Mege P., and Gauthier T., 2001. Dispersion of bubble flow properties in a turbulent FCC fluidized bed. In: *Fluidization X*, Kwauk M., Li J., and Yang W.-C., (eds.), Engineering Foundation, New York, USA. p.125.

[68] McKeen T.R., and Pugsley T.S., 2003. Simulation and experimental validation of a freely bubbling bed of FCC catalyst. *Powder Technol.*, **129**: 139.

[69] Kim H., and Arastoopour H., 2002. Extension of kinetic theory to cohesive particle flow. *Powder Technol.*, **122**: 83.

3

A 2D Numerical Study of the Fluidization Behavior of Geldart A Particles Using a Discrete Particle Model

ABSTRACT

This chapter reports on a numerical study of fluidization behavior of Geldart A particles by use of a 2D soft-sphere discrete particle model. Some typical features, including the homogeneous expansion, gross particle circulation in the absence of bubbles, and fast bubbles, can be clearly displayed if the interparticle van der Waals forces are relatively weak. An anisotropy of the velocity fluctuation of particles is found in both the homogeneous fluidization regime and the bubbling regime. The homogeneous fluidization is shown to represent a transition phase resulting from the competition of three kinds of basic interactions: the fluid-particle interaction, the particle-particle collisions (and particle-wall collisions) and the interparticle van der Waals forces. In the bubbling regime, however, the effect of the interparticle van der Waals forces vanishes and the fluid-particle interaction becomes the dominant factor determining the fluidization behavior of Geldart A particles. This is also evidenced by the comparisons of the particulate pressure with other theoretical and experimental results.

Based on: M. Ye, M. A. van der Hoef, and J.A. M. Kuipers, 2004. A numerical study of fluidization behavior of Geldart A particles using a discrete particle model, *Powder Technology*, 139(2):129-139.

M. Ye, M. A. van der Hoef, and J.A. M. Kuipers, 2004. Discrete particle simulation of the homogeneous Fluidization of Geldart A particles. in *Proc. Fluidization XI*, May 9-14, Ischia, Italy.

3.1 Introduction

It is well known that the fluidization behavior of Geldart A particles in gas-fluidized beds is quite different from that of Geldart B particles [1]. Geldart B particles will bubble immediately when the superficial gas velocity U_0 exceeds the minimum fluidization velocity U_{mf} whereas Geldart A particles display an interval of non-bubbling expansion (homogeneous fluidization) between U_{mf} and the minimum bubbling velocity, U_{mb}. Despite many detailed phenomenological investigations [1–4], the mechanism behind the homogeneous fluidization, however, has not yet been fully understood.

From the purely theoretical viewpoint, the homogeneous fluidization is closely related to the stability of continuum field conservation equations that govern the solid-gas two-phase flow inside a fluidized bed [5]. Jackson and his co-workers [6,7] were among the pioneers who tried to analyze this stability. They found that in addition to the inertia and drag force, a new term similar to the gas pressure is required to describe the motion of the particulate phase, otherwise the bed would be always unstable [7]. This new term, which was found to be a function of the porosity [8], has been considered as the particulate pressure. Unlike the pressure of a liquid or a gas, the particulate pressure is somewhat artificial since it has no clear physical meaning. However, the importance of the particulate pressure has been widely recognized and has prompted an ongoing discussion about its physical origin.

Foscolo and Gibilaro [9], in the spirit of Verloop and Heertjes [10], suggested that a shock wave due to the change of porosity (i.e. when porosity wave rises faster than the velocity of the so-called equilibrium disturbance) is the dominant factor that causes the instability of the homogeneous fluidization regime. They related the origin of the particulate pressure to the propagation of some kind of elasticity wave and defined an elasticity modulus to account for the stability of the bed. Although Foscolo and Gibilaro were able to predict the minimum bubbling points in many cases, not all phenomenona associated with the homogeneous fluidization in a gas fluidized-bed [11] can be explained. On the other hand, Rietema and his co-workers [4, 12] proposed that the interparticle forces should be responsible for the homogeneous fluidization behavior of small particles, rejecting Foscolo and Gibilaro's purely hydrodynamic analysis. Rietema and his co-workers [4,12] argued that the concept of effective elastic modulus could be related to some kind of mechanical structure induced by the interparticle van der Waals forces. Although the viewpoint of Rietema and his co-workers [4, 12] has a clear physical basis, it proves difficult to find a quantitative relation between the interparticle van der Waals forces and the macroscopic physical quantities of the bed. The reasons are twofold: Firstly, up to date there is no technique that can measure the detailed microscopic structure inside a gas-fluidized bed; Secondly, the interparticle van der Waals forces are short-range forces and strongly depend on the shape and surface properties of particles.

In this chapter, a 2D soft-sphere discrete particle model (DPM) has been used to simulate the fluidization behavior of Geldart A particles. One of the features of such

models is that realistic particle-particle (and particle-wall) interactions, such as the interparticle van der Waals forces and particle-particle collisions, can be readily incorporated. Since this kind of models have been proved very useful to study the complicated gas-solid flows in a gas-fluidized bed [13–15] so far, it allows for investigating the physical mechanism of the homogeneous fluidization. The drawback of such a detailed description, however, is the small size of the beds employed in the simulations. In this respect, the model should be regarded as a "learning" model.

3.2 Model description

The gas flow is modeled by the volume-averaged Navier-Stokes equations [18]

$$\frac{\partial(\varepsilon\rho_g)}{\partial t} + (\nabla \cdot \varepsilon\rho_g \mathbf{u}) = 0 \tag{3.1}$$

$$\frac{\partial(\varepsilon\rho_g \mathbf{u})}{\partial t} + (\nabla \cdot \varepsilon\rho_g \mathbf{u}\mathbf{u}) = -\varepsilon\nabla p - \mathbf{S}_p - \nabla \cdot (\varepsilon\overline{\tau}) + \varepsilon\rho_g \mathbf{g} \tag{3.2}$$

where ε is the porosity, and ρ_g, $\mathbf{u}$, $\overline{\tau}$ and p are the density, velocity, viscous stress tensor, and pressure of the gas phase respectively. The source term $\mathbf{S}_p$ is defined as

$$\mathbf{S}_p = \frac{1}{V}\int \sum_{a=0}^{Npart} \frac{\beta V_a}{1-\varepsilon}(\mathbf{u}-\mathbf{v}_a)\delta(\mathbf{r}-\mathbf{r}_a)dV.$$

Note that V is the volume of the fluid cell, V_a the volume of particle, $\mathbf{v}_a$ the particle velocity, and N_{part} the number of particles. The δ-function ensures that the drag force acts as a point force in the (central) position of a particle. To calculate the interphase momentum exchange coefficient β, we employed the well-known Ergun equation [19] for porosities lower than 0.8 and Wen and Yu correlation [20] for porosities higher than 0.8.

The gas phase equations are solved numerically with a finite differencing technique, in which a staggered grid was employed to ensure numerical stability. The porosity is calculated according to the method of Hoomans et al. [14],

$$\varepsilon = 1 - \frac{2}{\sqrt{\pi\sqrt{3}}}(1-\varepsilon_{2D})^{3/2} \tag{3.3}$$

where ε_{2D} is the local 2D void fraction calculated from the area occupied by particles. The equations of motion of an arbitrary particle, a, follow from Newton's second law

$$m_a \frac{d^2\mathbf{r}_a}{dt^2} = \mathbf{F}_{cont,a} + \mathbf{F}_{vdw,a} + \frac{V_a\beta}{1-\varepsilon}(\mathbf{u}-\mathbf{v}_a) - V_a\nabla p + m_a\mathbf{g} \tag{3.4}$$

$$I_a\Omega_a = I_a\frac{d\omega_a}{dt} = \mathbf{T}_a \tag{3.5}$$

where m_a is the mass of the particle, $\mathbf{F}_{cont,a}$ the contact force, $\mathbf{F}_{vdw,a}$ the van der Waals force, $\mathbf{T}_a$ the torque, I_a the moment of inertia, Ω_a the rotational acceleration, and ω_a the rotational velocity. Eq.(3.1) and Eq.(3.2) are solved numerically using a first-order time-integration scheme,

$$\begin{aligned} \mathbf{r}_a &= \mathbf{r}_a^{(0)} + \mathbf{v}_a \triangle t \\ \mathbf{v}_a &= \mathbf{v}_a^{(0)} + \mathbf{a}_a \triangle t \\ \omega_a &= \omega_a^{(0)} + \Omega_a \triangle t \end{aligned} \tag{3.6}$$

The contact force between two particles (or a particle and a sidewall) is calculated by use of the soft-sphere model developed by Cundall and Strack [21]. In that model, a linear-spring and a dashpot are used to formulate the normal contact force, while a linear-spring, a dashpot and a slider are used to compute the tangential contact force, where the tangential spring stiffness is two seventh of the normal spring stiffness [22]. Also we employed two different restitution coefficients. Thus a total of five parameters are required in order to describe the contact force in our model: the normal and the tangential spring stiffness, the normal and the tangential restitution coefficient, and the friction coefficient.

To calculate the interparticle van der Waals forces, we adopt the Hamaker scheme [23, 24]:

$$F_{vdw,ab}(S) = \frac{A}{3} \cdot \frac{2r_1 r_2 (S + r_1 + r_2)}{[S(S + 2r_1 + 2r_2)]^2} \left[\frac{S(S + 2r_1 + 2r_2)}{(S + r_1 + r_2)^2 - (r_1 - r_2)^2} - 1 \right]^2 \tag{3.7}$$

where S is the intersurface distance between two spheres, A the Hamaker constant, and r_1 and r_2 the radii of the two spheres respectively. However, Eq.(3.7) exhibits an apparent numerical singularity that the van der Waals interaction diverges if the distance between two particles approaches zero. In reality such a situation will never occur, because of the short-range repulsion between particles. In the present model, we have not included such a repulsion, however, we can avoid the numerical singularity by defining a cut-off (maximal) value of the van der Waals force between two spheres. In practice it is more convenient to use the equivalent cut-off value for the intersurface distance, S_0, instead of the interparticle force.

3.3 Numerical simulation

3.3.1 Input parameters

We consider a system consisting of monodisperse spheres with a diameter of 100 μm and a density of 900 kg/m^3, which are typically group A particles according to Geldart's classification [1]. The input parameters used in the simulations are shown in Table 1. The cut-off value of the intersurface distance between two spheres, S_0, should be less than the intermolecular center-to-center distance [24]. Here a commonly used value S_0= 0.4 nm is employed [25, 26]. Air is taken as the continuous phase.

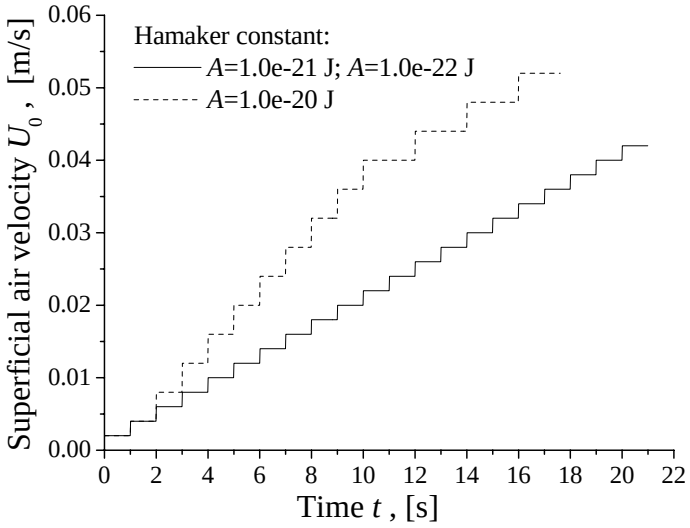

Figure 3.1: *The inlet conditions for the superficial gas velocity of the simulations. Three different Hamaker constants have been used.*

3.3.2 Procedure and initial condition

In principle, the Hamaker constant A can be related to the material properties such as the polarizability. In this research, however, the primary goal is to investigate the *effect* of the interparticle van der Waals forces on the homogeneous fluidization. To this end, three simulations have been conducted using three different levels of van der Waals forces, where the Hamaker constants A equals 10^{-20}, 10^{-21} and 10^{-22} J respectively. In each simulation, we follow the approach adopted by Rhodes et al. [27], in which the superficial gas velocity is increased from below the minimum fluidization velocity U_{mf} to above the minimum bubbling velocity U_{mb} step by step. If the interparticle van der Waals forces are relatively weak (A = 10^{-21} and 10^{-22} J), the simulation typically runs for 1 second in real time, for each velocity. In case of strong van der Waals force (A= 10^{-20} J), the simulation time for each velocity will be adjusted to ensure that the particles and fluid have enough time to interact with each other. Figure 3.1 shows the superficial gas velocities and the corresponding physical time.

A packed bed, typically used as the initial state, has been generated as follows: Firstly, the particles were placed at the sites of a SC lattice, and the superficial gas velocity was set to a relatively large value (0.04 m/s); When the bed bubbles, the superficial gas velocity is set to zero, which causes the particles to drop. The initial state then has been defined as the state where the pressure drop across the bed tends to zero and the bed height becomes stable. The average porosity of this initial state is 0.37.

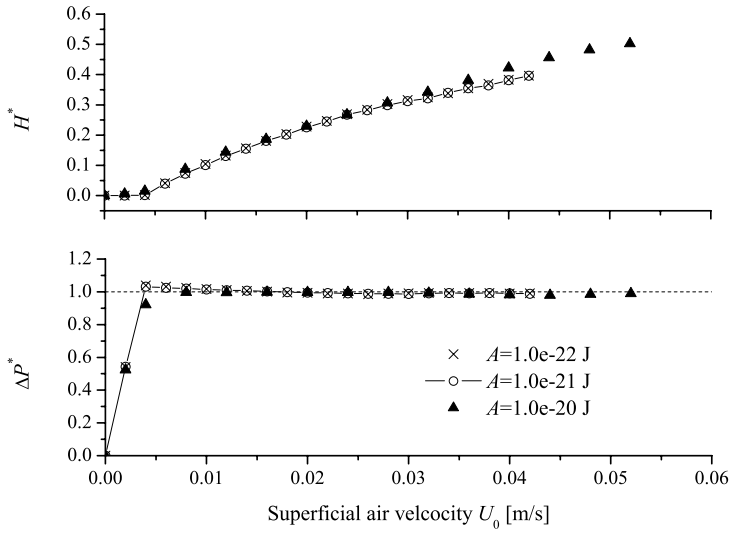

Figure 3.2: *The dimensionless bed height and pressure drop of the fluidized bed.*

3.4 Results and discussion

3.4.1 Macroscopic phenomena: observed from the simulations

Bed height and pressure drop

The bed height and pressure drop are two important parameters in the investigation of the homogeneous fluidization behavior. In this research, the bed height has been defined in the following way: First, the fluidized bed is divided into a number of narrow subregions along the x (i.e. width) direction. The width of each subregion is limited to two times the diameter of a single particle. Then the y coordinate (i.e. height) of the highest particle in each subregion is identified, which defines the height of this subregion. The average height of all subregions has been taken as the bed height.

The relative bed height H^* and pressure drop p^*, as a function of superficial gas velocity, are shown in Figure 3.2, where H^* and p^* are defined as

$$H^* = \frac{H - H_0}{H_0} \tag{3.8}$$

$$\triangle p^* = \frac{\triangle p}{\rho_p g\, H_0(1-\varepsilon_0)} \tag{3.9}$$

where H_0 and ε_0 are, respectively, the height and porosity of the initial packed bed.

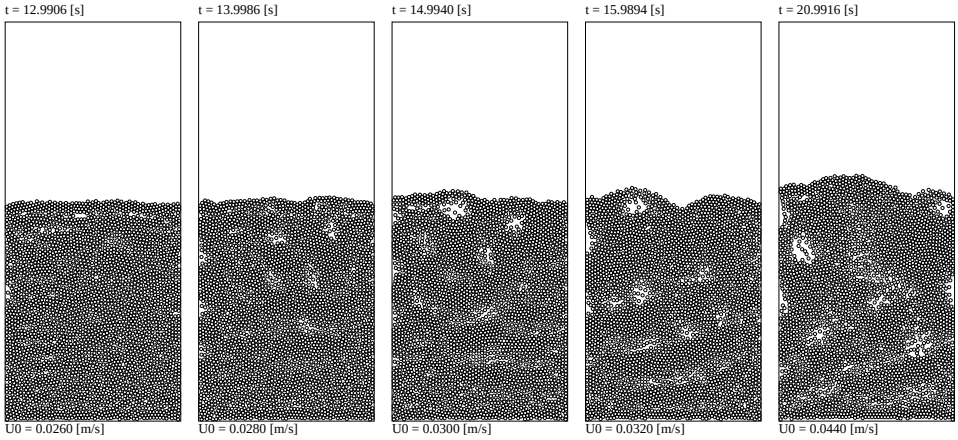

Figure 3.3: *Snapshots of simulation results for Hamaker constant $A = 10^{-22}$ J.*

Minimum fluidization velocity and minimum bubbling velocity

From Figure 3.2, it is clear that for all three levels of van der Waals forces the minimum fluidization velocity is nearly identical (U_{mf} = 0.004 m/s), which indicates that the effect of the van der Waals forces on the minimum fluidization point is small. This value, however, is over-predicted compared to the value calculated from the approximate relation of Wen and Yu (= 0.003 m/s) [29] with a porosity ε_{mf} =0.37.

It seems quite difficult to determine the minimum bubbling points solely from the data plotted in Figure 3.2. It has been found by previous researchers that there could be a decrease of the bed height near the minimum bubbling point [31]. The mechanism underlying this collapse is not well known. However, no such collapse has been observed in our simulations. This may be due to the relatively large particle size (d_p=100 μm) used in our simulations. In a recent paper of Menon and Durian [32], a collapse for particles with a diameter of 49 μm was observed, but not for particles with a diameter of 96 μm.

The minimum bubbling points, on the other hand, can be determined from the observation of the macroscopic motion of particles. Snapshots from the three simulations are shown in Figures 3.3 to 3.5. From Figure 3.3 it is obvious that the minimum bubbling velocity U_{mb} is about 0.028 m/s when the Hamaker constant $A = 10^{-22}$ J. In the case of $A = 10^{-21}$ J the first obvious bubble (see Figure 3.4) appears at U_{mb} = 0.030 m/s, which is somewhat higher than that for $A = 10^{-22}$ J. If the Hamaker constant becomes larger (i.e. $A = 10^{-20}$ J), however, no obvious bubble appears even for a superficial gas velocity U_0 as high as 0.052 m/s (see Figure 3.5). Instead a chainlike network can be found. A closer examination of the simulation results revealed that channels existed near the two sidewalls at U_0 = 0.04 m/s. It seems that the gas flows bypasses the bed by forming channels, which is a well-known behavior of Geldart C particles [1].

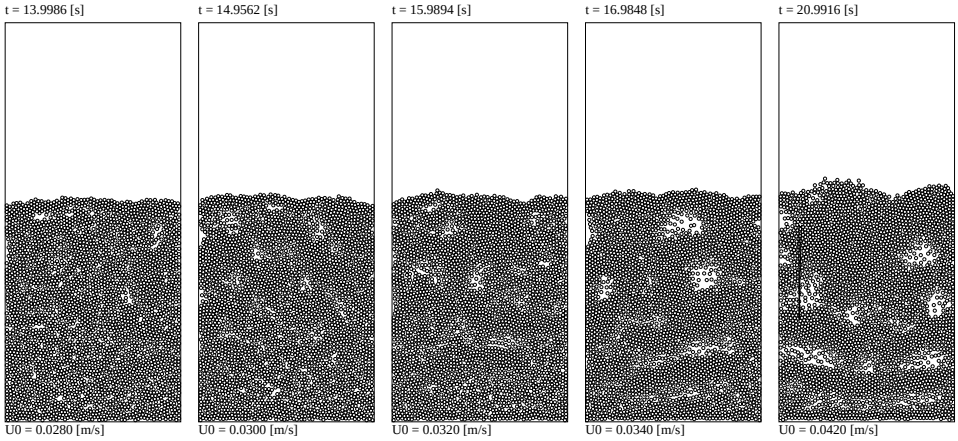

Figure 3.4: *Snapshots of simulation results for Hamaker constant* $A = 10^{-21}$ *J.*

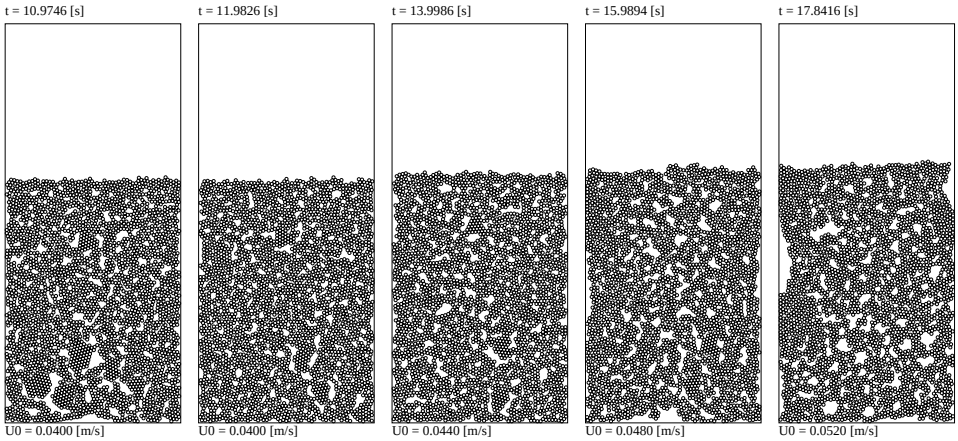

Figure 3.5: *Snapshots of simulation results for Hamaker constant* $A = 10^{-20}$ *J.*

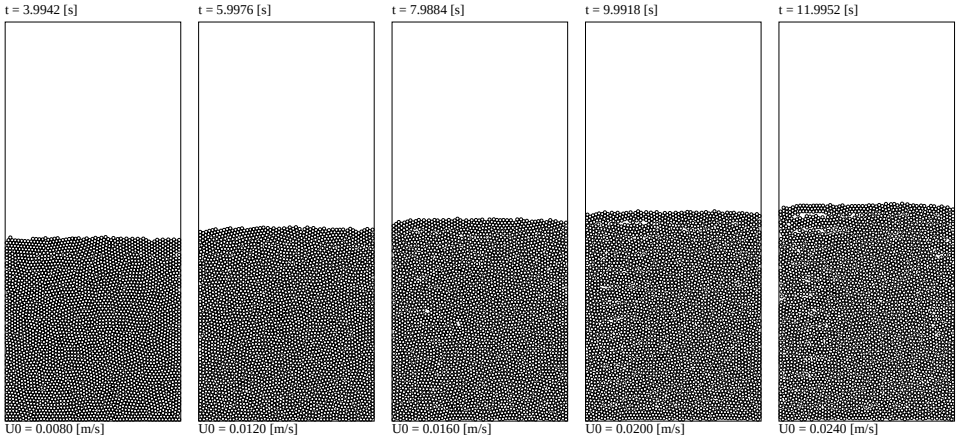

Figure 3.6: *The homogeneous expansion of Geldart A particles in a gas-fluidized bed. The Hamaker constant $A = 10^{-22}$ J.*

For the particles studied in this research, the minimum bubbling velocity estimated from the empirical correlations [29] is around 0.01 m/s, which is lower than the simulation results. In a DPM simulation for the similar type of particles Xu et al. [30] also obtained a value of $U_{mb} = 0.028$ m/s, which is very close to a specified experimental work by Donsi and Massimilla [33]. It is worthy mentioning that, although Xu et al. employed a larger A (2.1×10^{-21} J) for the homogeneous fluidization, the granular Bond number Bo (the ratio of the interparticle van der Waals force to the single particle weight) is in the same range compared to what we used [34].

Homogeneous expansion

In the case of relatively weak interparticle van der Waals forces ($A = 10^{-22}$ and 10^{-21} J), the homogeneous expansion of the bed can be observed, as shown in Figures 3.6 and 3.7. It has been found by previous researchers that for Geldart A particles the gross circulation of particles would prevail in the absence of obvious bubbles [1]. In Figure 3.8(a) and (b) we show the typical velocity fields of particles, corresponding to the central snapshots of Figures 3.6 and 3.7 respectively. It can be seen from Figure 3.8 that the particles near the bottom move upward from the middle zone while particles near the top of the bed move downward along two sidewalls. Such a circulation of particles eventually causes the system to become well mixed. Obviously the gas fed through the distributor and the friction between the particles and sidewalls are the main causes of such a macroscopic circulation. Besides this gross circulation, local small circulations can also be observed.

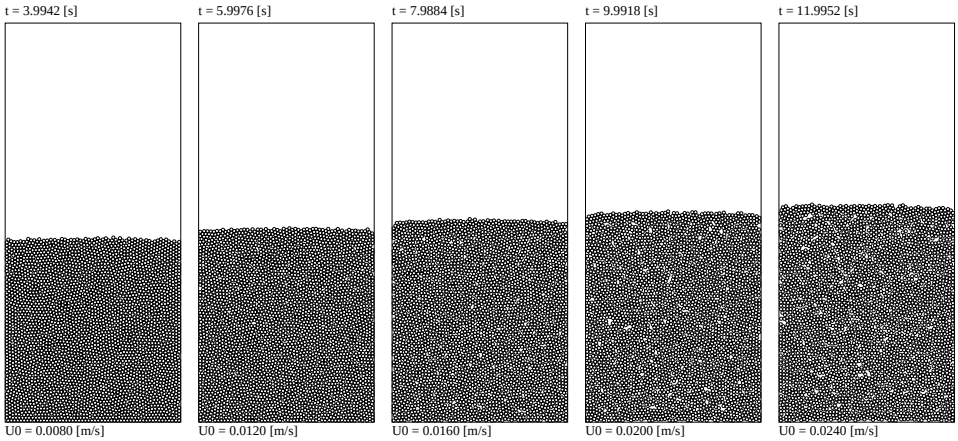

Figure 3.7: *The homogeneous expansion of Geldart A particles in a gas-fluidized bed. The Hamaker constant $A = 10^{-21}$ J.*

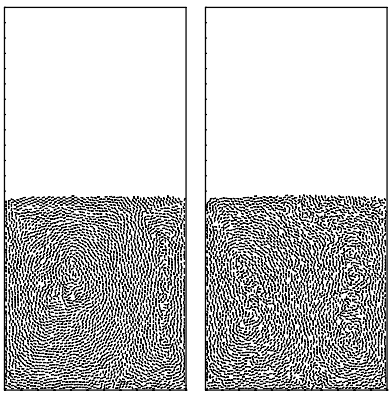

Figure 3.8: *The profile of particle velocity vector during the homogeneous expansion. (a) A=10^{-22} J. The snapshot shown in the center graph of Figure 3.6. (b) $A = 10^{-21}$ J. The snapshot shown in the center graph of Figure 3.7.*

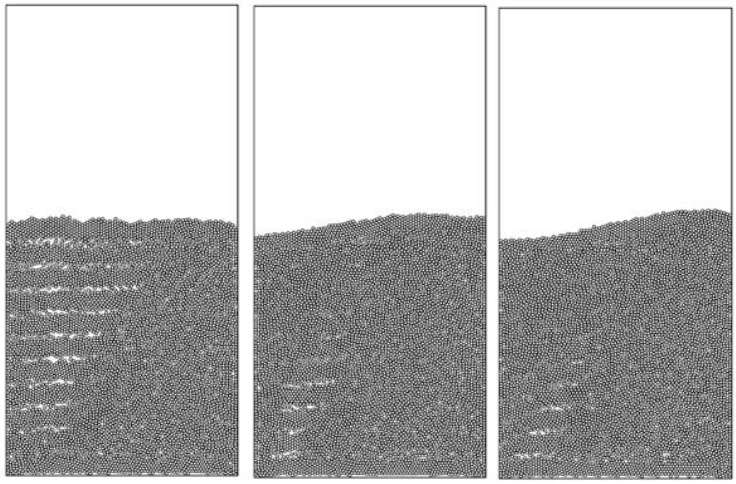

Figure 3.9: *: Snapshots obtained from simulations with different contact parameters. The number of particles is 6000 with a diameter of 60 μm and a density of 1129 kg/m^3. The normal and tangential spring stiffness are 7 N/m and 2 N/m respectively. The contact parameters in the pictures from left to right are: left: $e_n = e_t = 0.9$, $\mu_f = 0.3$; middle: $e_n = e_t = 0.6$, $\mu_f = 0.0$; right: $e_n = e_t = 0.9, \mu_f = 0.0$. The Hamaker constant is $A = 1.0 \times 10^{-20} J$.*

Void structures during homogeneous fluidization

Since in the homogeneous fluidization regime particle-particle contacts (or particle-particle collisions) occur frequently, a good understanding of their effect on the homogeneous fluidization is essential. The particle-particle contact is typically a dissipative process in which the kinetic energy of particles will be lost. In the soft-sphere model, two parameters will control the energy dissipation: the restitution coefficient and the friction coefficient. Simulations have been carried out for different restitution coefficients and friction coefficients (see Figure 3.9 for some typical snapshots). All the simulations have been performed under similar conditions, except for the values of the restitution and friction coefficients. It can be seen that in the absence of friction the cavities and channels are only found near the bottom of the bed, and furthermore wave-like surface is observed. If a non-zero friction coefficient is employed, we find the phenomena similar to those observed by Massimilla et al. [28]: channels are formed near the bottom of the bed which rise, grow and eventually disappear at the surface of the bed. Note that the surface of the bed is more flat in the presence of friction.

It may be deduced from the simulation results that the friction coefficient is the dominant parameters that affects the formation of channels and not the restitution coefficients. From granular physics, it is well-known that the kinetic energy dissipation between particle-particle contacts (collisions) will lead to the formation of clusters, and hence void structures such as cavities. This dissipation can be caused by two types of interactions: the inelastic collision between particles, which is con-

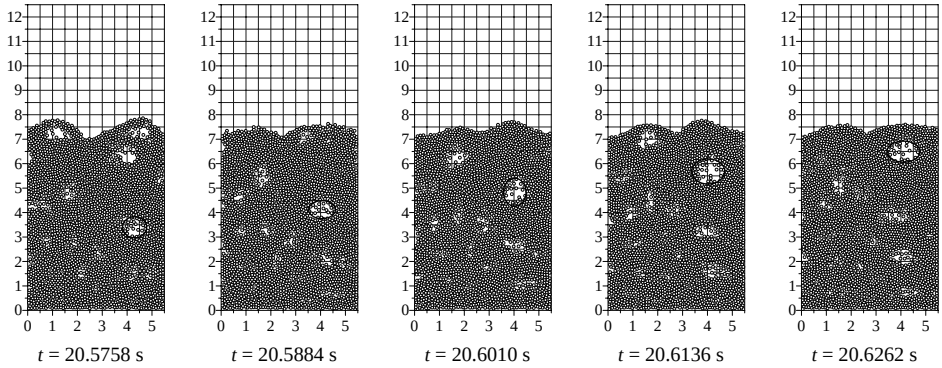

Figure 3.10: *The rise of a bubble inside the fluidized bed for a superficial gas velocity U_0=0.040 m/s. The Hamaker constant A=10^{-21} J.*

trolled by the restitution coefficient, and friction, which can be taken into account via the friction coefficient. From the viewpoint of energy balance, the homogeneous fluidization regime can be considered as a quasi-equilibrium state. Due to the absence of bubbles that carry the excess gas, the energy balance can be written as

$$E_i = E_o + E_d + E_p \tag{3.10}$$

where E_i is the kinetic energy provided by the inlet gas flow, E_o the kinetic energy carried out by the outlet gas flow, E_d the energy dissipated from particle-particle contacts, and E_p the potential energy necessary for maintaining the bed height. Interestingly, it is found from the simulation results that the average bed height will not change by modifying the contact parameters, as long as the inlet gas velocity is kept constant. Therefore the energy balance will be greatly affected by the dissipation of kinetic energy of particles due to particle-particle collisions. The presence of friction, on the other hand, may enhance the energy dissipation caused by particle-particle collisions. The wave-like surface of the bed in the absence of friction may relate to the energy distribution. We argue that in the absence of friction, the restitution coefficients in our simulations are not sufficient to keep the energy balance between E_i and E_d , and the gas motion may manifest in other complex forms. This suggests that the contact parameters, especially the frictional coefficients, will influence the energy distribution and hence the bed dynamics.

Fast bubbles

In Figure 3.10 the rise of a typical bubble has been visualized. The rise velocity of this bubble can be estimated from a detailed analysis of the snapshots, and amounts 0.055 m/s, which is much higher than the interstitial velocity of gas around this bubble ($0.001 \sim 0.02$ m/s). It is therefore a fast bubble that can only be found in the fluidization of fine particles [29]. In Figure 3.11 the velocity field of the

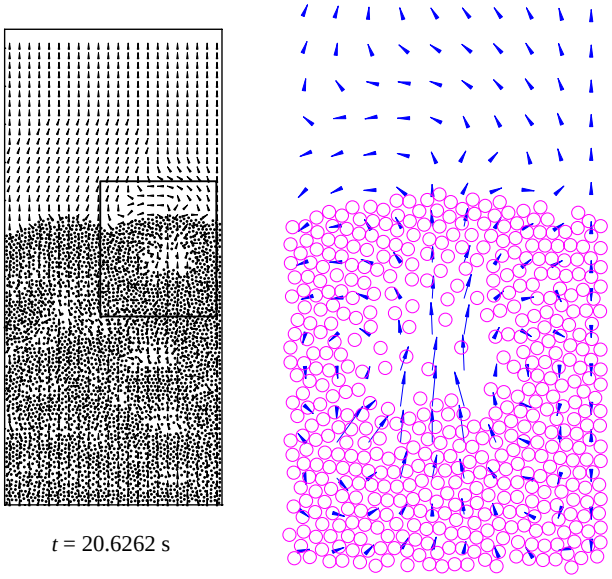

Figure 3.11: *The gas flow around a single bubble. Left: The instantaneous velocity field of gas phase of the bed. Right: The instantaneous velocity flied of gas flow around a single bubble. The figure corresponds to the snapshot shown in the far right graph of Figure 3.10.*

gas phase around the bubble has been plotted. The circulation of gas around the bubble is clearly demonstrated, which is believed to be one of the most important features of a fast bubbles [29].

3.4.2 The forces structure during homogeneous fluidization

Here we will present a more detailed analysis of the magnitude of the various forces in the homogeneous fluidization regime. From Eq.(3.1), we have the following total force (F_t), acting on a single particle

$$F_t = F_{conta,c} + F_{cont,f} + F_{vdw} + F_{drag} + F_g \tag{3.11}$$

with $F_{cont,c}$ the elastic force due to particle-particle contact, $F_{cont,f}$ the friction force due to particle-particle contact, F_{vdw} the van der Waals force, F_{drag} the drag force, and F_g the gravitational force. Simulations have been carried out both with and without interparticle van der Waals forces. In a recent paper [30] it was shown that in the homogeneous fluidization regime the contact forces acting on the particle are balanced by the interparticle van der Waals forces. In Figure 3.12 we show the forces acting on each particle. In the presence of van der Waals forces it can be seen that the sum of normal contact force and interparticle van der Waals force is not strictly zero for most particles, but rather fluctuates around zero. If we turn

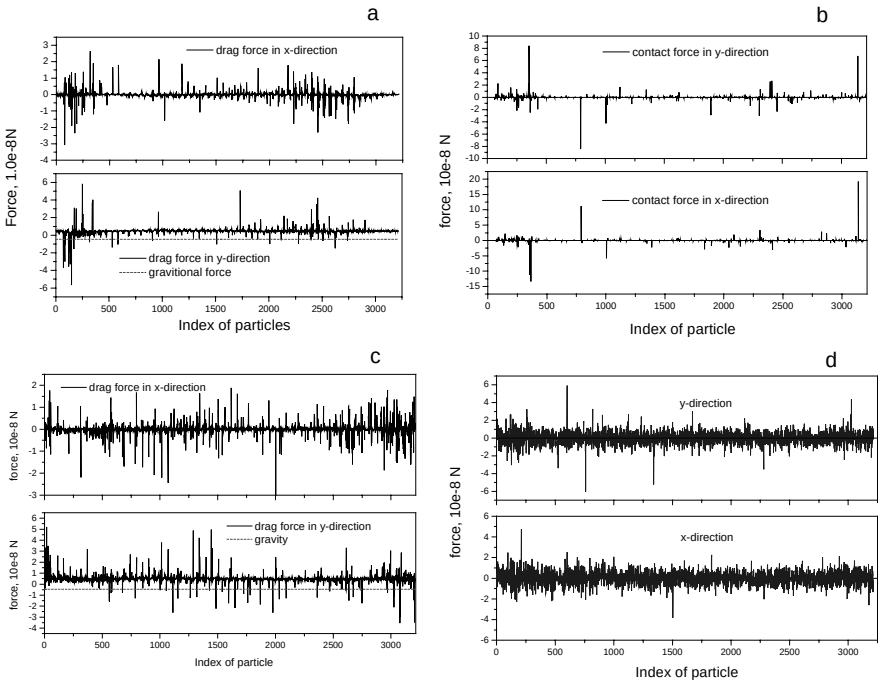

Figure 3.12: *: Instantaneous forces acting on the particles during homogeneous fluidization, taken at some random moment for different values of the Hamaker constant A. The number of particles is 3214 with a diameter of 100 μm and a density of 900 kg/m^3. The normal and tangential spring stiffness are 7 N/m and 2 N/m, respectively. The contact parameters are: $e_n = e_t = 0.9$, $\mu_f = 0.2$. (a) Drag force and gravitational force for $A = 0$; (b) Normal contact force for $A = 0$; (c) Drag force and gravitational force for $A = 1.0 \times 10^{-20} J$; (d) The sum of van der Waals force and normal contact force for $A = 1.0 \times 10^{-20} J$.*

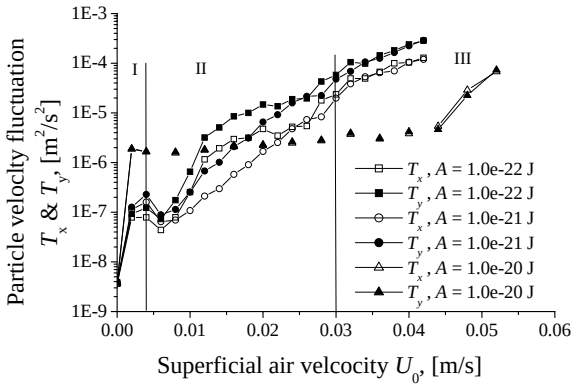

Figure 3.13: *The time-averaged velocity fluctuation of particles in both the x and y direction.*

off the interparticle van der Waals force the normal contact force becomes extremely small (for most of particles it vanishes). Meanwhile, in both situations the x-components of the drag forces acting on the particles also fluctuate around zero while the y-components fluctuate around $-F_g$. The frictional forces between particles, however, are not balanced by any kinds of force. Since the frictional forces are essentially working along the tangential direction, they may contribute much more to the rotational motion rather than the translational motion. Clearly, an exact balance of the forces seems to exist only at the macroscopic-level, but not at the level of individual particles, which confirms that the homogeneous fluidization regime is actually a quasi-equilibrium state. The drag forces and van der Waals forces are two important sources of the local force fluctuations, which consequently form the sources of velocity fluctuation of particles.

3.4.3 Analysis of the velocity fluctuation

An important property of the system with regard to the understanding of the fluidization behavior is the granular temperature, which is defined as the mean squared velocity fluctuation of particles. Since the velocity fluctuation is not always isotropic [37], it is essential to separately consider the mean square fluctuation of the x (defined perpendicular to the sidewalls) and y (parallel to the sidewalls) component of particle velocities. The velocity fluctuation is given by

$$T_x = \langle v_x^2 - \langle v_x \rangle^2 \rangle, \quad T_y = \langle v_y^2 - \langle v_y \rangle^2 \rangle \tag{3.12}$$

where v_x and v_y are x and y component of the instantaneous particle velocity respectively. The brackets, $\langle \cdot \rangle$, denote an ensemble average. The granular temperature in the 2D fluidized beds is defined as

$$T = (2T_x + T_y)/3 \tag{3.13}$$

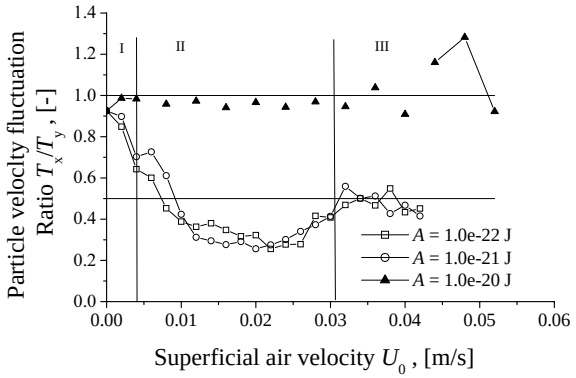

Figure 3.14: *The ratio of the time-averaged velocity fluctuation of particles between the x and y direction.*

in accordance with Koch and Sangani [37].

In this research, the following method has been used to determine T_x and T_y from the simulation data: Firstly, for each cell (CFD grid) the local velocity fluctuation of particles is calculated by use of Eq.(3.12); From this, the total velocity fluctuation of the particles inside the bed is calculated as the volume fraction weighted time-average [38]

$$T_{k,av} = \frac{1}{\triangle t}\int_t^{t+\triangle t}(\sum T_k\varepsilon_i/\sum\varepsilon_i)dt \qquad (k=x,y) \tag{3.14}$$

Weak interparticle van der Waals force

In Figure 3.13, we show the velocity fluctuation of particles inside the bed. If the interparticle van der Waals forces are relatively weak, i.e. $A = 10^{-22}$ and 10^{-21} J, we note that there exist three distinct regimes: (1) Regime I ($U_0 = 0.00 \sim 0.004$ m/s), where the particle velocity fluctuation is nearly isotropic, i.e. $T_x/T_y \simeq 1$ as shown in Figure 3.14. Moreover, the variations of both T_x and T_y are negligible and the velocity fluctuation can be approximately considered as a constant $T = 3.5\times10^{-8}$ m^2/s^2. (2) Regime II ($U_0 = 0.006 \sim 0.03$ m/s), in which the velocity fluctuation of particles increases as the superficial gas velocity increases. However, a rather large anisotropy with respect to the x and y direction is found. As shown in Figure 3.14, for both levels of van der Waals forces the ratio T_x/T_y decreases from $0.6 \sim 0.7$ to $0.3 \sim 0.4$ and then increases to about 0.5, with a minimum value 0.3 at about U_0= 0.022 m/s. However, the velocity fluctuation in both x and y direction are obviously different for $A = 10^{-22}$ and 10^{-21} J, which implies that the van der Waals force could affect the velocity fluctuation in this regime. (3) Regime III ($U_0 \geq 0.03$ m/s). In this regime, the velocity fluctuation still increases with superficial gas velocity U_0, however the ratio T_x/T_y in this regime is nearly constant, i.e. $T_x/T_y \simeq 0.5$. Moreover, the velocity fluctuation in both directions are nearly equal for $A = 10^{-22}$

and $A = 10^{-21}$ J. This can be understood from the fact the van der Waals force is a short range interaction: the porosity is higher in this regime, and as a result the mean interparticle distance increases and the effect of van der Waals force becomes extremely weak.

It should be mentioned that the occurrence of three regimes as observed from the variation of the velocity fluctuation, i.e. Figures 3.13 and 3.14, agrees well with the analysis based on the macroscopic motion of particles. In principle, there are three kinds of basic interactions in fluidized beds that can cause velocity fluctuations of the particles. The first one is the fluid-particle interaction, which is believed to be the dominant factor causing a strong fluctuation of particle velocity in y direction. The other two are the particle-particle collisions (and particle-wall collisions) and the interparticle van der Waals forces. These two kinds of interactions, which have no directional preference, should contribute equally to the fluctuation of particle velocity in both x and y direction. Regime I is actually the fixed bed regime. In this regime, the superficial gas velocity is relatively low and the fluid-particle interaction is not important compared to the particle-particle interactions (including the particle-particle collisions and the interparticle van der waals forces). As a result, the bed of particles act like a solid, with no obvious anisotropy of the velocity fluctuation. Regime II corresponds to the homogeneous fluidization regime. In this regime the fluid-particle interaction starts to play an important role, however the particle-particle interaction is still relatively strong. Therefore, this represents a transient phase where all three kinds of interactions, i.e. the fluid-particle interaction, the particle-particle collisions (and particle-wall collisions), and the interparticle van der Waals forces, are the prime sources of the velocity fluctuation of the particles in this regime. Regime III is the bubbling regime. In this regime, the fluid-particle interaction becomes dominant over the particle-particle collisions while the effect of the interparticle van der Waals forces is significantly reduced. On the other hand, the constant ratio T_x/T_y = 0.5 probably indicates there exists a dynamic equilibrium between the fluid-particle interaction and the particle-particle collisions (and particle-wall collisions) as far as the contribution to the velocity fluctuation of particles is concerned.

Strong interparticle van der Waals force

When the interparticle van der Waals force is strong ($A = 10^{-20}$ J), quite different fluidization behavior is observed. As shown in Figure 3.5, we find a chainlike network which dominates the fluidization behavior. The bed of particles behave like a solid during a relatively long interval of $U_0 = 0.0 \sim 0.044 m/s$. Obviously the interparticle van der Waals forces are the dominate sources of the velocity fluctuation of particles. In this case, as shown in Figures 3.13 and 3.14, the ratio T_x/T_y is nearly 1.0, which reflects the isotropy of the velocity fluctuation of particles. But if the superficial gas velocity becomes sufficient high ($U_0 \geq 0.04$ m/s), a fluid-like behavior can also be found. As mentioned above, however, no obvious bubble arises. Also no breakdown of the chainlike network has been observed. This means that in the case of the strong interparticle van der waals forces the Geldart A particles can

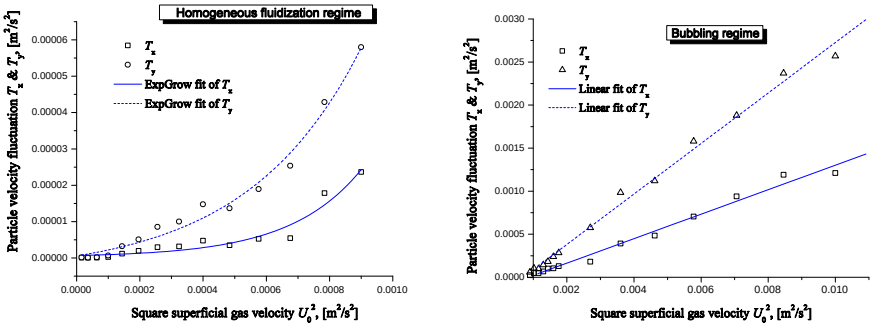

Figure 3.15: *: The dependence of the velocity fluctuation of particles on the square superficial gas velocity. Simulations are carried out under the same conditions as indicated in Figure 3.12 except that the contact parameters are:* $e_n = e_t = 0.9$, $\mu_f = 0.2$ *and the Hamaker constant* $A = 1.0 \times 10^{-20} J$.

display the fluidization behavior of Geldart C particles.

Effect on the gas flows

Direct measurement of the velocity fluctuation of particles (i.e. granular temperature) in a gas-fluidized bed has proved difficult, and only very recently some experimental results have become available. Cody et al. (1) measured the granular temperature in a gas-fluidized bed by use of a Acoustic Shot Noise (ASN) method. Menon and Durian [32] measured the sand motion in a gas-fluidized bed with a diffusing wave spectroscopy (DWS). In a recent experiment [36] the fluctuation velocity was estimated from the measured diffusion coefficient D_f by use of the kinetic theory. The velocity fluctuation of particles, with respect to the squared superficial gas velocity, obtained in our 2D simulations is plotted in Figure 3.15, It shows that the velocity fluctuation of particles is essentially zero before the bed begins to bubble, in agreement with the observation of Cody et al. [35] and Menon and Durian [32]. Menon and Durian [32] concluded that the homogeneous fluidization is a completely static state. Actually the velocity fluctuation of particles in the homogeneous fluidization regime is quite low (only 1% of that in bubbling regime), as shown in Figure 3.15, which is quite difficult to be measured by using a single measuring system due to the limited range of resolution. In this respect, the discrete particle simulations are ideally suited for obtaining this type of information.

Cody et al. [35] found that beyond the minimum bubbling point the average velocity fluctuation of particles is a linear function of the squared superficial gas velocity. It can be seen that in bubbling regime our simulation results agree very well with the findings by Cody et al. [35]. In the homogeneous fluidization regime, however, we do not observe such a linear dependence, instead, we find an exponential dependence. It is noteworthy that in the experiments by Valverde et al. [36] an exponential dependence of the fluctuation velocity on gas velocity was found

up to a maximum value corresponding to the maximum bed expansion point. In fact the interval of homogeneous fluidization in the experiments of Cody et al. [35] is quite short ($u_{mb}/u_{mf} < 2.0$, where both u_{mb} and u_{mf} have their usual meaning) and the exponential dependence of velocity fluctuation may be screened by the relatively long interval of the bubbling regime. By contrast, Valverde et al. [36] obtained a long interval of homogeneous fluidization ($u_{mb}/u_{mf} \sim 40$) by adding flow conditioners to particles with average diameter of 8.53 mm, where the cohesion of particles has been greatly reduced and a Geldart A type fluidization behavior is observed. So far the constant ratio of T_x/T_y in the bubbling regime, as found above, is actually due to the linear dependence of the velocity fluctuation of particles on the square superficial gas velocity.

The mechanism behind the transition from an exponential dependence to a linear dependence may be explained from the viewpoint of energy balance. The linear dependence may indicate that the fluctuation energy in the bubbling regime mainly comes from the energy provided by the inlet gas, while an exponential dependence hints at a more complicated picture. This will be the subject of further study.

The role of interparticle van der Waals forces

From the above analysis, it seems that the instability of the homogenous fluidization of Geldart A particles is mainly induced by the strong fluid-particle interaction, which leads to a much stronger velocity fluctuation of particles in the y (vertical) direction than that in the x (horizontal) direction. The presence of the particle-particle collisions and the interparticle van der Waals forces can prevent, or reduce, such an instability since they contribute equally to the velocity fluctuation in both x and y direction. This can be evidenced by the presence of Geldart C fluidization behavior of Geldart A particles when the interparticle van der Waals forces are strong, as discussed above. As the interparticle van der Waals forces are always present for the true Geldart A particles, it is essential to consider their effect on the homogenous fluidization behavior.

3.4.4 Particulate pressure: comparison with other work

Like in a dense molecular gas, the particulate pressure can be defined as

$$p_p = \rho_p(1-\varepsilon)T. \tag{3.15}$$

On the other hand, Koch and Sangani [37] proposed a different expression for the particulate pressure by assuming that the velocity fluctuation of particles is anisotropic:

$$p_p = [(\phi + 8B/5)T_y + (12/5)BT]\rho_p U_t, \tag{3.16}$$

where B is a function of the particle concentration $\phi = 1-\varepsilon$ [37]. Eq.(3.16) is slightly different from Eq.(3.15) in ref.([37]) since the latter one is normalized by $\rho_p U_t$ where U_t is the particle terminal velocity.

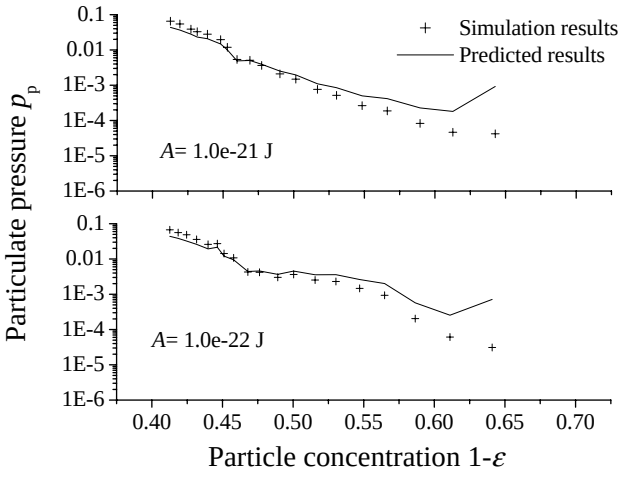

Figure 3.16: *The time-averaged particle pressure of the fluidized bed. The unit of the particulate pressure is kg/m·s^2.*

In Figure 3.16 results for p_p based on both Eq.(3.16) (plus symbols) and Eq.(3.15) (line). Clearly the difference between these two sets of results is more pronounced in the dense regime (i.e. homogeneous fluidization regime) than in the dilute regime (bubbling regime). Since Koch and Sangani [37] did not consider the effect of the interparticle van der Waals forces, this is not surprising because in homogeneous fluidization regime (the dense regime) the interparticle van der Waals forces have a direct impact on the velocity fluctuation of particles.

The local particle pressure inside the bed can be obtained by using Eq.(3.15). Figure 3.17 shows the distribution of particle pressure inside a bubbling fluidized bed, corresponding to the snapshot shown in the far right picture of Figure 3.10. From Figure 3.17, we found that the particle pressure is larger in the bottom and at sides of a bubble. Above the bubble the particle pressure is relatively small. This is in agreement with the recent experimental results by Rahman and Campbell [39].

3.5 Conclusions

In this paper we reported on the simulation results of the fluidization behavior of Geldart A particles by using a 2D soft-sphere based discrete particle model. Some typical features of fluidization behavior of Geldart A particles have been observed. If the interparticle van der Waals forces are not too strong, an interval of homogeneous fluidization can be displayed between the minimum fluidization point and the minimum bubbling point, where the gross circulation of particles in the absence of bubbles is found. The formation of cavities and channels is related to the contact parameters, especially the friction coefficient. In the bubbling regime a

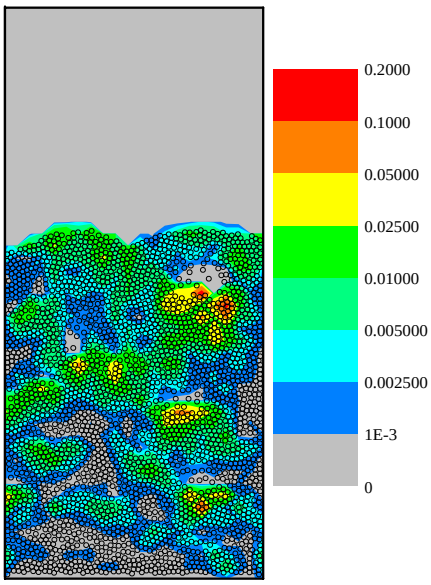

Figure 3.17: *The instantaneous particle pressure distribution of the bubbling fluidized bed. The snapshots shown in the far right graph of Figure 3.10. The unit of the particulate pressure is kg/m·s^2.*

detailed check suggests that the bubbles are typically fast bubbles, and the circulation of gas flow around the bubble is also clearly demonstrated. The structure of the forces acting on the particles is also studied, and the homogeneous fluidization regime is shown to be a quasi-equilibrium state where a force balance only exists at the macroscopic-level but not at the level of individual particles. The drag forces and van der Waals forces are two important sources of the local force fluctuations, and thus of the velocity fluctuation of the particles. It proves that, by use of a discrete particle model, the important features of homogeneous fluidization can be qualitatively described.

An analysis of the velocity fluctuation of particles has been carried out. It is shown that an anisotropy of the velocity fluctuation of particles exists in both the homogeneous fluidization regime and the bubbling regime. At least three basic interactions, i.e. the fluid-particle interaction, the particle-particle collisions (and the particle-wall collisions), and the interparticle van der Waals forces, can be identified as the main sources of velocity fluctuations of particles. The homogeneous fluidization is actually a transition phase resulting from the competition of these three interactions. In the bubbling regime, however, the effect of the interparticle van der Waals forces vanishes and the fluid-particle interaction becomes the dominant factor determining the fluidization behavior of Geldart A particles. Further analysis suggests that the ratio of the velocity fluctuation of particles in the x and y direction is nearly constant, which indicates that a dynamic equilibrium of the con-

tribution to the fluctuation energy of particles may exist between the fluid-particle interaction and the particle-particle collisions (and particle-wall collisions) in the bubbling regime. Additionally, we find that the velocity fluctuation of the particles is an exponential function of the squared superficial gas velocity in the homogeneous fluidization regime, and not a linear function as found by Cody et al. [35].

The comparison of the particulate pressure obtained from our simulations with the theoretical prediction by Koch and Sangani [37] suggests that the difference is more pronounced in the homogeneous fluidization regime than that in the bubbling regime. This further indicates that the fluid-particle interaction is a dominant factor responsible for the bubbling regime but not for the homogeneous fluidization. Our results in bubbling regime are also found to be in a good agreement with the experimental results by Rahman and Campbell [39].

We stress, however, that the current results are for 2D only, and can therefore only serve to get a *qualitative* insight into the physical principles underlying the fluidization behavior of Geldart A particles. For a true, quantitative comparison with experiments, clearly full 3D simulations are required, on which we report in the next chapter.

References

[1] Geldart D., 1973. Types of gas fluidization. *Powder Technol.*. **7**: 285.

[2] de Jong J.A.H., and Nomden J.F., 1974. Homogeneous gas–solid fluidization. *Powder Technol.*. **9**: 91.

[3] Abrahamsen A. R., and Geldart D., 1980. Behaviour of gas-fluidized beds of fine powders. Part I: Homogeneous expension. *Powder Technol.*. **26**: 35.

[4] Rietema K., and Piepers H.W., 1990. The effect of interparticle forces on the stability of gas-fluidized beds–I. Experimental evidence. *Chem. Engng. Sci.*. **45**: 1627.

[5] Homsy G.M., 1998. Nonlinear waves and the origin of bubbles in fluidized beds. *Appl. Sci. Res.*. **58**: 251.

[6] Jackson R., 1963. The mechanics of fluidized beds: I. The stability of the state of uniform fluidization. *Trans. Inst. Chem. Engrs.*, **41**: 13.

[7] Anderson T.B., and Jackson R., 1968. Fluid mechanical description of fluidized beds. Stability of the state of uniform fluidization. *Ind. Engng Chem. Fundam.*, **8**: 137.

[8] Grag S.K., and Pritchett J.W., 1975. Dynamics of gas fluidized beds. *J. Appl. Phys.*, **46**: 4493.

[9] Foscolo P.U., and Gibilaro L.G., 1984. A fully predictive criterion for the transition between particulate and aggregate fluidization. *Chem. Engng. Sci.*, **39**: 1667.

[10] Verloop J., and Heertjes P.M., 1970. Shock waves as a criterion for the transition from homogeneous to heterogeneous fluidization, *Chem. Engng. Sci.*, **25**: 825.

[11] Lettieri P., Brandam S., Yates J.G., and Newton D., 2001. A generalization of the Foscolo and Gibilaro particle-bed model to predict the fluid bed stability of some fresh FCC catalysts at elevated temperatures. *Chem. Engng. Sci.*, **56**: 5401.

[12] Rietema K., Cottaar E.J.E., and Piepers H.W., 1993. The effects of interparticle forces on the stability of gas-fluidized beds–II. Theoretical derivation of bed elasticity on the basis of van der Waals forces between powder particles. *Chem. Engng. Sci.*, **48**: 1687.

[13] Y. Tsuji, T. Kawaguchi and T. Tanaka, T., Discrete particle simulation of two dimensional fluidized bed, Powder Technol. 77 (1993), 79.

[14] B. P. B. Hoomans, J. A. M. Kuipers, W. J. Briels, and W. P. M. van Swaaij, Discrete particle simulation of bubble and slug formation in a two-dimensional gas-fluidised bed: a hard-sphere approach. Chem. Engng. Sci. 51 (1996), 99.

[15] B. H. Xu, A. B. Yu, Numerical simulation of the gas-solid flow in a fluidized bed by combining discrete particle method with computational fluid dynamics. Chem. Engng. Sci. 52 (1997), 2785.

[16] T. Kobayashi, T. Mukai, T. Kawaguchi, T. Tanaka, and Y. Tsuji, DEM analysis of flow patterns of Geldart's group A particles in fluidized bed. The 4th World Congress of Particle Technology Sydney, Australia, 21- 26 July ,2002.

[17] B. H. Xu, Y. C. Zhou, A. B. Yu, and P. Zulli, Force structures in gas fluidized beds of fine powders. The 4th World Congress of Particle Technology Sydney, Australia, 21- 26 July ,2002.

[18] J. A. M. Kuipers, K. J. van Duin, F. P. H. van Beckum, and W. P. M. van Swaaij, A numerical model of gas-fluidized beds, Chem. Engng. Sci. 47 (1992), 1913.

[19] S. Ergun, Fluid flow through packed columns. Chem. Engng. Progs. 48 (1952), 89.

[20] C. Y. Wen and Y. H. Yu, Mechanics of fluidization. Chem. Engng. Prog. Symp. Ser., 62 (1966), 100.

[21] P. A. Cundall and O. D. Strack, A discrete numerical model for granular assemblies, Géotechnique, 29 (1979), 47.

[22] S. Luding, Collisions and contacts between two particles, in: Physics of dry granular Media, eds. H. J. Herrmann, J.-P. Hovi, and S. Luding, Kluwer Academic Publishers, Dordrecht, 1998.

[23] B. Chu, Molecular forces, John Wiley & Sons, New York, 1967.

[24] J. Israelachvili, Intermolecular & surface forces, Academic Press, London, 1991.

[25] J. P. K. Seville, C. D. Willett, and P. C. Knight, Interparticle forces in fluidization: a review. Powder Tech., 113 (2000), 261.

[26] Y. Iwadate, and M. Horio, Agglomerating fluidization of wet powders and group C powders: a numerical analysis. In L.-S. Fan, and T. M. Knowlton (Eds.), Fluidization IX, p.293, New York: Engineering Foundation.

[27] M. J. Rhodes, X. S. Wang, M. Nguyen, P. Stewart and K. Liffman, Use of discrete element method simulation in the studying fluidization characteristics: influence of interparticle force. Chem. Engng. Sci. 56 (2001), 69.

[28] Massimilla L., Donsi G., and Zucchini C., 1972. *Chem. Engng. Sci.*, **27**: 2005.

[29] J. F. Davidson, R. Clift R. and D. Harrrison, Fluidization. Academic Press. 1985, London.

[30] Xu B.H., Zhou Y.C., Yu A.B., and Zulli P., 2002. Force structures in gas fluidized beds of fine powders. The 4th World Congress of Particle Technology Sydney, Australia, 21-26 July 2002.

[31] N. P. Cheremisinoff and P. N. Cheremisinoff, Hydrodynamics of gas-solids fluidization. Gulf, Houston, 1984.

[32] N. Menon and D. J. Durian, Particle motions in a gas-fluidized bed of sand. Phys. Rev. Lett. 79 (1997), 3407.

[33] G. Donsi and L. Massimilla, Bubble-free expansion of gas-fluidized beds of fine particles. AIChE J., 19 (1973), 1104.

[34] A. B. Yu, and B. H. Xu, Particle-scale modelling of gas-solid flow in fluidization. J. Chem. Technol. Biotechnol. 78 (2003), 111.

[35] Cody G.D., Goldfarb D.J., Storch G.V., and Norris A.N., 1996. Particle granular temperature in gas fluidized beds. *Powder Technol.*. **87**: 211.

[36] Valverde J.M., Castellanos A., and Quintanilla M.A.S., 2001. Self-diffusion in a gas-fluidized bed of fine powder. *Phys. Rev. Lett.*, **86**: 3020.

[37] D. L. Koch and A. S. Sangani, Particle pressure and marginal stability limits for a homogeneous monodisperse gas-fluidized bed: kinetic theory and numerical simulations. J. Fluid Mech. 400 (1999), 229.

[38] Goldschmidt M., Hydrodynamic modelling of fluidised bed spray granulation. Ph.D. Thesis, Twente University, 2001.

[39] K. Rahman and C. S. Campbell, Particle pressures generated around bubbles in gas-fluidized beds. J. Fluid. Mech. 455 (2002), 103.

4

Effects of Gas and Particle Properties on the Fluidization of Geldart A Particles

ABSTRACT

In this chapter we report on 3D computer simulations based on the soft-sphere discrete particle model (DPM) of Geldart A particles in a 3D gas-fluidized bed. The effects of particle and gas properties on the fluidization behavior of Geldart A particles are studied, with focus on the predictions of U_{mf} and U_{mb}, which are compared with the classical empirical correlations by Abrahamsen and Geldart [2]. It is found that the predicted minimum fluidization velocities are consistent with the correlation given by [2] for all cases that we studied. The overshoot of the pressure drop near the minimum fluidization point is shown to be influenced by both particle-wall friction and the interparticle van der Waals forces. A qualitative agreement has been found between the predicted U_{mb} with the correlation for different particle-wall friction coefficients, interparticle van der Waals forces, particle densities, particle sizes, and gas densities. For fine particles with a diameter $d_p < 40\mu$m, a deviation has been found between the predicted U_{mb} and the correlation. This may be due to the fact that the interparticle van der Waals forces are switched off in the simulations while they can play an important role in this size range. The simulation results with different gas viscosities, however, manifest a systematic deviation from the correlation. We found that with an increasing gas shear viscosity the U_{mb} experiences a minimum point near $2.0 \times 10^{-5}\mathrm{Pa}\cdot\mathrm{s}$, while in the correlation the minimum bubbling velocity decreases monotonously for increasing μ_g.

Based on: M. Ye, M. A. van der Hoef, and J.A. M. Kuipers, 2004. Effects of gas and particle properties on the fluidization of Geldart A particles in a gas-fluidzed bed, accepted by *Chem. Engng. Sci.*

4.1 Introduction

The great relevance of fluidization of Geldart A particles [1] for industrial applications has long been recognized in chemical reaction engineering, in particular in the context of fluidized bed reactors of fluid catalytic cracking (FCC) powders. A typical property of Geldart A particles is that they display an interval of non-bubbling expansion (homogeneous fluidization) between the minimum fluidization velocity U_{mf} and the minimum bubbling velocity U_{mb}, which is absent in the fluidization of large particles (Geldart B and D particles). It is precisely this homogeneous fluidization which is of practical importance for both heat and mass transfer in the reactors. Over the past years these systems have been the subject of intense research, in order to shed light on the origin of the homogeneous fluidization. Unfortunately, to date no comprehensive theoretical approach has been found which is capable of describing homogeneous fluidization *and* bubbling behavior on the basis of gas and particle properties. Foscolo and Gibilaro [3] suggested that the fluid-particle interaction is the dominant factor that controls the stability of the homogeneous fluidization regime. On the other hand, Rietema and his co-workers [4,5] proposed that the interparticle forces should be responsible for the homogeneous fluidization behavior of small particles. It has since then been a matter of intense debate between researchers. Experimental results by Tsinontides and Jackson [6] and Menon and Durian [7] suggest the state of homogeneous fluidization is actually solid-like where the enduring contacts make particles stay at rest, which supports the role of interparticle forces in the formation of homogeneous fluidization. However, Cody et al. [8] showed a pronounced increase of the particle velocity fluctuation during the transition from Geldart B to Geldart A fluidization behavior in their experiments, which means the bed of particles displays a fluidlike behavior. In a recent experiment Valverde et al. [9] fluidized very small particles ($d_p \sim 8.53\mu$m) with flow conditioners in a gas-fluidized bed, and observed a relatively long interval of homogeneous fluidization. They found that even during the homogeneous fluidization, both the solidlike and fluidlike behavior can be distinguished. This finding bridges the gap between the experimental results by Tsinontides and Jackson [6] and Menon and Durian [7] and Cody et al. [8]. However, as Valverde et al. [9] used Geldart C particles, it is not clear whether the solidlike or the fluidlike behavior is dominant for true Geldart A particles in gas-fluidized beds. Koch and Sangani [10] derived a very detailed kinetic theory by taking into account the fluid-particle interaction and particle-particle collisions. From detailed linear stability analysis of their equations, Koch and Sangani [10] showed that homogeneous fluidization is not stable, unless other non-hydrodynamical mechanisms such as interparticle forces are considered. Buyevich and his co-workers [11, 12] developed a similar kinetic theory based on the concept of induced random fluctuation of particles. Based on this theory, very recently Sergeev et al. [13] found that the apparent stability of uniform fluidization can also be explained without taking into account interparticle forces. So far, however, the physics behind the homogeneous fluidization is not completely understood. As the direct experimental evidence supporting either of these viewpoints is still not available, a detailed

study of the particle-particle interactions and particle-fluid interaction at a more fundamental level is highly desirable.

Computer simulations can play a valuable role in such studies. Discrete particle models (DPM) have been widely used in the study of gas-fluidized beds, for example, the hard-sphere approach by Hoomans et al. [14] and Li and Kuipers [15], and soft-sphere approach by Tsuji et al. [16], Xu and Yu [17], Mikami et al. [18], and Kafui and Thorton [19]. The idea of discrete particle simulation is to trace the motion of each particle in the system by solving the Newtonian equations of motion. In DPM the details of the particle-particle (and particle-wall) collisions, including friction, can be readily incorporated. Furthermore, through the *two-way coupling* DPM allows studying the influence of particle properties on the gas flow or vice versa [15]. The details of this simulation method are given in Chapter 2.

Recently several attempts have been made [20, 21, 30] to study the fluidization behavior of Geldart A particles by use of 2D discrete particle simulations. Kobayashi et al. [20] studied the effect of both the lubrication forces and the van der Waals forces on the fluidization of Geldart A particles. Xu et al. [21] investigated the force structure in the homogeneous fluidization regime, where they found that the van der Waals forces acting on the particles are balanced by the contact forces. In the previous chapter, we observed many of the typical features of gas-fluidized Geldart A particles, such as the homogeneous expansion, gross particle circulation in the absence of bubbles, and fast bubbles emanating at fluidization velocities beyond U_{mb} [30]. It was found that homogeneous fluidization actually represents a transition phase resulting from the competition of three kinds of basic interactions: the fluid-particle interaction, the particle-particle collisions (and particle-wall collisions) and the interparticle van der Waals forces [30]. In this work, we will study the influence of the properties of both the particulate phase and gas phase on the fluidization behavior of Geldart A particles with a full 3D discrete particle model, with focus on the prediction of U_{mf} and U_{mb} and comparisons with the classical empirical correlations by [2]. In section 2 the discrete particle model is briefly described. Subsequently the details of the simulation procedure are discussed in section 3, which is followed by a presentation of the simulation results. The chapter ends with a discussion and conclusions.

4.2 Discrete particle model

In the discrete particle model, the gas-phase hydrodynamics is derived from the volume-averaged Navier-stokes equations, following the approach of [22], which is reported in more detail in Chapter 2.

$$\frac{\partial(\varepsilon\rho_g)}{\partial t} + (\nabla \cdot \varepsilon\rho_g \mathbf{u}) = 0 \tag{4.1}$$

$$\frac{\partial(\varepsilon\rho_g \mathbf{u})}{\partial t} + (\nabla \cdot \varepsilon\rho_g \mathbf{u}\mathbf{u}) = -\varepsilon\nabla p - \mathbf{S}_p - \nabla \cdot (\varepsilon\overline{\tau}) + \varepsilon\rho_g \mathbf{g} \tag{4.2}$$

where the coupling with the particulate phase is included by means of a source term $\mathbf{S}_p$, defined as

$$\mathbf{S}_p = \frac{1}{V}\int \sum_{a=0}^{Npart} \mathbf{F}_{drag,a}\delta(\mathbf{r}-\mathbf{r}_a)dV. \tag{4.3}$$

In solving the gas-phase hydrodynamical equations, there are two types of boundary conditions that can in principle be used to account for the sidewalls: no-slip and free-slip boundary conditions. For the free-slip boundary conditions, the normal components of the gas velocity near the sidewalls are zero and the normal gradient of the tangential components vanishes. In the case of no-slip boundary conditions, both the normal and tangential components of gas velocity at the sidewalls vanish [22]. The no-slip boundary conditions have been widely used in the simulation of fluidized beds and are considered to be more physically accurate. In this research, we use either no-slip or free-slip boundary conditions for the sidewalls. As we will see in the following sections, in our particular case, the free-slip wall boundary conditions produces smaller minimum bubbling velocities than the no-slip boundary conditions, which are more close to the values calculated from the empirical correlations [2]. The minimum fluidization points, on the other hand, are not affected by the wall boundary conditions.

The particulate phase is described by solving the Newtonian equations of motion for each individual particle in the system. The equation of motion of a single particle a is given by

$$m_a\frac{d^2\mathbf{r}_a}{dt^2} = \mathbf{F}_{c,a} + \mathbf{F}_{vdw,a} + \mathbf{F}_{drag,a} - V_a\nabla p + m_a\mathbf{g} \tag{4.4}$$

$$I_a\frac{d\omega_a}{dt} = \mathbf{T}_a \tag{4.5}$$

The first and second term on the RHS of Eq.(4.4) are, respectively, the total contact force and the van der Waals force exerted by neighboring particles.

The contact force between two particles (or a particle and a wall) is obtained from a soft-sphere model originally proposed in [23]. In that model, a linear-spring and a dashpot are used to formulate the normal contact force, while a linear-spring, a dashpot and a slider are used to compute the tangential contact force. The details of this model can be found in Chapter 2.

The interaction of particle a with surrounding fluid follows from a drag force $F_{drag,a}$, which depends on the relative velocity of the two phases, and can be written as

$$\mathbf{F}_{drag,a} = 3\pi\mu_g\varepsilon^2 d_p(\mathbf{u}-\mathbf{v}_p)f(\varepsilon) \tag{4.6}$$

In Eq.(6.4), the effect of the neighboring particles on the drag force experienced by particle a is included via the so-called porosity function $f(\varepsilon)$, which depends on the local porosity ε. In this research, the well-known Ergun equation [24] is employed for porosities lower than 0.8 and the Wen and Yu correlation [25] for porosities higher than 0.8. In terms of the porosity function, the Ergun-Wen-Yu

drag model can be written as

$$f(\varepsilon) = \frac{150(1-\varepsilon)}{18\varepsilon^3} + \frac{1.75Re_p}{18\varepsilon^3} \qquad \varepsilon < 0.8 \tag{4.7}$$

$$f(\varepsilon) = (1 + 0.15Re_p^{0.687})\varepsilon^{-4.65} \qquad \varepsilon \geq 0.8 \tag{4.8}$$

This drag model used in many other studies is used in the present study as well.

To calculate the interparticle van der Waals force between two spheres, we adopt the Hamaker expression [26, 27]:

$$F_{vdw,ab}(S) = \frac{A}{3} \cdot \frac{2r_a r_b(S + r_a + r_b)}{[S(S + 2r_a + 2r_b)]^2} \left[\frac{S(S + 2r_a + 2r_b)}{(S + r_a + r_b)^2 - (r_a - r_b)^2} - 1 \right]^2 \tag{4.9}$$

Note that Eq.(4.9) exhibits an apparent numerical singularity if the intersurface distance S between two particles approaches zero. In the present model, we define a cut-off (maximal) value of the van der Waals force between two spheres to avoid such a numerical singularity when two particles approach very close or/and start to compress. In practice, an equivalent cut-off value S_0 for the intersurface distance is used instead of the interparticle force [28].

4.3 Simulation procedures

4.3.1 Fluidizing the system

In the simulations, the superficial gas velocity U_0 is set to increase linearly with time

$$U_0 = Kt. \tag{4.10}$$

Here the slope K is chosen sufficiently low, such that sudden changes of the fluidization conditions are avoided. This procedure was found to be more efficient, compared to the "step-wise" procedures adopted by [29] and [30]. In the step-wise procedure, the gas velocity is increased step by step, and for each gas velocity a sufficiently long computing time is required to ensure that the bed reaches a final dynamical equilibrium, since a sudden change of the gas flow will lead to large fluctuations in the flow conditions. We stress, however, that this linearly-increasing approach differs from the common experimental procedure, and could cause some systematic errors when compared to the experimental correlations. Nevertheless, the linear-increasing procedure is expected to be useful for investigating the origin of bubbling fluidization.

The optimum value of K is determined by preliminary simulations using different slopes. From the simulations, it has been found that the larger the slope K, the higher the predicted minimum bubbling point U_{mb} under the same conditions. A smaller K predicts a U_{mb} more close to that obtained in the step-wise procedure, which, however, requires a much longer computing time. An optimum value $K = 0.03$ m/s^2 is determined from the fact that the computing time is not

Table 4.1: *Parameters used in the simulations.*

parameters	value
Particle number,	36000
Normal restitution coefficient, e_n	0.9
Tangential restitution coefficient, e_t	0.9
Friction coefficient between particles, μ_f	0.2
Normal spring stiffness, k_n	7 or 3.5 N/m
Tangential spring stiffness, k_t	2 or 1 N/m
CFD time step,	1.0×10^{-5} or 2.0×10^{-5} s
Particle dynamics time step,	1.0×10^{-6} or 2.0×10^{-6} s
Minimum interparticle distance, S_0	0.4 nm
Number of cells	48×12×5
Gas temperature, T	293 K
Gas constant, R	8.314 J/(mol·K)

significantly longer, while the relation between pressure drop (and bed height as well) and gas velocity shows relatively small deviation from that obtained via the step-wise procedure. In this paper, if not specified otherwise, the slope K is set to 0.03 m/s^2.

Some input parameters that have been used in the simulations are listed in Table 4.1. Other parameters not indicated here will be specified in the individual simulations.

4.3.2 The determination of minimum bubbling point

One of the most important quantities which characterize the fluidization behavior of Geldart A particles is the minimum bubbling point U_{mb}, which is generally defined as the instant at which the first obvious bubble appears [1]. However, such a definition is difficult to utilize in a quantitative way. It has been found that the change of the spatial fluctuation of local porosities is the most outstanding observation [20,30], although a temporal fluctuation of pressure drop and granular temperature can also be observed near the transition from homogeneous fluidization to bubbling fluidization. The typical fluctuation of local porosities with respect to the gas velocity is shown in Figure 4.1. Here the fluctuation of local porosities is calculated from

$$\triangle\varepsilon = \sqrt{\frac{1}{N_{sub}-1}\left[\sum_{k=1}^{N_{sub}}\varepsilon_k^2 - \frac{1}{N_{sub}}\left(\sum_{k=1}^{N_{sub}}\varepsilon_k \sum_{k=1}^{N_{sub}}\varepsilon_k\right)\right]} \tag{4.11}$$

with ε_k is the local porosity in the subdomain k. As can be seen from Figure 4.1, there are two clear transitions occurring for the fluctuation of local porosities with an increasing gas velocity. A detailed analysis shows that these two transition

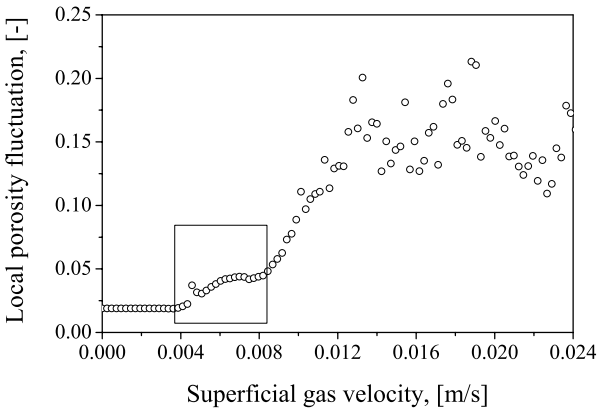

Figure 4.1: *The spatial fluctuation of local porosities. The simulation is carried out with free-slip boundary conditions for the sidewalls. Other parameters not listed in Table 4.1 are: particle diameter $d_p = 75\mu$m; Hamaker constant $A = 0.0$; particle density $\rho_p = 1495$ kg/m^3; gas shear viscosity $\mu_g = 1.8\times10^{-5}$Pa·s; gas molar mass $M_g = 2.88\times10^{-2}$ kg/mole; size of the fluidized bed 12.0×3.0×1.2 mm; initial bed height $H_0 = 3.68$ mm; and particle-wall friction coefficient $\mu_f = 0.2$.*

points are very close to the minimum fluidization point (0.0034 mm/s) and minimum bubbling point (0.0082 mm/s) determined from the visualization of simulation results. The window of homogeneous expansion in the discrete particle simulations can thus be determined by the transition points of porosity fluctuation. In this research, however, the minimum bubbling point is determined by the visualization check.

The U_{mb} calculated from the correlation derived by [2] is used for the comparison, which is given by

$$U_{mb} = \frac{2.07\, d_p \rho_g^{0.06}}{\mu_g^{0.347}} \exp(0.176\, W_{45}) \tag{4.12}$$

where W_{45} is the weight fraction of particles having a diameter less than 45 μm.

4.3.3 The determination of minimum fluidization point

The determination of the minimum fluidization velocity U_{mf} is straightforward. The pressure drop $\Delta\, p_0$ across the bed will just support the weight of particles at the minimum fluidization point, so that the following relation should hold:

$$\frac{\Delta\, p_0}{H_0} = \varepsilon_0 \rho_g g + (1-\varepsilon_0)\rho_p g. \tag{4.13}$$

Therefore in the simulation the minimum fluidization point is determined as the first instant at which the pressure drop across the bed equals $\Delta\, p_0$. The theoretical

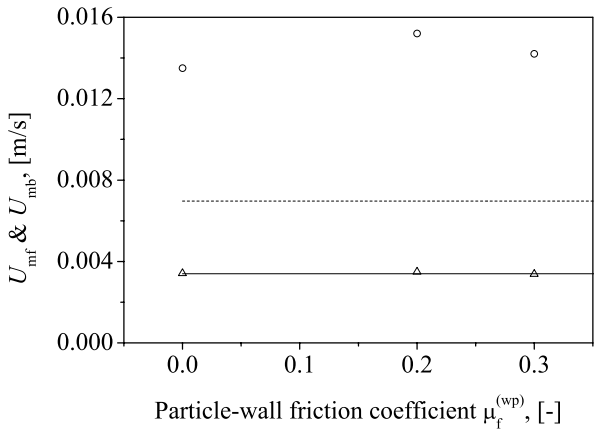

Figure 4.2: *The effect of particle-wall friction on U_{mf} and U_{mb}. Shown are the simulation results for U_{mb} (circles) and U_{mf} (triangles), as well as the theoretical predictions for U_{mb} from Eq.(4.12) (dashed line) and U_{mf} from Eq.(4.14) (solid line). The simulations are carried out with no-slip boundary conditions for the sidewalls. Other parameters not listed in Table 4.1 are: particle diameter $d_p = 75\mu$m; Hamaker constant $A = 1.0 \times 10^{-22}$ J; particle density $\rho_p = 1495$ kg/m^3; gas shear viscosity $\mu_g = 1.8{\times}10^{-5}\mathrm{Pa \cdot s}$; gas molar mass $M_g = 2.88{\times}10^{-2}$ kg/mole; size of the fluidized bed 12.0×3.0×1.2 mm; and initial bed height $H_0 = 3.68$ mm.*

minimum fluidization point U_{mf} is given by [2]

$$U_{mf} = \frac{9.0 \times 10^{-4}\, d_p^{1.8}[(\rho_p - \rho_g)g]^{0.934}}{\rho_g^{0.066}\mu_g^{0.87}} \tag{4.14}$$

4.4 Simulation results

4.4.1 The effect of sidewalls

Since our simulations have been carried out in a "tiny" fluidized bed, it is essential to check first the effect of the sidewalls on the fluidization behavior.

The effect of particle-wall friction

A number of simulations have been carried out with different particle-wall friction coefficients under no-slip boundary conditions. The results are given in Figure 4.2. It is shown that the predicted minimum fluidization velocities U_{mf} agree well with the values calculated from the correlation given by Eq.(4.14). By contrast, the minimum bubbling velocities are overestimated in the simulation, compared to the correlation (4.12). It is worthwhile to mention that the influence of the particle-wall friction on the minimum bubbling point is negligible, however. In Figure 4.3 we show the pressure drop for different particle-wall friction coefficients μ_f. It is

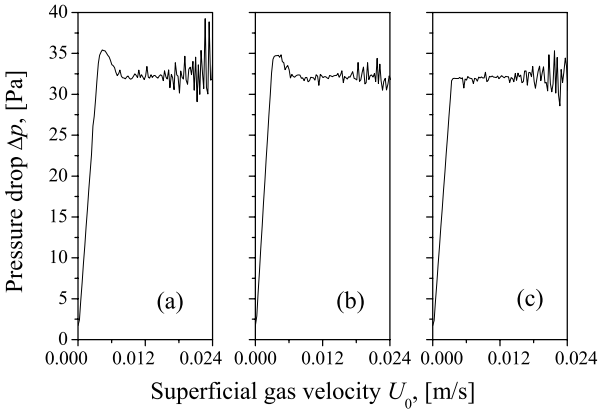

Figure 4.3: *The effect of particle-wall friction on the pressure drop. Hamaker constant $A = 0$. Other simulation conditions are the same as Fig.4.2. The particle-wall friction coefficient $\mu_f^{(wp)}$ is (a) 0.3; (b) 0.2; (c) 0.0.*

found that the overshoot of pressure drop near the minimum fluidization point obviously depends on the particle-wall friction coefficients. The bigger the particle-wall friction coefficient, the higher the overshoot of the bed pressure drop. Without interparticle van der Waals forces ($A = 0$), the overshoot is nearly zero for a zero particle-wall friction coefficient. These findings are in accordance with the recent experimental results obtained by [31].

The effect of gas boundary conditions

To quantify the effect of wall boundary conditions on the fluidization behavior, we compare the simulation results obtained for no-slip with free-slip boundary conditions. In Figure 4.4 we show the fluctuation of local porosities obtained in the simulations. In both cases the first transition occurs at nearly the same gas velocity, which means that the minimum fluidization point is not influenced by the imposed wall boundary conditions. This is not surprising since the inception of fluidization only depends on the weight of particles inside the bed. As can be seen, however, in case of the no-slip boundary condition the second transition occurs much later than in case of the free-slip boundary condition, i.e. the transition from homogeneous fluidization to bubbling fluidization is delayed due to the no-slip boundary conditions. A detailed check of the simulation data indicates a $U_{mb} = 0.0128$ m/s in case of the no-slip boundary condition, while a value of 0.0082 m/s is obtained in the case of free-slip boundary condition, for the simulation conditions given in Figure 4.4. In fact, we carried out two sets of simulations with either no-slip or free-slip boundary conditions, and in general qualitative agreement has been found in all the cases we studied, except that always a higher U_{mb} is obtained in the case of no-slip boundary conditions. According to the correlation by [2], a

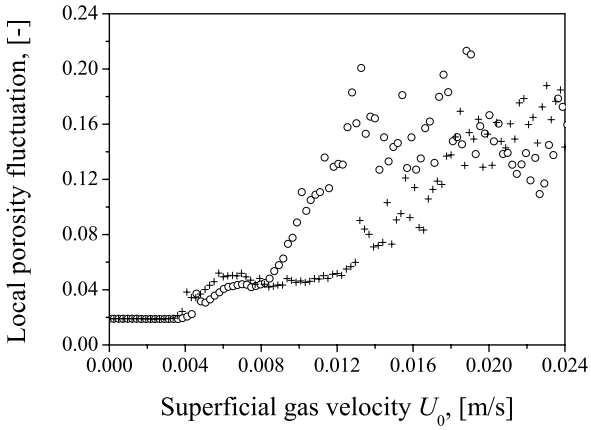

Figure 4.4: *The effect of wall boundary conditions on the fluctuation of local porosities. Circle: free-slip condition; Cross: no-slip conditions. The simulations are carried out under the same conditions as in Figure 4.1.*

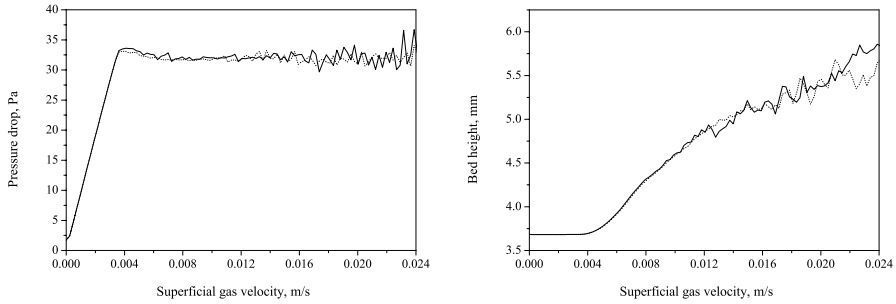

Figure 4.5: *The effect of wall boundary conditions on pressure drop and bed height. Solid line: no-slip conditions; Dotted line: free-slip conditions. The simulations are carried out under the same conditions as in Figure 4.1.*

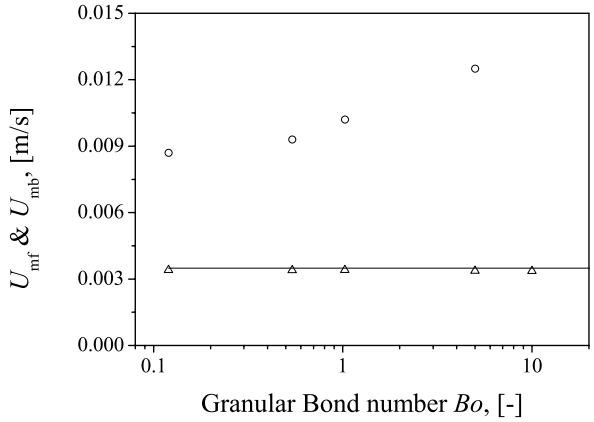

Figure 4.6: *The effect of the interparticle van der Waals forces on U_{mf} and U_{mb}. The simulation results of U_{mf} (circles) and U_{mb} (triangles), as well as U_{mf} by Eq.(4.14), are plotted out. The simulations carried out under free-slip boundary conditions. Other parameters not listed in Table 4.1 are: particle diameter $d_p = 75\mu$m; particle density $\rho_p = 1495$ kg/m^3; gas shear viscosity $\mu_g = 1.8\times10^{-5}\mathrm{Pa}\cdot\mathrm{s}$; gas molar mass $M_g = 2.88\times10^{-2}$ kg/mole; size of the fluidized bed 12.0×3.0×1.2 mm; initial bed height $H_0 = 3.68$ mm; and the particle-wall friction coefficient $\mu_f = 0.2$.*

$U_{mb} = 0.0070$ m/s is expected for the specified system indicated in Figure 4.4. The simulated U_{mb} is 17% over-predicted under free-slip boundary conditions (=0.0082 m/s) and 82% over-predicted under no-slip boundary conditions (=0.0128 m/s). On the other hand, the pressure drop and bed height do not show big deviations for these two different wall boundary conditions, as depicted in Figure 4.5.

4.4.2 The effect of interparticle van der Waals force

In Fig. 4.6, we show the effect of the strength of the van der Waals forces on the minimum bubbling point and minimum fluidization point. The strength of the van der Waals forces has been formulated in terms of granular Bond number B_o, which is defined by the ratio of the interparticle van der Waals force acting between two identical spheres and the single particle weight. The simulations have been conducted under free-slip boundary conditions. It is found that the influence of interparticle van der Waals forces on U_{mf} is negligible, and that the predicted minimum fluidization velocities U_{mf} again agree well with the value obtained from Eq.(4.14). On the other hand, the predicted U_{mb} increases with an increasing Bond number Bo, as shown in Figure 4.6. This means that the cohesive interactions between particles may delay the minimum bubbling point in the gas-fluidized bed, which is in accordance with previous experimental work. In the case of quite strong cohesive forces, for instance, $Bo \geq 10$, the bed behaves like Geldart C system, and a minimum bubbling point in the normal sense is not observed.

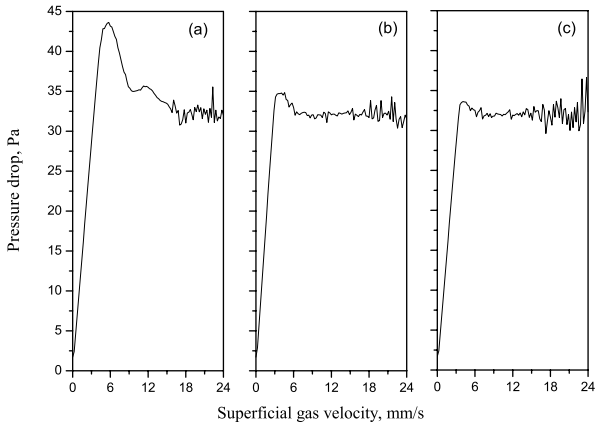

Figure 4.7: *The effect of the interparticle van der Waals forces on the pressure drop. Simulation conditions are the same as Fig.4.6. The Hamaker constant A is (a) 10^{-21} J; (b) $A = 10^{-22}$ J; (c) 0.*

In Fig. 4.7 the profiles of pressure drop for different Hamaker constants are shown. It is found that the overshoot is also affected by the interparticle van der Waals force: the stronger the interparticle van der Waals force, the higher the overshoot of the pressure drop near the minimum fluidization point. So on the basis of our discrete particle simulations, we conclude that the overshoot of the bed pressure drop for Geldart A particles is due to the particle-wall friction as well as the interparticle van der Waals forces. This confirms the conclusion of [4].

4.4.3 The effects of particle density

In Fig. 4.8 we show the results of U_{mf} and U_{mb} for different particle densities. Again, the predicted minimum fluidization points U_{mf} agree well with the correlation given by Eq.(4.14). When the particle density becomes higher, U_{mf} increases rapidly. By contrast, only a weak dependence of U_{mb} on particle density is found. The predicted U_{mb} changes slightly from 0.0082 mm/s to 0.0094 mm/s by increasing the particle density from 900 to 2995 kg/m^3. Hence the window of homogeneous fluidization is decreased for heavy particles, but this is mainly due to the increase in U_{mf}. Note that the correlation reported in [2], as shown in Eq.(4.12), does not include any information about the particle density, which suggests a negligible effect of particle density on U_{mb}. Our simulation results seem to support this conclusion.

4.4.4 The effects of particle size

In Fig. 4.9 the results for U_{mf} and U_{mb} for different particle diameters are shown. The predicted minimum fluidization points U_{mf} agree well with the correlation

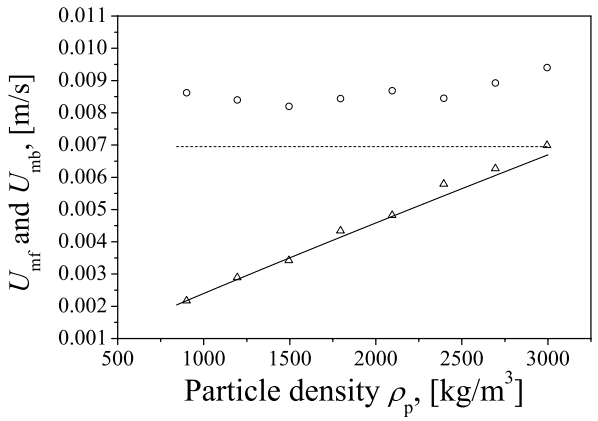

Figure 4.8: *The effect of particle density on U_{mf} and U_{mb}. The simulation results of U_{mb} (circles) and U_{mf} (triangles), as well as the U_{mf} by Eq.(4.14) (solid-line) and U_{mb} by Eq.(4.12) (dash line), are shown. The simulations are carried out under free-slip boundary conditions. Other parameters not listed in Table 4.1 are: particle diameter $d_p = 75\mu$m; gas shear viscosity $\mu_g = 1.8\times10^{-5}$Pa · s; gas molar mass $M_g = 2.88\times10^{-2}$ kg/mole; size of the fluidized bed 12.0×3.0×1.2 mm; initial bed height $H_0 = 3.68$ mm; and the particle-wall friction coefficient $\mu_f^{(wp)} = 0.2$.*

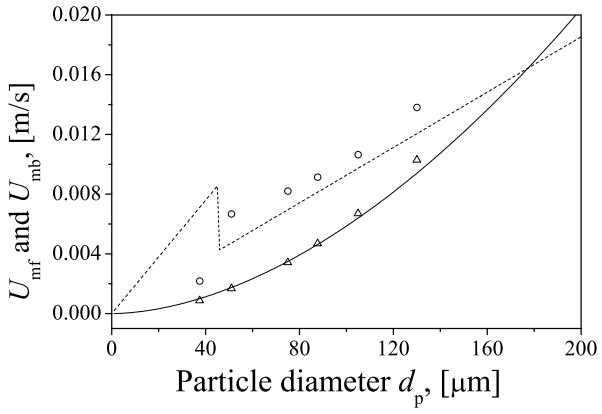

Figure 4.9: *The effect of particle diameter on U_{mf} and U_{mb}. The simulation results of U_{mb} (circles) and U_{mf} (triangles), as well as the U_{mf} by Eq.(4.14) (solid-line) and U_{mb} by Eq.(4.12) (dash line), are shown. The simulations are carried out under free-slip boundary conditions. Other parameters not listed in Table 4.1 are: particle density $\rho_p = 1495$ kg/m^3; gas shear viscosity $\mu_g = 1.8\times10^{-5}$Pa · s; gas molar mass $M_g = 2.88\times10^{-2}$ kg/mole; and the particle-wall friction coefficient $\mu_f^{(wp)} = 0.2$.*

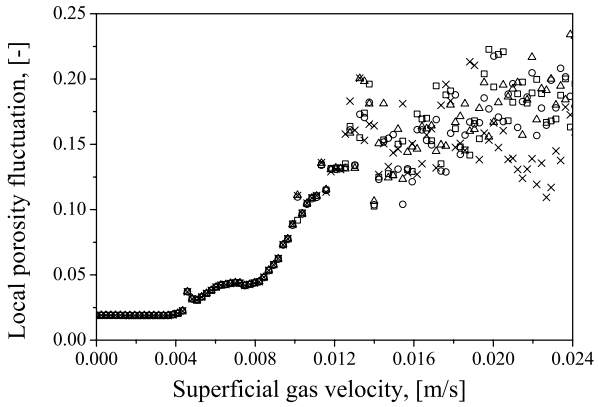

Figure 4.10: *The effect of gas density on U_{mf} and U_{mb}. The inlet gas densities used in the simulations are 0.5990 (square), 1.1979 (cross), 1.4974 (triangle) and 2.2461 (circle) kg/m^3. The simulations are carried out under free-slip boundary conditions. Other parameters not listed in Table 4.1 are: particle diameter $d_p = 75\mu$m; particle density $\rho_p = 1495$ kg/m^3; gas shear viscosity $\mu_g = 1.8\times10^{-5}$Pa $\cdot$ s; size of the fluidized bed 12.0×3.0×1.2 mm; initial bed height $H_0 = 3.68$ mm; and the particle-wall friction coefficient $\mu_f = 0.2$.*

given by Eq.(4.14): the bigger the particle diameter d_p, the higher the U_{mf}. A general qualitative agreement is found for U_{mb} when the particle diameter d_p is larger than 40 μm. The values of U_{mb} are typically over-predicted by 15% to 25% compared to the correlation given in [2]. For fine particles with a diameter $d_p < 40\mu$m, the predicted U_{mb} shows an apparent deviation with the correlation. For instance, with a particle diameter $d_p = 37.5\mu$m, a lower U_{mb} (=0.0022 m/s) is obtained. We remind that we turned off the interparticle van der Waals forces in this particular simulation (i.e. Hamaker constant $A = 0$). As mentioned before, the incorporation of interparticle van der Waals forces can delay the minimum bubbling point and extend the interval of homogeneous fluidization. For fine particles with a diameter d_p less than 40 μm, the interparticle van der Waals forces may become stronger, and will shift U_{mb} to a higher value, compared to what is normally observed in the experiments. Thus it can be argued that for fine particles interparticle van der Waals forces are playing an important role for homogeneous fluidization.

4.4.5 The effects of the gas density

In the present study, the equation of state of ideal gas is used, which gives the relation between gas pressure and density as follow:

$$\rho_g = \frac{M_g\, p}{RT} \tag{4.15}$$

where M_g is the molar mass of gas phase, R the gas constant (=8.314 J/(mole$\cdot$ K)), and T gas temperature. To change the gas density, we can either change the mo-

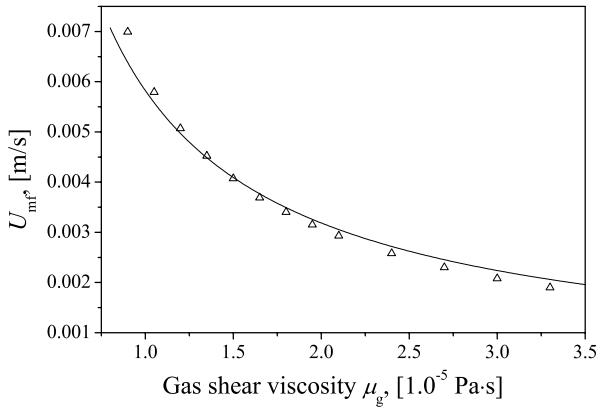

Figure 4.11: *The effect of gas shear viscosity on U_{mf}. The triangles denote the simulation results while slid line stands for the calculation by Eq.(4.14). The simulations carried out under free-slip boundary conditions. Other parameters not listed in Table 4.1 are: particle diameter $d_p = 75\mu$m; particle density $\rho_p = 1495$ kg/m^3; size of the fluidized bed 12.0×3.0×1.2 mm; initial bed height $H_0 = 3.68$ mm; and the particle-wall friction coefficient $\mu_f = 0.2$.*

lar mass M_g or the gas pressure p. We stress, however, that the gas density is not uniform inside the fluidized bed since the gas pressure is spatially heterogeneous. Note that the gas density is taken as the density at the inlet. In fact the bed pressure drop used in the simulation is quite small compared to the absolute gas pressure, thus the gas density can be determined solely by the inlet gas pressure. First we change the molar mass M_g of the gas phase from 1.44×10^{-2} to 5.04×10^{-2} kg/mole. The impact on the fluctuation of local porosity is shown in Figure 4.10. As can be seen, except in the bubbling regime, we can hardly observe the differences for different gas densities. It means that the effect of gas density on both U_{mf} and U_{mb} are negligible. Actually in the correlations given in [2], as shown in Eqs.(4.14) and (4.12), only a weak dependence of U_{mb} and U_{mf} on gas density is found, i.e. $U_{mb} \sim \rho_g^{0.06}$ and $U_{mf} \sim \rho_g^{-0.066}$.

4.4.6 The effect of the gas viscosity

In Figures 4.11 and 4.12 we show U_{mf} and U_{mb} for different gas shear viscosities. For simplicity, the interparticle van der Waals forces are switched off by setting the Hamaker constant $A = 0$. Again, the minimum fluidization velocities agree well with the values calculated from Eq.(4.14). U_{mf} experiences a continuous decrease as μ_g increases. The minimum bubbling velocities, however, manifest a systematic deviation from the empirical correlation given in [2]. As illustrated in Figure 4.12, U_{mb} first drops and subsequently increases for an increasing shear viscosity, passing a minimum point at $\mu_g = 2.0 \times 10^{-5}\mathrm{Pa}\cdot\mathrm{s}$. This is obviously in contradiction with Eq.(4.12), where the minimum bubbling velocity decreases monotonously for

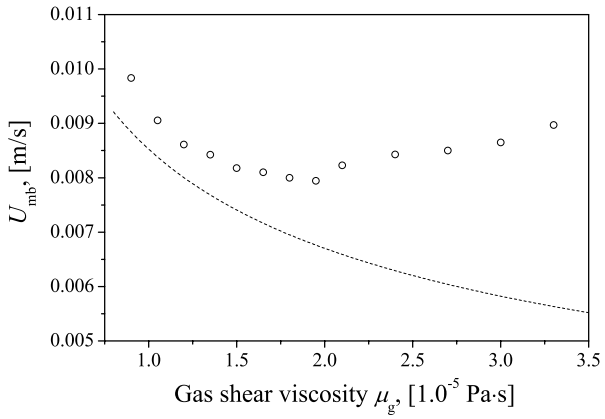

Figure 4.12: *The effect of gas shear viscosity on U_{mb}. The circles denote the simulation results while dash line stands for the calculation by Eq.(4.12). The simulations are carried out under the same conditions as in Figure 4.11.*

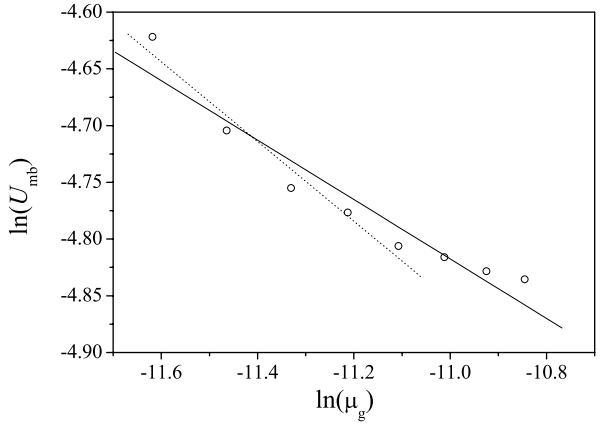

Figure 4.13: *The predicted U_{mb} with different gas shear viscosities, plotted on a log-log scale. The crosses denote the simulation results up to μ_g $2.0\times10^{-5}\mathrm{Pa}\cdot\mathrm{s}$, the solid-line is obtained by fitting all the data, and the dash-line is a linear fit of the first 5 data. The simulations are carried out under the same conditions as in Figure 4.11.*

increasing μ_g. At present, we have no explanation why a minimum in U_{mb} is observed in our simulations. We should mention, however, that the correlation of [2] was actually obtained with gas shear viscosities ranging from 0.9 to 2.0 $\times 10^{-5}\mathrm{Pa}\cdot\mathrm{s}$. In this regime, the U_{mb} as predicted from our simulations also experiences a continuous decrease with an increasing gas shear viscosity. It would be interesting to preform experiments with gas shear viscosities larger than $2.0\times 10^{-5}\mathrm{Pa}\cdot\mathrm{s}$, where our simulations predict an *increase* in U_{mb}.

To further compare with the correlation of [2], we fit these data to a linear function, which yields a slope of -0.267. This value is not far off from the slope given by Eq.(4.12), namely -0.347. If we only fit data up to $1.8\times 10^{-5}\mathrm{Pa}\cdot\mathrm{s}$, which corresponds to the shear viscosity of air under normal condition (T=293 K), a slope of -0.354 is obtained.

4.5 Conclusions and discussions

In this research, computer simulations based on the soft-sphere discrete particle model (DPM) have been used to investigate the fluidization behavior of Geldart A particles. The simulations have been carried out in a 3D fluidized bed, with interparticle van der Waals forces that follow from the Hamaker theory. We first studied the effects of the sidewalls on the fluidization behavior. It has been found that the generation of the overshoot of the pressure drop near the minimum fluidization point is affected by both the particle-wall friction and the interparticle van der Waals forces, which confirm the experimental results by [31] and [4].

In all the cases we studied in this research, the predicted U_{mf} was in a good agreement with the correlation by [2]. The minimum bubbling velocity U_{mb}, in general, shows a qualitative agreement with this correlation. First, the wall boundary conditions are found to have a significant impact on the predicted U_{mb}. The free-slip boundary conditions seems to predict a lower U_{mb} compared to the no-slip boundary conditions in our small-scale simulations. The predicted U_{mb} under free-slip boundary conditions is found 15% to 25% higher than the value calculated from the correlation, while under no-slip boundary conditions this amounts more than 80%. Second, the action of the interparticle van der Waals force is found to delay the origin of bubbles and extend the interval of homogeneous fluidization. The higher the granular Bond number, the higher U_{mb}, until a transition to Geldart C behavior is encountered, where no U_{mb} can be discerned. Third, the particle density and gas density are shown to have a weak effect on U_{mb}. For heavy particles, the window of homogeneous fluidization is decreased mainly due to the increase in U_{mf}. By contrast, it has been found that the particle size has a strong effect on U_{mb}. The predicted U_{mb} for different particle diameter agrees with the correlation except for fine particles with a diameter $d_p < 40\mu$m. This may be due to the fact that we turn off the interparticle van der Waals forces in these particular simulations. It can be argued that for larger particles with a diameter $d_p > 40\mu$m the interparticle van der Waals forces may have a negligible effect on the formation of homogeneous fluidization. For fine particles, however, a proper incorporation of interparticle van

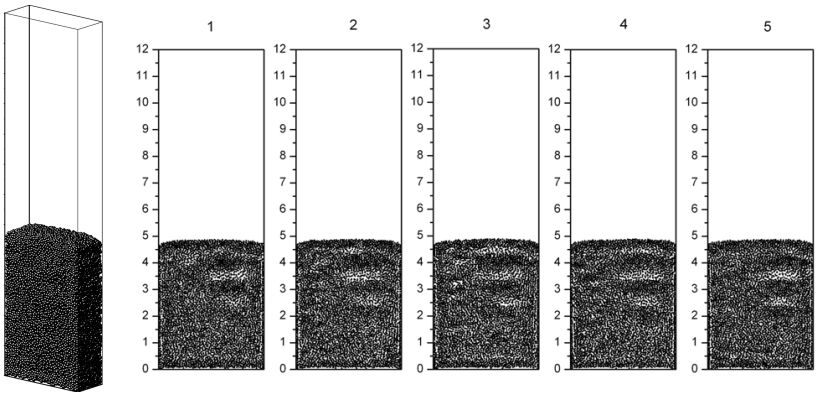

Figure 4.14: *The snapshots of the simulation results of the homogeneous fluidization of Geldart A particles. The far left graph shows the fluidized bed in 3D. In the graphs 1 to 5, the cross sections of the bed (cutting through the width direction) are shown. The simulation conditions are the same as in Figure 4.1.*

der Waals forces is highly desired. Finally, the effect of the gas viscosity has been examined. We found that the minimum bubbling velocities from our simulations for different gas viscosity show a systematic deviation from the empirical correlation by [2]. We found that with an increasing gas shear viscosity the U_{mb} experiences a minimum point near $2.0 \times 10^{-5}\mathrm{Pa} \cdot \mathrm{s}$, while in the correlation by [2] the minimum bubbling velocity decreases monotonously for increasing μ_g. Interestingly, if we fit the data up to $2.0 \times 10^{-5}\mathrm{Pa} \cdot \mathrm{s}$, a slope of -0.267 has been obtained, which is not far away from the value (=-0.347) given by Eq.(4.12). Clearly a more elaborate study of the effect of gas viscosity is required, both experimentally and numerically.

We want to stress, however, that it is a non-trivial task to determine the minimum bubbling velocity U_{mb}, since there is no unique, quantitative formalism to relate U_{mb} to parameters that can be directly measured in the discrete particle simulations. This is directly related to the fact that the minimum bubbling point is rather loosely defined, namely, as the instant at which "the first obvious bubble" appears in the fluidized bed. At present, the most accurate and reliable way to determine the minimum bubbling point is probably by direct observation of the snapshots of the simulation results. But this is of course prone to errors, which is especially the case when there are some void structures present in the homogeneous fluidization. In Figures 4.14 and 4.15, we illustrate the typical results for both homogeneous fluidization and bubbling fluidization. As can be seen, even during the homogeneous fluidization, we can still find some void structures. It would be extremely difficult to define a formalism (i.e. a computer code) which could discriminate the voids and cavities of homogeneous fluidization from the first obvious bubble, just on the basis of the particle coordinates.

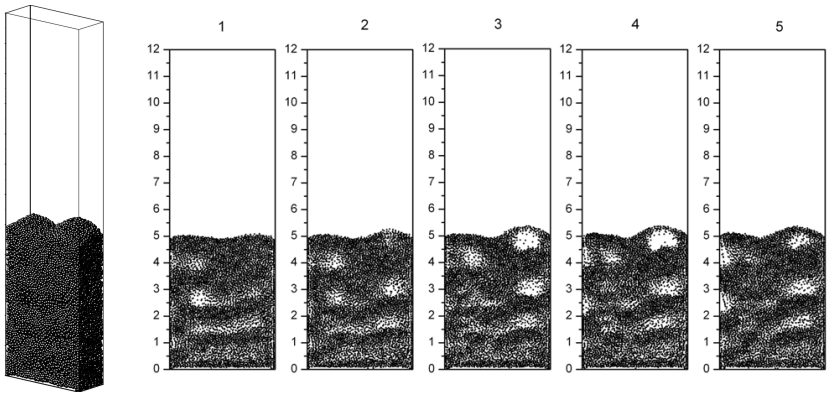

Figure 4.15: *As in Fig.4.14, but for the bubbling fluidized bed. The simulation conditions are the same as in Figure 4.1*

References

[1] Geldart D., 1973. Types of gas fluidization. *Powder Technol.* **7**: 285.

[2] Abrahamsen A.R., and Geldart D., 1980. Behavior of gas-fluidized beds of fine powders. part I: homogeneous expansion. *Powder Technol.* **26**: 35.

[3] Foscolo P.U., and Gibilaro L.G., 1984. A fully predictive criterion for the transition between particulate and aggregate fluidization. *Chem. Engng. Sci.*, **39**: 1667.

[4] Rietema K., and Piepers H.W., 1990. The effect of interparticle forces on the stability of gas-fluidized beds–I. Experimental evidence. *Chem. Engng. Sci.*, **45**: 1627.

[5] Rietema K., Cottaar E.J.E., and Piepers H.W., 1993. The effects of interparticle forces the stability of gas-fluidized beds–II. Theoretical derivation of bed elasticity on the basis of van der Waals forces between powder particles. *Chem. Engng. Sci.*, **48**: 1687.

[6] Tsinontides S.C., and Jackson R., 1993. The mechanics of gas fluidized beds with an interval of stable fluidization. *J. Fluid Mech.*, **225**: 237.

[7] Menon N., and Durian D.J., 1997. Particle motions in a gas-fluidized bed of sand. *Phys. Rev. Lett.*, **79**: 3407.

[8] Cody G.D., Kapbasov S.K., and Buyevich Y.A., 1999. Particulate fluctuation velocity in gas fluidized beds—fundamental models compared to recent experimental data. *AIChE Symp. Ser.* **95**: 7.

[9] Valverde J.M., Castellanos A., and Quintanilla M.A.S., 2001. Self-diffusion in a gas-fluidized bed of fine powder. *Phys. Rev. Lett.*, **86**: 3020.

[10] Koch D.L., and Sangani A.S., 1999. Particle pressure and marginal stability limits for a homogeneous monodisperse gas-fluidized bed: kinetic theory and nu-

merical simulations. *J. Fluid Mech.*, **400**: 229.

[11] Buyevich Y.A., 1999. Particulate stresses in dense disperse flow. *Ind. Eng. Che,. Res.* **38**: 731.

[12] Buyevich Y.A., and Kapbasov S. K., 1999. Particulate pressure in disperse flow. *Int. J. Fluid Mech.*, **26**: 72.

[13] Sergeev Y.A., Swailes D.C., and Petrie C.J.S., 2004. Stability of uniform fluidization revisited. *Physica A*, **335**: 9.

[14] Hoomans B.P.B., Kuipers J.A.M., Briels W.J., and van Swaaij W.P.M., 1996. Discrete particle simulation of bubble and slug formation in a two-dimensional gas-fluidised bed: a hard-sphere approach. *Chem. Engng. Sci.*, **51**: 99.

[15] Li J., and Kuipers J.A.M., 2003. Gas-particle interactions in dense gas-fluidized beds. *Chem. Engng. Sci.*, **58**: 711.

[16] Tsuji Y., Kawaguchi T., and Tanaka T., 1993. Discrete particle simulation of two-dimensional fluidized bed. *Powder Technol.*, **77**: 79.

[17] Xu B.H., and Yu A.B., 1997. Numerical simulation of the gas-solid flow in a fluidized bed by combining discrete particle method with computational fluid dynamics. *Chem. Engng. Sci.*, **52**: 2785.

[18] Mikami T., Kamiya H., and Horio M., 1998. Numerical simulation of cohesive powder behavior in a fluidized bed. *Chem. Engng. Sci.*, **53**: 1927.

[19] Kafui K.D., Thornton C., and Adams M.J., 2002. Discrete particle-continuum fluid modelling of gasCsolid fluidised beds. *Chem. Engng. Sci.*, **57**: 2395.

[20] Kobayashi T., Kawaguchi T., Tanaka T., and Tsuji Y., 2002. DEM analysis on flow patterns of Geldart's group A particles in fluidized bed. In: *Proc. of World Congress on Particle Technology 4* (CD-ROM). July 21-25, Sydney, Australia.

[21] Xu B.H., Zhou Y.C., Yu A.B., and Zulli P., 2002. Force structures in gas fluidized beds of fine powders. In: *Proc. of World Congress on Particle Technology 4* (CD-ROM). July 21-25, Sydney, Australia.

[22] Kuipers J.A.M., van Duin K.J., van Beckum F.P.H., and van Swaaij W.P.M., 1992. A numerical model of gas-fluidized beds. *Chem. Engng. Sci.*, **47**: 1913.

[23] Cundall P. A., and Strack O. D. L., 1979. A discrete numerical model for granular assemblies. *Geotechniques.* **29**: 47.

[24] Ergun S., 1952. Fluid flow through packed columns. *Chem. Engng. Progs.*, **48**: 89.

[25] Wen C.Y. and Yu Y.H., 1966. Mechanics of fluidization. *Chem. Engng. Prog. Symp. Ser.*, **62**: 100.

[26] Chu B., 1967. *Molecular forces*, John Wiley & Sons, New York, USA.

[27] Israelachvili J., 1991. *Intermolecular & surface forces*, Academic Press, London, UK.

[28] Seville J.P.K., Willett C.D., and Knight P.C., 2000. Interparticle forces in fluidiza-

tion: a review. *Powder Technol.*, **113**: 261.

[29] Rhodes M.J., Wang X.S., Nguyen M., Stewart P., and Liffman K., 2001. Use of discrete element method simulation in studying fluidization characteristics: influence of interparticle forces. *Chem. Engng. Sci.* **56**: 69.

[30] Ye M., van der Hoef M.A., and Kuipers J.A.M., 2004. A numerical study of fluidization behavior of Geldart A particles using a discrete particle model. *Powder Technol.*. **139**: 129.

[31] Loezos P.N., Costamagna P., and Sundaresan S., 2002. The role of contact stresses and wall friction on fluidization. *Chem. Engng. Sci.*. **2002**: 5123.

5

Kinetic theory of granular flows for Geldart A particles: test by a discrete particle model

ABSTRACT

The classical two-fluid model, based on the kinetic theory of granular flows (KTGF), provides a very promising theoretical framework for predicting large-scale gas-solid two-phase flows. However, thus far the two fluid model has not been successful in describing gas-solid flows of Geldart A particles. As the kinetic theory was originally developed for cohesiveless particles, it is essential to check if the theory can still work for Geldart A particles, which are slightly cohesive. In this research, a soft-sphere discrete particle model (DPM) is used to study the detailed particle-particle interactions in periodic boundary domains, where interparticle van der Waals forces are taken into account, and with no gas phase present. In our simulations, we (1) compare the results for both the hard-sphere and the soft-sphere discrete particle model for cohesiveless particles, with the theoretical predictions obtained from the kinetic theory of granular flows, and (2) study the effect of the cohesive forces in the soft-sphere model and explore a way to modify the current kinetic theory according to the soft-sphere DPM simulation results. The information obtained from these simulations can be further incorporated into the KTGF based two-fluid model.

Based on: M. Ye, M. A. van der Hoef and J. A. M. Kuipers, 2004. From discrete particle model to a continuous model of Geldart A particles. Accepted by *Chemical Engineering Research and Design.*

5.1 Introduction

Group A particles of the Geldart classification [1] are often encountered in chemical engineering. An important example is the fluid catalytic cracking (FCC) catalysts, which are widely used for production of gasoline from oil. For certain gas velocities, this type of particles are found to display a unique homogeneous expansion in gas-fluidized bed reactors, where the solid fraction is normally very high (in the range of 0.5∼0.6). However, up to date, the physical mechanism behind this homogeneous fluidization is still not completely understood. This greatly prevents construction of a reliable continuous model for dense gas-solid two-phase flow with Geldart A particles. Such models, however, are of great practical interest in the design and scale-up of engineering-size scale fluidized bed reactors.

Recently Lettieri et al. [2] used the particle-bed model, originally developed by Chen et al. [3], to investigate the homogeneous fluidization of Geldart A particles. It was demonstrated that a homogeneous expansion can be obtained in this particle-bed model, however, in this particle-bed model an artificial particle-phase elasticity force is required. In the past decades, two-fluid models based on the kinetic theory of granular flows (KTGF) have experienced a rapid development and are widely applied to various types of gas-solid two-phase flows [4–7]. However, most of the studies have focused on either large particles (Geldart B or D particles) or dilute systems (circulating fluidized beds). Very little work has been done on dense systems of fine particles, in particular Geldart A particles. Recently, McKeen and Pugsley [8] reported a simulation of bubbling fluidization of Geldart A particles. It was shown that without modifying the drag laws, the bed expansion is over-predicted and the flow patterns observed in the simulations depart significantly from those observed in real bubbling fluidized beds. Since the diameter of Geldart A particles is less than 120 μm, it is expected that the surface cohesion between particles will play a role in the fluidization behavior. McKeen and Pugsley [8] argued that due to cohesion, the particles would tend to form clusters, which will reduce the average drag force acting on a single particle. Nevertheless, the influence of the cohesion on the KTGF has not been fully investigated. The KTGF was originally developed from the kinetic theory of dense gases, by taking into account the inelasticity of particle-particle collisions [9]. Recently, Kim and Arastoopour [10] tried to extend the kinetic theory to cohesive particles, however, the final expression for the particulate stress is quite complex and difficult to incorporate in the current continuous models.

In this chapter, a soft-sphere discrete particle model (DPM) will be used to test the kinetic theory of granular flows, with the emphasis on the excess compressibility since it plays a central role in calculation of particle phase pressure and other transport coefficients. In order to test our simulation procedure, we first compare the results from both the soft-sphere model and the hard-sphere model for simple elastic spheres with the prediction from kinetic theory. Once we have established that the soft-sphere model yields results similar to those from the hard-sphere model, we investigate the effect of the "heating" procedures, the coefficients of restitution, and the spring stiffness on the excess compressibility. Finally, we turn

on the cohesive forces and investigate the influence of the cohesion on the excess compressibility. Note that at present, the effect of the gas phase is not considered.

5.2 Kinetic theory of granular flows

5.2.1 Elastic particles

If no energy dissipation is present during particle-particle collisions, the kinetic theory of molecular gases, as originally developed by Chapman and Enskog [11], can be applied directly. The simplest situation is the ideal gas, where the motion of particles is considered as the only source for momentum and kinetic energy transfer in the system. In that case the particulate pressure p_0, the shear viscosity μ_0 and thermal conductivity λ_0 are [11]:

$$p_0 = nk_BT \tag{5.1}$$

$$\mu_0 = \frac{5}{16d^2}\sqrt{\frac{mk_BT}{\pi}} \tag{5.2}$$

$$\lambda_0 = \frac{75mk_B}{64d^2}\sqrt{\frac{mk_BT}{\pi}} \tag{5.3}$$

where n is the particle number density, k_B the Boltzmann constant, m is the mass of a single particle, d the particle diameter, and T the granular temperature, which is defined as:

$$T = \frac{2E_k}{3Nk_B} \tag{5.4}$$

with E_k representing the kinetic energy of the system, and N the particle number. For the dense gas system, however, the collisions between particles will also contribute significantly to the transfer of momentum and kinetic energy. The effect of the particle-particle collisions was first studied by Enskog [11]. Based on the standard Enskog theory (SET), the particle pressure is given by:

$$p_1 = nk_BT(1 + 4\varepsilon_s\chi) \tag{5.5}$$

where ε_s is the solid volume fraction, and χ the radial distribution function. From Eq.(5.1), it follows that Eq.(5.5) can be rewritten in term of the excess compressibility $y_1 = 4\varepsilon_s\chi$,

$$p_1 = p_0(1 + y_1) \tag{5.6}$$

According to the SET, the shear viscosity and the thermal conductivity are completely determined by the excess compressibility via:

$$\mu_1 = 4\varepsilon_s\mu_0\left(\frac{1}{y_1} + \frac{4}{5} + 0.7614y_1\right) \tag{5.7}$$

$$\lambda_1 = 4\varepsilon_s\lambda_0\left(\frac{1}{y_1} + \frac{6}{5} + 0.7574y_1\right) \tag{5.8}$$

5.2.2 Inelastic particles

For the inelastic particles, there is a general consensus on the form of the particle pressure in the literature, which is given as [9]:

$$p_2 = p_0 \left[1 + 2(1+e)\varepsilon_s \chi\right] \tag{5.9}$$

In the case of $e = 1$, Eq.(5.9) reduces to Eq.(5.5). We can write Eq.(5.9) again in terms of an excess compressibility y_2:

$$p_2 = p_0(1 + y_2), \tag{5.10}$$

with

$$y_2 = 2(1+e)\varepsilon_s \chi = y_1 + 2(e-1)\varepsilon_s \chi.$$

The effect of the dissipation is thus that the excess compressibility is modified by a factor $(e+1)/2$ compared to the elastic case. In terms of the modified excess compressibility y_2, the expression for the shear viscosity and thermal conductivity then take the same form as Eq.(5.7) and (5.8), only with a slightly different prefactor [7]:

$$\mu_2 = 4.064\varepsilon_s \mu_0 \left(\frac{1}{y_2} + \frac{4}{5} + 0.761 y_2\right) \tag{5.11}$$

$$\lambda_2 = 4.10052\varepsilon_s \lambda_0 \left(\frac{1}{y_2} + \frac{6}{5} + 0.748 y_2\right) \tag{5.12}$$

5.2.3 Radial distribution function

As shown in the previous paragraph, the radial distribution function χ is of fundamental importance in the kinetic theory of dense granular flows. In essence, the radial distribution function gives the correction to probability of a collision due to the presence of other particles. In the case of slightly inelastic collisions, where the collisional anisotropy plays a negligible role, the radial distribution function only depends on the local particle volume fraction. In the kinetic theory of granular flows, normally only the value at the point of contact is of interest. Therefore in literature, the radial distribution at the point of particle contact is mostly given as $\chi_0(\varepsilon_s)$.

In the early work of granular flows [9], the radial distribution function for dense rigid spherical gases proposed by Carnahan and Starling [12] is applied:

$$\chi_0(\varepsilon_s) = \frac{2 - \varepsilon_s}{2(1-\varepsilon_s)^3}. \tag{5.13}$$

This expression is in almost exact agreement with the results from molecular dynamics simulations for particle volume fractions up to about 0.55, but above this it predicts values that are too low. To obtain better agreement for high volume fractions, and prevent particle volume fractions higher than the theoretically

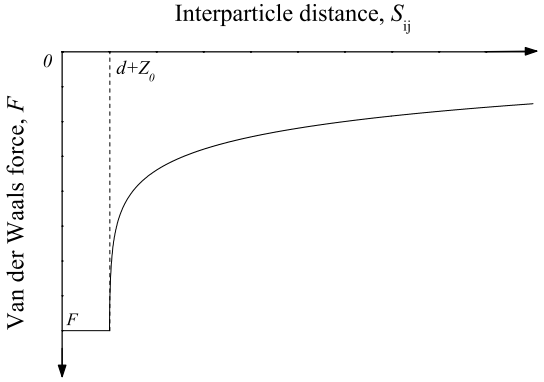

Figure 5.1: *The interparticle van der Waals force according to the Hamaker theory.*

maximum packing density for uniform spheres, $\varepsilon_s^{max} = 0.7405$, Savage [13] used a simple approximate expression for the radial distribution in his later work:

$$\chi_0(\varepsilon_s) = \left[1 - \left(1 - \frac{\varepsilon_s}{\varepsilon_s^{max}}\right)^{1/3}\right]^{-1}. \tag{5.14}$$

Subsequently, Ding and Gidaspow [5] modified Eq.(5.14) to get a better match with the molecular dynamics data of Alder and Wainright [14] for high solid fractions:

$$\chi_0(\varepsilon_s) = \frac{3}{5}\left[1 - \left(1 - \frac{\varepsilon_s}{\varepsilon_s^{max}}\right)^{1/3}\right]^{-1}. \tag{5.15}$$

However, this radial distribution function does not approach 1 for dilute systems. The best fit to the data by Alder and Wainright [14] is presented by Ma and Ahmadi [15]:

$$\chi_0(\varepsilon_s) = \frac{1 + 2.5\varepsilon_s + 4.5904\varepsilon_s^2 + 4.515439\varepsilon_s^3}{\left[1 - (\varepsilon_s/\varepsilon_s^{max})^3\right]^{0.67802}} \tag{5.16}$$

with $\varepsilon_s^{max} = 0.64356$.

5.3 Discrete particle model

In a discrete particle model, the equations of motion of the particles are solved for each individual particle. The discrete particle models can be roughly divided into two groups: time driven ("soft-sphere") and event-driven ("hard sphere"). In hard-sphere simulations the particles are assumed to interact through instantaneous, binary collisions. In between the collisions, one has free flight of the particles (no force), so the system evolves directly from one collision to the next [16, 17].

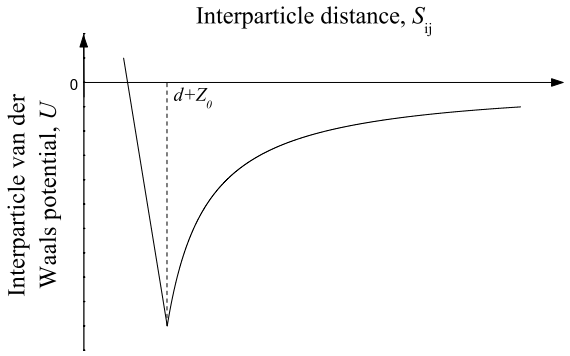

Figure 5.2: *The interparticle van der Waals potential according to the force shown in Figure 5.1.*

In soft-particle simulations, the system evolves in time from Newton's law, using a fixed time step, and the particles are allowed to overlap slightly [18, 19]. The contact forces are calculated from the deformation history of the contact, for which different models can be used. The simplest and most widely used soft-sphere approach is the linear spring/dash-pot model originally developed by Cundall and Strack [20]. In this study, we will use the soft-sphere approach, although the hard-sphere interaction was a basic assumption in developing the kinetic theory. The reasons for using the soft-sphere model are twofold: (1) in the hard-sphere approach the occurrence of multiple contacts at the same time is not possible; (2) the incorporation of cohesive force between particles is not straightforward in the hard-sphere model, since the update of the coordinates in that model is not based on forces.

5.3.1 Contact force

Following the approach by Cundall and Strack [20], the contact force between two spheres is formulated by

$$\mathbf{F}_{ij}^{(c)} = -K\delta\,\mathbf{n}_{ij} - \eta\,\mathbf{v}_{ij} \tag{5.17}$$

where K is the spring stiffness, δ the overlap between particles, $\mathbf{n}_{ij}$ the unit vector pointing from particle i to j, $\mathbf{v}_{ij}$ the relative velocity between particles. The damping coefficient η is determined by the coefficient of restitution e. The details of this model can be found in Chapter 2. No frictional force has been considered at present since it typically is ignored in the KTGF.

5.3.2 Cohesive force

The cohesive interactions between particles are typically short-range in nature. Subject to different conditions, the cohesive forces can include van der Waals

forces, liquid bridges, etc. In "dry" granular flows of fine particles, the van der Waals force is the dominating cohesive force, and will be the only one considered in this study. The formulation of the interparticle van der Waals force was first derived by Hamaker [21]. For two spheres with the same diameter d, and with interparticle distance (from center to center) $r_{ij} > d$, the van der Waals force equals

$$\mathbf{F}_{ij}^{(v)} = \frac{Ad}{12Z_{ij}^2}\mathbf{n}_{ij}, \tag{5.18}$$

with Z_{ij} $(= r_{ij} - d)$ the intersurface distance. To avoid the singularity that arises when two spheres are at contact ($Z_{ij} = 0$), we define the van der Waals force for $Z_{ij} \leq Z_0$ as:

$$\mathbf{F}_{ij}^{(v)} = \frac{Ad}{12Z_0^2}\mathbf{n}_{ij}, \tag{5.19}$$

where Z_0 is a pre-defined cut-off value. The interparticle potential corresponding to these forces is:

$$U = -\frac{Ad}{12Z_{ij}} \quad (Z_{ij} > Z_0), \tag{5.20}$$

$$U = -\frac{Ad}{12Z_0^2}(r_{ij} - d) \quad (Z_{ij} \leq Z_0), \tag{5.21}$$

In Figures 5.1 and 5.2, we show the interparticle van der Waals interaction as a function of the interparticle surface distance. Note that the minimum of the cohesive potential is:

$$U_{\min} = -\frac{Ad}{12Z_0}. \tag{5.22}$$

In a system with gravity present, the magnitude of the cohesive force is normally related to the weight of a single particle. Since the gravitational forces are absent in this work, it is essential to find different gauge for the cohesive force. As in molecular simulations, we scale the cohesive potential with the average kinetic energy of a single particle. Thus we define a scaling factor φ as:

$$\varphi = \frac{|U_{\min}|}{k_B T} = \frac{Ad}{12Z_0} \cdot \frac{1}{k_B T}. \tag{5.23}$$

For a particle with a diameter $d < 100\mu\,\mathrm{m}$, a value $Z_0 = 4.0$ nm is commonly used [22]. In this research, we keep the ratio d/Z_0 constant, which has a value of

$$\frac{d}{Z_0} \sim 2.5 \times 10^5.$$

We take the radius of a single particle as the unit of length in this research, i.e. $r = 1.0$; In these units the cut-off value of the inter-surface distance is set to $Z_0 = 8.0 \times 10^{-6}$. Furthermore the Boltzmann constant k_B is defined as 1.0, so that scaling factor φ equals

$$\varphi = \frac{5}{24} \times 10^5 \frac{A}{T}. \tag{5.24}$$

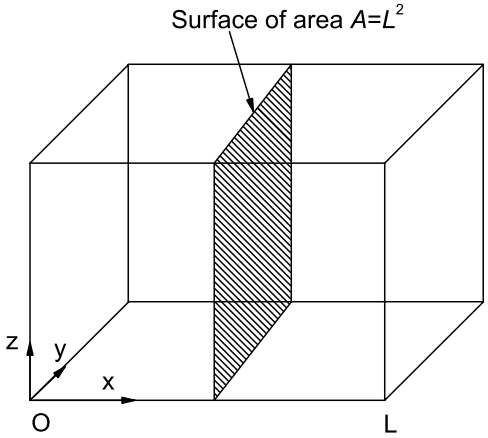

Figure 5.3: *The imaginary surface inside the cubic box.*

It is also important to compare the magnitudes of the cohesive forces with the contact force. As the maximum overlap between two particles was pre-defined as $0.005d$, the maximum contact force will be $0.005Kd$. The ratio between the cohesive force and contact force is then

$$\frac{F_{ij}^{(v)}}{F_{ij}^{(c)}} \sim \frac{1}{0.005Kd} \cdot \frac{Ad}{12Z_0^2} = 2.6 \times 10^{11} \frac{A}{K}. \tag{5.25}$$

In any case we should keep the ratio $F_{ij}^{(v)}/F_{ij}^{(c)}$ in the range 0∼10% to prevent very strong cohesion between particles, since that could give rise to clusters, the study of which is beyond the scope of this research.

The measurement of key quantities in discrete particle model provides a close look of the physics of these quantities. In the next part, the methods that are used to measure the particle pressure P and shear viscosity μ_p in the soft-sphere code are described.

5.4 Particle pressure Measurement

We consider a cubic box having a volume V and side length L, which contains N particles. Imagine an arbitrary surface of area $A = L^2$ inside the box, see Figure 5.3. For convenience, it is assumed that this surface is perpendicular to the x axis. The particle pressure can be defined as the force per unit area acting normal to this surface

$$P_x = \frac{F_x}{A} \tag{5.26}$$

According to Newton's second law, this can be written as

$$P_x = \frac{1}{A} \cdot \frac{d(mx)}{dt} \tag{5.27}$$

The overall particle phase pressure is

$$P_p = \frac{1}{3}(P_x + P_y + P_z) \tag{5.28}$$

Thus the pressure is actually a momentum flux, which is the amount of momentum that crosses a unit area of the surface in unit time. In general this flux is composed of two parts: (a) P_m, the momentum carried by the particles themselves as they cross the area during the time interval dt. This part is called kinetic pressure. (b) P_f, the momentum transferred as a result of forces acting between particles that lie on different sides of the surface. This term is called collision pressure. So we have

$$P_p = P_m + P_f \tag{5.29}$$

The kinetic pressure P_m, which is the momentum flux carried by the motion of particles, can be directly obtained from the kinetic energy:

$$P_m = \frac{2N}{3V}\bar{E}_k. \tag{5.30}$$

An expression for P_f in terms of the interparticles forces can be obtained via the virial theorem. This gives that (e.g. see Haile [23]) P_f can be written as

$$P_f = \frac{1}{A}\sum_i \sum_j \mathbf{F}_{ij} \cdot \mathbf{r}_{ij}, \tag{5.31}$$

where F_{ij} is the pair-wise interparticle force. Thus the total instantaneous particle pressure P_p is given as

$$P_p = \frac{2N}{3V}\bar{E}_k + \frac{1}{A}\sum_i \sum_j \mathbf{F}_{ij} \cdot \mathbf{r}_{ij}. \tag{5.32}$$

The collision pressure, if normalized by the kinetic pressure, is actually the so-called excess compressibility y. For the soft-sphere model, the excess compressibility y is given by

$$y = \frac{1}{2\bar{E}} \sum_{i=1}^{N-1} \sum_{j=i+1}^{N} \mathbf{F}_{ij} \cdot \mathbf{r}_{ij}, \tag{5.33}$$

while for the hard-sphere model [23]

$$P_p = \frac{m}{2\bar{E}t} \sum_{i=1}^{N_c} \Delta\, \mathbf{v}_{ij} \cdot \mathbf{r}_{ij}. \tag{5.34}$$

Table 5.1: *parameters used in the simulations.*

Parameters	Value
Particle number, N	500
Particle radius, r	1
Particle density, ρ_s,	1
(Soft-sphere model) Normal spring stiffness, K,	70000
Time step, Δt	10^{-4}
Granular temperature, T, 1 or 0.01	
Boltzmann constant, k_B,	1
Cut-off value for inter-surface distance between particles, Z_0,	10^{-6}

Note: all parameters are normalized.

5.5 Simulation procedure

In this research, periodic boundary domains are used in order to minimize the effects of the size of the container, since we have a relatively small amount of particles ($N = 500$) in our system, for reasons of computational efficiency. Due to the inelastic collisions, the particles will continuously dissipate energy, which would eventually cause the particles come to a quiescent state. In this work, we therefore drive the system by two different techniques: (1) rescaling the particle velocities every time step, according to the desired granular temperature; (2) accelerating the particles randomly. All the parameters are normalized by the particle radius, particle density, and granular temperature. The parameters that are not varied in the simulations are listed in Table 5.1. The values of other parameters will be given in the appropriate section.

5.5.1 Rescaling

In this procedure, suppose $\mathbf{v}^{(0)}$ is particle velocity vector at the end of each time step, we rescale the particle velocity by

$$\mathbf{v} = L\mathbf{v}^{(0)}, \tag{5.35}$$

where L equals

$$L = \sqrt{\frac{3N_{part}T}{2E^{(0)}}}. \tag{5.36}$$

Here $E^{(0)}$ is the kinetic energy at the end of each time step.

5.5.2 Random accelerating

Another method of driving is by applying a random force to each particle. In this case, the velocity $\mathbf{v}$ is given by

$$\mathbf{v} = \mathbf{v}^{(0)} + \alpha\, R\mathbf{u}\Delta t, \tag{5.37}$$

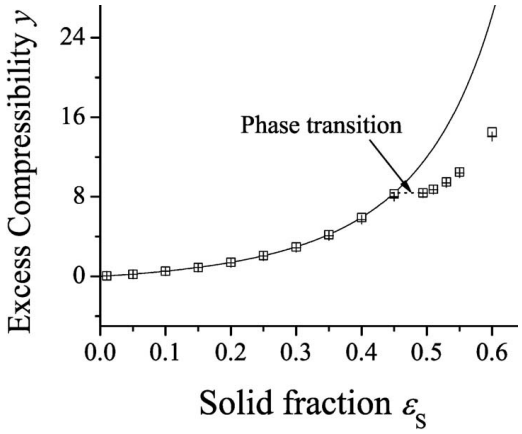

Figure 5.4: *Simulation results for both the soft-sphere model (squares) and the hard-sphere model (the crosses), compared to the Carnahan-Starling equation (solid-line). The particles are initially arranged in a face-centered cubic (FCC) configuration. Spring stiffness* $K = 70000$*, Hamaker constant* $A = 0.0$*, granular temperature* $T = 1.0$*, and coefficient of restitution* $e = 1.0$*. The system is driven by rescaling.*

where $R \in (-1, 1)$ is a random number, and $\mathbf{u}$ the unit vector. The parameter α is used to control the magnitude of the acceleration.

5.6 Results

5.6.1 Comparisons with the hard-sphere results

First, we should check whether the soft-sphere model gives results comparable to those from the hard-sphere model. To this end, we carried out several sets of simulations with particles starting either from random positions or face-centered cubic (FCC) positions. The hard-sphere simulation results for these two configurations have been well documented by many researchers [12, 24–26]. It has been shown that the Carnahan-Starling equation can excellently represent these results up to the solid-fraction of 0.55 [12]. According to the Carnahan-Starling equation, the excess compressibility of a hard-sphere system can be represented as:

$$y = \frac{4\varepsilon_s - 2\varepsilon_s^2}{(1-\varepsilon_s)^3}. \tag{5.38}$$

In Figure 5.4 we show our simulation results for smooth, elastic and cohesiveless spheres in periodic boundary domains, where the particles are initially placed in the face-center cubic (FCC) grids. For such systems, Hoover et al. [25] observed a phase transition from the fluid state to a solid state at $y = 7.27$. As can be seen, both the hard-sphere and soft-sphere simulations clearly display this transition point.

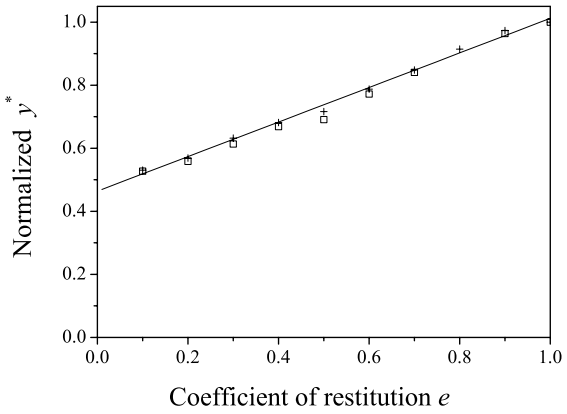

Figure 5.5: *Excess compressibility as in Figure 5.4, but now as a function of the coefficient restitutions, for one solid fraction ($\varepsilon_s = 0.05$). The excess compressibility has been normalized by y obtained in the case of coefficient of restitution $e = 1.0$. The system is driven by rescaling.*

We also compared the simulation results with inelastic spheres, which are shown in Figure 5.5. The solid fraction in the initial configuration is fixed at 0.05. It is shown that in this dilute system, the soft-sphere model can reproduce the results of the hard-sphere simulations, and both simulations results are in agreement with Eq.(5.38) (solid line). We will show in the following sections, thar also for the dense system, very good agreement between the hard-sphere and soft-sphere results can be found. The conclusion is therefore that the soft-sphere model can be used as an alternative for the hard-sphere model, as far as the calculation of the excess compressibility is concerned.

5.6.2 Effect of the procedures

To accurately calculate the excess compressibility, it is essential to have the system in an equilibrium state. As discussed before, the collisions between particles will dissipate kinetic energy of the system, so that an equilibrium state can only be reached when the system is driven by external forces. The two procedures discussed above can in principle be used to drive the system. However, we find these two procedures can lead to different behaviors of the granular system. In Figure 5.6, we show the simulation results for the face-centered cubic (FCC) configurations driven by rescaling procedure. As can be seen, for all solid fractions an equilibrium state is reached. However, this equilibrium is found to be metastable, as after some time (depending on the solid fraction) the compressibility already decreases. This break-down of the equilibrium might be due to the formation of clusters, which is a well-known feature of granular system with inelastic collisions. However, it is extremely difficult to distinguish the clusters from the snapshots in very dense sys-

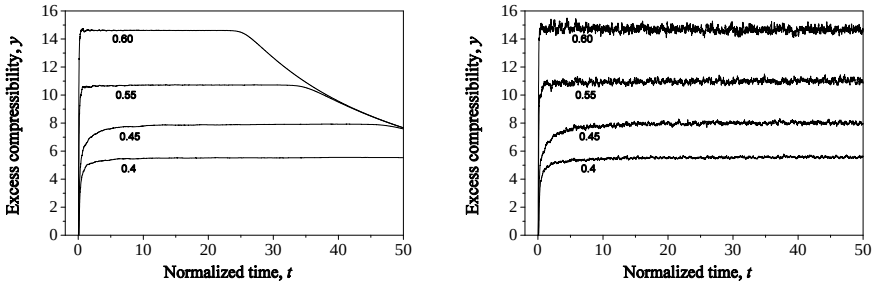

Figure 5.6: *The evolution of excess compressibility for dense systems with solid fraction* $\varepsilon_s = 0.40, 0.45, 0.55$*, and 0.60, respectively. The coefficient of restitution* $e = 0.9$*. The particles are initially arranged in a face-centered cubic (FCC) configuration. The system is driven by either rescaling (left) or random acceleration (right).*

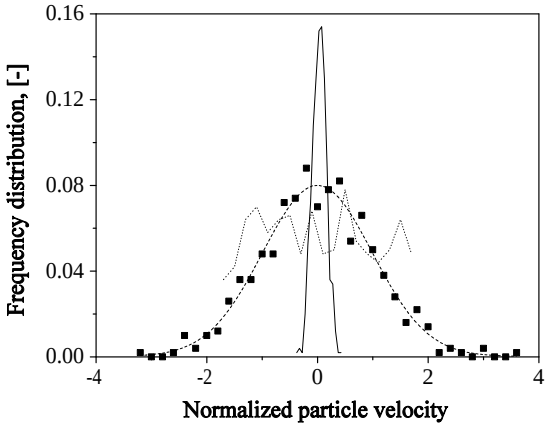

Figure 5.7: *The instantaneous velocity distribution for a granular system with solid fraction* $\varepsilon_s = 0.60$*. The excess compressibility is shown in Figure 5.6. The velocity distribution is taken for the* y *direction at: t=0 (dotted line); t=25 (squares); and t=35 (solid line). The dash line is a fit of the squares using a Gaussian function.*

tems. Alternatively, we check the velocity distribution of particles. In Figure 5.7, the typical instantaneous velocity distributions for different instants have been shown. The initial velocities of particles are generated randomly. After a sufficient number of particle-particle collisions, the velocity distribution develops into a Gaussian distribution, which leads the system to an equilibrium state. But after a quite large number of collisions, the velocity distribution becomes very narrow, which means most of particles are having a very small velocity or even at rest. This may indicate that denser regimes have formed where particles experience more frequent collisions, and their kinetic energy dissipates more quickly. Thus the velocities of particles in the denser regime are relatively smaller than particles in the dilute regime. In the rescaling procedure, the slower particles will gain less kinetic energy and remain slower.

This break-down is also found in random configurations. In Figure 5.8 we show the simulation results for random systems. As can be seen, the system quickly transforms to a non-equilibrium state and it is difficult to get the statistical information for the equilibrium sate. It is not clear at present whether the transition from the equilibrium to the non-equilibrium is an inherent phenomenon or not. Also, it is not understood why in the non-equilibrium state, the curves for y seem to collapse onto one single curves (see Figure 5.6). Nevertheless, the transition to the non-equilibrium state can be avoided by using the random acceleration procedure. In Figure 5.6 we show the results using this method. It is clearly demonstrated that, at least within current simulation time, that the system remains in equilibrium. Also, the plateau value for y corresponds with the intermediate plateau value of the metastable state of the system driven by scaling.

However, we would point point that, although the random acceleration procedure can generate a stable equilibrium state, it requires a relatively longer simulation time. On the other hand, the rescaling procedure is quite efficient for lower solid fractions (less than 0.45). Thus in this study, if not specified, the random acceleration procedure will be used to simulate the denser system with a solid fraction higher than 0.45 while the rescaling procedure is used to lower solid fraction (less than 0.45), where we take the plateau value found in the metastable equilibrium state as the final results for the excess compressibility.

5.6.3 Dependence on the spring stiffness

Although the linear spring/dashpot model provides a convenient way to calculate the interparticle contact force, it is still too simple for investigating the detailed particle-particle interactions. For example, the definition of the spring stiffness, K, is somewhat artificial in this model. It has been argued that a rigorous selection of the spring stiffness should be directly related to the material properties of the particles. Yet this may lead to a relatively large value of the spring stiffness, and consequently an unrealistic small time step for the discrete particle simulations. In our soft-sphere model, the selection of the spring stiffness is based on the following criteria: (1) the corresponding time step should be reasonable; (2) the overlap should have a maximum value equal to 0.5% of the diameter of the particle. Clearly

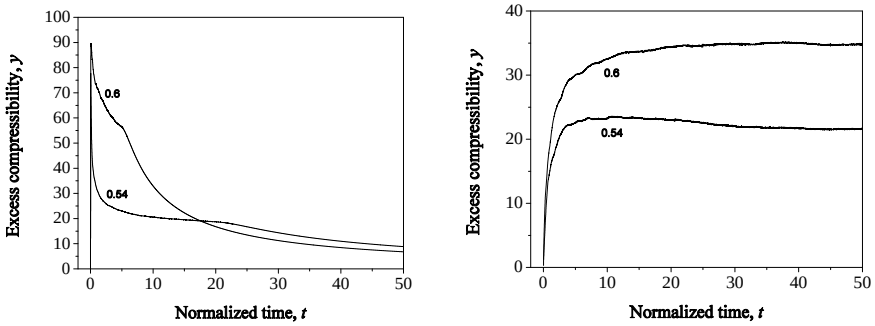

Figure 5.8: *The instantaneous velocity distribution for a granular system with solid fraction $\varepsilon_s = 0.54$ and 0.60. The coefficient of restitution $e = 0.9$. The particles are initially placed randomly. The system is driven by either rescaling (left) or random acceleration (right).*

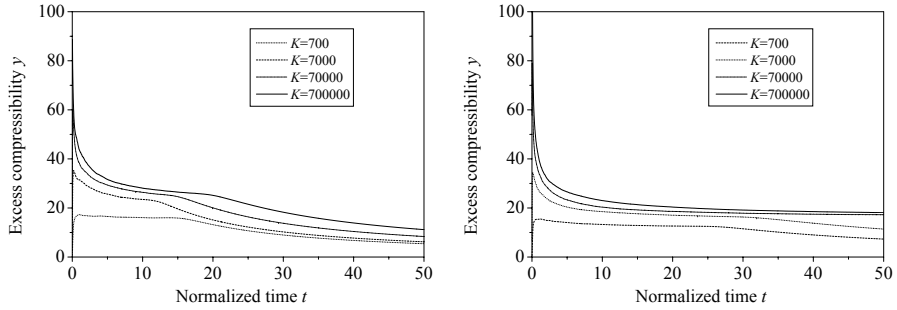

Figure 5.9: *The evolution of the excess compressibility in soft-sphere simulations for random initial particle positions. Hamaker constant $A = 0.0$, granular temperature $T = 1.0$, and solid fraction $\varepsilon_s = 0.54$, and the coefficient of restitution $e = 0.9$ (right) and 1.0 (left). The system is driven by rescaling.*

the larger the spring stiffness, the closer it resembles a hard-sphere system. Yet, the computation will be very expensive. The classical kinetic theory of granular flows is based on the assumption of instantaneous and binary collisions of hard-spheres. In soft-sphere simulations with a finite spring stiffness, multiple contacts will always be present. Therefore, it is a prerequisite to investigate how the presence of multiple contacts will influence the kinetic theory of granular flows. To this end, we carry out two sets of simulations with exactly the same initial configuration, using four different spring stiffness: 700, 7000, 70000, and 700000. In the first and second set of simulations the coefficient of restitution is set to 1.0 and 0.9, respectively. In both sets of simulations, the solid fraction is fixed to 0.54, which is a dense regime typically encountered in the homogeneous fluidization of Geldart A particles.

In Figure 5.9, we show the evolution of the excess compressibility with time. For small spring stiffness ($K = 700$ or 7000), the system displays the feature of a non-equilibrium state for both elastic and inelastic system, since the excess com-

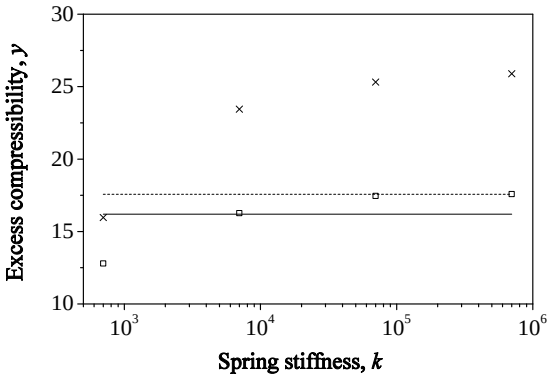

Figure 5.10: *The comparisons with the excess compressibility from different spring stiffness. The simulation conditions are specified in Figure 5.9. Crosses are the simulation results for* $e = 0.9$*, and squares for* $e = 1.0$*. The solid line represents the correlation by Ma and Ahmadi, and dash line represents the correlation by Carnahan and Starling.*

pressibility continuously decreases with time, and the equilibrium "plateau" value is not reached. This suggests that an artificially small spring stiffness may lead to the failure of prediction of excess compressibility. For large spring stiffness ($K =$ 70000 and 700000), the simulations with a system of elastic particles ($e = 1.0$) are shown in Figure 5.9. As can be seen, an equilibrium state is reached. In Figure 5.10 we compare the steady state values with correlations for hard-sphere systems. From Figure 5.10, it can be argued that a reasonably large spring stiffness can be used to get the correct excess compressibility. We also check with an inelastic system ($e = 0.9$). For large spring stiffness ($K = 70000$ and 700000) only a short equilibrium phase has first been established, after which a break-down of this equilibrium state is observed (as shown in Figure 5.9). As discussed before, this indicates that the dissipative nature of the particle-particle collisions will lead the system to form clusters, which leads to a non-equilibrium state. The excess compressibility is over-predicted for inelastic systems. Therefore to calculate the excess compressibility for dense inelastic systems, it is essential to use the random acceleration procedure.

5.6.4 Effect of the coefficient of restitution

As can be seen from Eq.(5.9), the kinetic theory of granular flow predicts that the excess compressibility is a linear function of the coefficient of restitution e,

$$y = 2(1 + e)\varepsilon_s\chi. \tag{5.39}$$

Note that the Eq.(5.9) is derived under the assumption that the particles are slightly inelastic, i.e. $e \sim 1.0$. Therefore, it is necessary to examine the effect of the coefficient of restitution on the excess compressibility and check the validity of Eq.(5.9).

We performed several sets of simulations for different coefficients of restitution. As was discussed above, in the case of dense regime, the rescaling procedure will not lead to a steady excess compressibility. Thus we use the random acceleration procedure for the solid fraction higher than (including) 0.45 and the rescaling procedure for solid fraction less than 0.45. In Figure 5.11, the excess compressibility has been shown as a function of the solid fraction for different coefficients of restitution e. These results are compared with the Eq.(5.39), where the radial distribution function χ is taken either from the Ma-Ahmadi correlation or from the Carnahan-Starling correlation. As can be seen the excess compressibility agrees well with both correlations for a solid fraction ε_s up to 0.55. For extremely dense systems, i.e. $\varepsilon_s > 0.55$, the Ma-Ahmadi correlation presents a much better estimate of the excess compressibility for slightly elastic particles ($e = 0.8 \sim 1$). A more detailed comparison with the Ma-Ahmadi correlation is shown in Figure 5.12. Therefore the Ma-Ahmadi correlation is suggested to be a good representative of the radial distribution function in the kinetic theory of granular flows.

5.6.5 Effect of the cohesive force

For Geldart A type particles, the cohesive van der Waals forces cannot be neglected. However, the influence of such forces on the excess compressibility has not been reported before. In Figure 5.12, the results for the excess compressibility for different Hamaker constants A are shown. For simplicity a coefficient of restitution $e = 1.0$ is used. We consider two different Hamaker constants: $A = 3.0 \times 10^{-12}$ and $A = 3.0 \times 10^{-10}$. From Figure 5.12, we see that for these two Hamaker constants, the simulation results show a very good agreement with Eq.(5.39) if the radial distribution function χ is calculated from the Ma-Ahmadi correlation. Only a very small deviation has been found in the dense regimes, which suggests that the cohesion has only a quite weak influence on the excess compressibility, at least for the values of Hamaker constant that we studied.

However, it should be noted that the quantification of the cohesive force is not straightforward, since there is no reference force (such as gravitational force) in these systems. We consider these systems as slightly cohesive since the ratio of the cohesive potential and the average kinetic energy per particle is small, i.e. $\varphi = 6.25 \times 10^{-8} \sim 6.25 \times 10^{-6}$. At the same time, the ratio between the cohesive force and contact force ranges from 1.11×10^{-5} to 1.11×10^{-3}. If a strong cohesive force is present, particles in the system may form complicated structures, whereas a homogeneous state is one of the basic assumptions underlying the kinetic theory of granular flow. It is extremely difficult to directly measure the cohesive forces between Geldart A particles since this type of forces strongly depend on the surface properties of particles. From our simulation results, it becomes clear that the kinetic theory of granular flows still holds for slightly cohesive granular system.

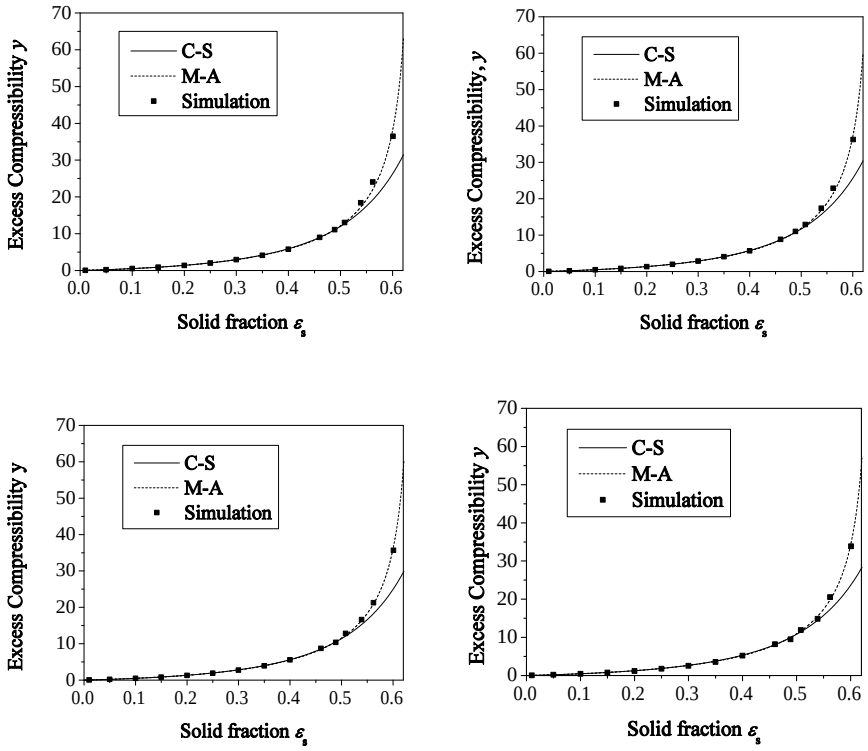

Figure 5.11: *The excess compressibility from soft-sphere simulations, with random initial particle positions. Hamaker constant $A = 0.0$, granular temperature $T = 1.0$, and the coefficient of restitution (a) $e = 1.0$ (top-right); (b) $e = 0.95$ (top-left); (c) $e = 0.90$ (bottom-right); (d) $e = 0.80$ (bottom-left). Spring stiffness $K = 70000$. The results are compared with Eq.(5.39) based on both Carnahan-Starling (solid line) and Ma-Ahmadi (dash line) correlation.*

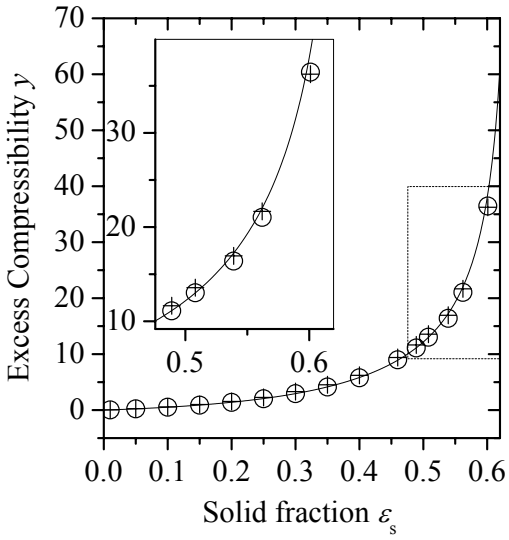

Figure 5.12: *The effect of the cohesive force on the excess compressibility. The coefficient of restitution* $e = 1.0$*, and granular temperature* $T = 1.0$*. The Hamaker constant* $A = 3.0 \times 10^{-12}$ *(circles) and* 3.0×10^{-10} *(crosses).*

5.6.6 The contribution of cohesion to the excess compressibility

In order to check to what extent the cohesive forces influence the excess compressibility, we calculate the contribution of the cohesive force to the excess compressibility, which we define as

$$y_3 = \frac{1}{2\bar{E}} \sum_{i=1}^{N-1} \sum_{j=i+1}^{N} \mathbf{F}_{ij}^{(v)} \cdot \mathbf{r}_{ij}. \tag{5.40}$$

Here $\mathbf{F}_{ij}^{(v)}$ is the van der Waals force between two spheres. In Figures 5.13 and 5.14, we show the results obtained in a system with constant granular temperature $T = 1.0$, the overall excess compressibility of which are shown in Figure 5.12. These results are plotted as a function of ε_s, ε_s^2, ε_s^3, and ε_s^4. From Figures 5.13a and 5.14a, we can see that with an increasing solid fraction the magnitude of y_3 experiences a continuous increase. Also for the same solid fraction ε_s a larger cohesive force will lead to a larger contribution y_3. For a weak cohesive force ($A = 3.0 \times 10^{-12}$), as shown in Figure 5.13(c-d), the contribution y_3 is essentially a linear function of ε_s^3 or ε_s^4, which can be well fitted by a function $y_3 \sim -C_1\varepsilon_s^3 - C_2\varepsilon_s^4$. If the cohesive interaction becomes stronger, say $A = 3.0 \times 10^{-10}$, the contribution y_3 manifests a linear dependence on the solid fraction ε_s or ε_s^2. Thus for slightly cohesive particles,

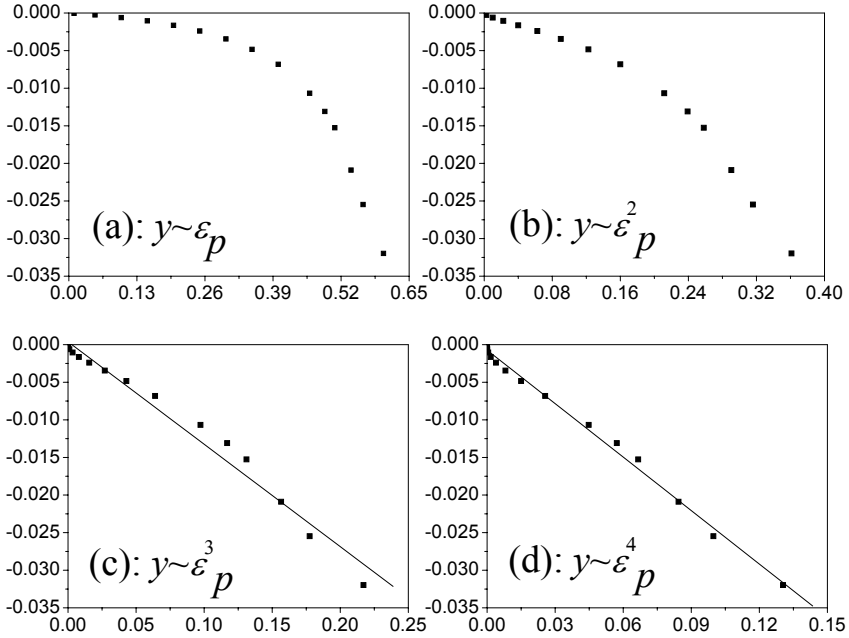

Figure 5.13: *The contribution of the cohesive force to the excess compressibility, y_3. The coefficient of restitution $e = 1.0$, granular temperature $T = 1.0$ and the Hamaker constant $A = 3.0 \times 10^{-12}$ in these results. The solid lines in (c) and (d) are linear fittings of the data.*

we can write the contribution y_3 of cohesion to excess compressibility as

$$y_3 = -\sum_{i}^{Nc} C_i \varepsilon_s^i \tag{5.41}$$

The coefficients C_i strongly depend on the magnitude of cohesive force.

5.7 Conclusion and discussions

The reliability of the classical two-fluid models for Geldart A particles depends very much on the accuracy of the correlations for drag coefficient, particle pressure, and other transport coefficients. Much research has been devoted to obtaining accurate drag correlations, from either experiments or direct numerical simulations [27]. For particle pressure and other transport coefficients, however, results are few and far between. It is becoming more popular nowadays to use the constitutive closures based on kinetic theory of granular flows for a continuous representation for the particle phase. It is still not clear whether the kinetic theory of granular flows, which was originally developed for cohesiveless particles, can

be applied to slightly cohesive systems (such as Geldart A particles). It is also not obvious to what extent the kinetic theory of granular flows can be used for dense granular systems.

In this chapter we use a soft-sphere discrete particle model to test the kinetic theory, with an emphasis on the excess compressibility as it is the key quantity in KTGF for calculating the particle pressure and other transport coefficients. However, the excess compressibility should be obtained from the equilibrium state. Due to the dissipative nature of particle-particle collision, it is not possible for a granular system to stay at equilibrium without any other external energy sources. Therefore it is essential to find some manners that can be used to continuously "heat" the granular system. On the other hand, however, the dissipation will lead to form dense regimes. In these dense regimes the particles frequently collide with others and continuously lose kinetic energy, which eventually leads to a very narrow velocity distribution. This clustering phenomenon is a typical feature of granular systems. A simple rescaling procedure is not sufficient to keep the system running for a long time in an equilibrium state. In the rescaling procedure, the fast particles will gain more energy while the slower particles will gain less energy. Since the particles in the dense regimes normally have a lower velocity, they will gradually slow down, which eventually leads to an inhomogeneous situation. In this case, it is not possible to get a steady value of excess compressibility. Therefore it is necessary to use another "heating" manner: the random accelerating approach. By accelerating each particle with a random acceleration, the granular system is found to stay in the equilibrium state. However, it is not as computationally efficient as the rescaling procedure. So for dense systems with a solid fraction higher than 0.45, we use the random accelerating procedure. The rescaling procedure can be efficiently used in dilute systems.

Clearly, the equation of state given by Eq.(5.39) can be justified for a coefficient of restitution $e \sim 1.0$, however, for high solid fraction, better prediction can be obtained if the Ma-Ahmadi correlation is taken as the radial distribution function.

For slightly cohesive particles, only a very small deviation has been found from Eq.(5.39), which suggests that with the Hamaker constants tested in the range used in this research the cohesion only has a weak influence on the excess compressibility. However, it should be noted that the quantification of the cohesive force is not straightforward, since there is no reference force (such as gravitational force) in these systems. We consider these systems as slightly cohesive since the ratio of the cohesive potential and the average kinetic energy per particle is small. It is expected that in the presence of a strong cohesive force, particles will form complicated agglomerates. In this case, an equilibrium state may not exist, for which the validity of kinetic theory of granular flows is questionable. It is extremely difficult to directly measure the cohesive forces between Geldart A particles as these forces strongly depend on the surface properties.

Basically a correction of the KTGF can be made by using a modified excess compressibility that accounts for the effects of cohesion between particles. The excess compressibility due to cohesion, y_3 depend on the magnitude of the cohesive force and solids volume fractions. For a weak cohesive force ($A = 3.0 \times 10^{-10}$), y_3 can be

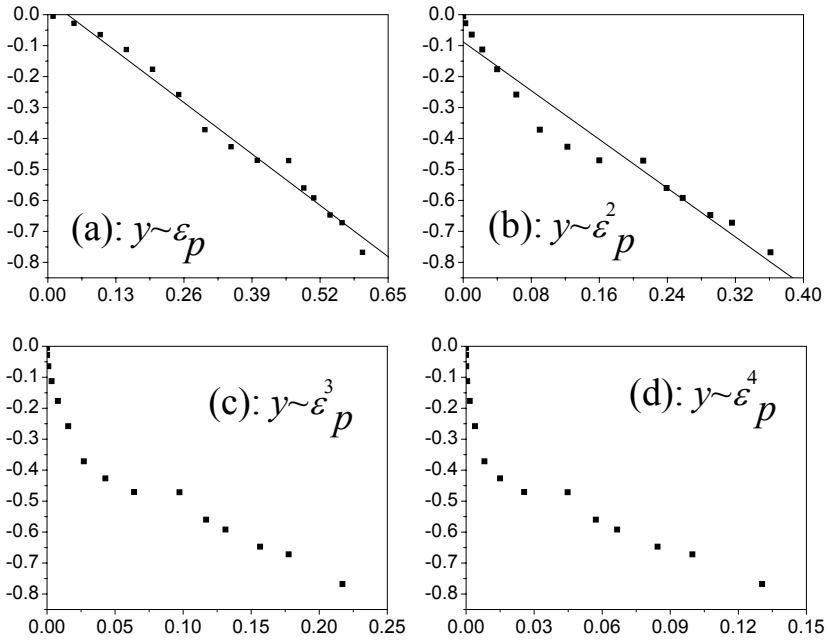

Figure 5.14: *The same as in Figure 5.13, but the Hamaker constant* $A = 3.0 \times 10^{-10}$. *The solid lines in (a) and (b) are linear fittings of the data.*

well represented by $y_3 \sim -C_1\varepsilon_s^3 - C_2\varepsilon_s^4$. For a strong cohesive force tested as well in this study, $y_3 \sim -C_3\varepsilon_s - C_4\varepsilon_s^2$.

References

[1] D. Geldart, 1973. Types of gas fluidization. *Powder Technol.*, **7**: 285.

[2] Lettieri P., Cammarata L., Micale G.D.M., and Yates J., 2003. CFD simulations of gas fluidized beds using alternative Eulerian-Eulerian modeling approaches. *Int. J. Chem. Reactor Engng.*, **1**: A5.

[3] Chen Z., Gibilaro L.G., and Foscolo P.U., 1999. Two-dimensional voidage waves in fluidized beds. *Ind. Eng. Chem. Res.*, **38**: 610.

[4] Sinclair J.L., and Jackson R., 1989. Gas-particle flow in a vertical pipe with particle-particle interactions. *AIChE J.*, **35**: 1473.

[5] Ding J., and Gidaspow D., 1990. A bubbling fluidization model using kinetic theory of granular flow. *AIChE J.*, **36**: 523.

[6] Samuelsberg, A., and Hjertager B.H., 1996. Computational modeling of gas/particle flow in a riser. *AIChE J.*, **42**: 1536.

[7] Nieuwland J.J., van Sint Annaland M., Kuipers J.A.M., and van Swaaij W.P.M., 1996. Hydrodynamic modeling of gas/particle flows in riser reactors. *AIChE J.*, **42**: 1569.

[8] McKeen T.R., and Pugsley T.S., 2003. Simulation and experimental validation of a freely bubbling bed of FCC catalyst. *Powder Technol.*, **129**: 139.

[9] Lun C.K.K., Savage S.B., Jeffrey D.J., and Chepurniy N., 1984. Kinetic theories for granular flow: inelastic particles in Couette flow and slightly inelastic particles in a general flow field. *J. Fluid Mech.*, **140**: 223.

[10] Kim H., and Arastoopour H., 2002. Extension of kinetic theory to cohesive particle flow. *Powder Technol.*, **122**: 83.

[11] Chapman S., and Cowling T.G., 1970. *The mathematical theory of nonuniform gases*. Cambridge University Press, Cambridge, UK.

[12] Carnahan N.F., and Starling K.E., 1969. Equation of state for non-attracting rigid spheres. *J. Chem. Phys.*, **51**: 635.

[13] Savage S.B., 1988. Streaming motions in a bed of vibrationally fluidized dry granular material. *J. Fluid Mech.*, **194**: 457.

[14] Alder B.J., and Wainright T.E., 1960. Studies in molecular dynamics. II. Behavior of a small number of elastic spheres. *J. Chem. Phys.*, **33**: 1439.

[15] Ma D., and Ahmadi G., 1986. An equation of state for dense rigid sphere gases. *J. Chem. Phys.*, **84**: 3449.

[16] Hoomans B.P.B., Kuipers J.A.M., Briels W.J., and van Swaaij W.P.M., 1996. Discrete particle simulation of bubble and slug formation in a two-dimensional gas-

fluidized bed: a hard sphere approach. *Chem. Engng. Sci.*. **51**: 99.

[17] Ouyang J., and Li J., 1999. Particle-motion-resolved discrete model for simulating gas-solid fluidization. *Chem. Eng. Sci.* **54**: 2077.

[18] Tsuji Y., Kawaguchi T., and Tanaka T., 1993. Discrete particle simulation of two-dimensional fluidized bed. *Powder Technol.* **77**: 79.

[19] Xu B.H., and Yu A.B., 1997. Numerical simulation of the gas-solid flow in a fluidized bed by combining discrete particle method with computational fluid dynamics. *Chem. Engng. Sci.* **52**: 2785.

[20] Cundall P.A., and Strack O.D.L., 1979. A discrete numerical model for granular assemblies. *Géotechnique*, **29**: 47.

[21] Israelachvili J., *Intermolecular & surface forces*, Academic Press, London, 1991.

[22] Seville J.P.K., Willett C.D., and Knight P.C., 2000. Interparticle forces in fluidization: a review. *Powder Technol.*, **113**: 261.

[23] Haile J.M., 1992. *Molecular dynamics simulation: elementary methods*. John Wiley & Sons, Inc., New York, USA.

[24] Alder B.J., and Wainwright T.E., 1957. Phase transition for a hard sphere system. *J. Chem. Phys.*, **27**: 1208.

[25] Hoover W.G., and Ree F.H., 1969. Melting transition and communal entropy for hard spheres. *J. Chem. Phys.*, **49**: 3609.

[26] Erpenbeck J.J., and Wood W.W., 1984. Molecular dynamics calculations of the hard-sphere equation of state. *J. Stat. Phys.*, **35**: 321.

[27] Van der Hoef M.A., Beetstra R., and Kuipers J.A.M., 2005. Lattice Boltzmann simulations of the low Reynolds number flow past mono and bidisperse arrays of spheres: results for the permeability and drag force. *J. Fluid Mech.* In press.

6

The Two-fluid Modeling of Geldart A Particles in Gas-fluidized Beds

ABSTRACT

In this chapter we investigate the effect of cohesion and drag models on the bed hydrodynamics of Geldart A particles based on the two-fluid model. For a high gas velocity $U_0 = 0.03$ m/s, we found a transition from the homogeneous fluidization to bubbling fluidization with an increase of the coefficient C_1, which is used to account for the contribution of cohesion to the excess compressibility. Thus cohesion can play a role in the bed expansion of Geldart A particles. However, in order to get a better prediction of bed expansion, the influence of the drag models should be considered as well. We test the commonly-used drag model which is given by Wen and Yu with an exponent $n = 4.65$. It has been found at low gas velocity, this drag model gives under-prediction of the bed expansion. Alternatively, we used a large exponent $n = 9.6$ reported in experimental studies of gas-fluidization, which was shown to given a better prediction of the bed expansion. These findings suggest that at low gas velocity, a scale-down of the commonly-used drag model is required. On the other hand, however, a scale-up of the commonly-used drag model is necessary at high gas velocity, for example $U_0 = 0.2$ m/s. Therefore a simple scaling-up or -down of the drag force cannot be generally adopted. A detailed study of drag model for Geldart A particles is definitely required.

6.1 Introduction

Computational Fluid Dynamics (CFD) has proved to be a powerful tool in almost every branch of single-phase flows, from aerospace propulsion to weather prediction. The applications of CFD in dispersed multi-phase flows, however, are still under development. First, due to the great variation of the properties of the dispersed phase, the establishment of a general form of the governing equations is difficult; second, a good coupling technique is necessary to fully include the interactions between the carrying phase and dispersed phase; last and most importantly, suitable closure laws for closing the set of governing equations for dispersed phase are required. A typical feature of these closure is that they should represent the average effect of detailed microscopic processes as accurately and widely applicable as possible. One of the examples is dense solid-gas two-phase flows, where the solids are being carried by a gas. Despite the fact that the particle-particle and particle-gas interactions take place at a scale smaller than the size of particles, the governing equations of both the solid and gas phase are formulated by the volume-averaged Navier-Stokes type of equations, which constitutes the so-called two-fluid model [1]. The closure laws for the gas phase are well established in single-phase flows, however, the closure laws for the solid phase lack the underlying theoretical framework of the gas phase, and have to be estimated. Normally the solid phase pressure and viscosity are either simply taken as constants or are derived from the kinetic theory of granular flows [2, 3]. The two-fluid model developed so far has been successfully applied to the solid-gas two-phase flows in many different applications [4].

A great challenge in CFD modeling of solid-gas two-phase flows is to obtain realistic predictions of the fluidization behavior of small particles such as Geldart A particles [5]. The standard two-fluid models have been used by several researchers to predict the bubbling fluidization of Geldart group A particles. Ferschneider and Mege [6] have reported a major overestimation of bed expansion in a bubbling bed of FCC particles. Bayle et al. [7] obtained the same result in a turbulent bed of FCC particles. Recently Lettieri et al. [8] used a particle-bed model, originally developed by Chen et al. [9] to investigate the homogeneous fluidization of Geldart A particles. It has been demonstrated that a homogeneous expansion can be obtained in this particle-bed model. However, in this model an artificial particle-phase elasticity force is required.

McKeen and Pugsley [10] used the two-fluid CFD code MFIX to simulate a freely bubbling bed of FCC catalyst for $U_0 = 0.05 \sim 0.2$ m/s and compared the results to experimental data obtained from ECT measurements. In accordance with the observations by Ferschneider and Mege [6], McKeen and Pugsley [10] also found that the standard CFD model greatly over-predicted bed expansion in case the standard drag closures are used. By using a scale constant of 0.25 to the standard gas-solid drag laws, they found that their results could well reproduce the experimental results. They argued that their modification can be attributed to the formation of clusters with a size smaller than the CFD grid size, leading to an overall smaller drag force acting in the particle bed. The existence of such small scale clusters have

not been reported before, certainly not for particles with a size of 75 μm. For this kind of particles, the van der Waals force will be small and therefore only slightly cohesive forces will prevail.

In fact, one of the findings of our discrete particle simulations (see chapter 3 and 4) is that the interparticle van der Waals forces will, to some extent, affect the fluidization behavior of Geldart A particles, however, they are not the *dominate* factor with respect to the transition of flow regimes. In Chapter 5 we showed that for slightly cohesive particles the kinetic theory of granular flows still holds, even for dense systems, where only a very small correction due to the cohesive forces is required. However, *if* the particles form cluster-like structures, the application of the current version of kinetic theory of granular flows should be seriously questioned in any case. In other words, it would be unlikely that a simple reduction of only gas-particle drag, as suggested by McKeen and Pugsley [10], would suffice in that case.

In this chapter, a two-fluid model based on kinetic theory of granular flows is used to investigate the fluidization of Geldart A particles, with an emphasis on the dense homogeneous expansion. The effects of different parameters on the formation of homogeneous fluidization is discussed.

6.2 The Two-fluid model

6.2.1 Governing equations

In the two-fluid model, both the gas and particulate phase are considered as a continuous medium. The continuity and momentum equations of the gas phase are given by [1]:

$$\frac{\partial(\varepsilon\rho_g)}{\partial t} + (\nabla\cdot\varepsilon\rho_g\mathbf{u}) = 0, \tag{6.1}$$

and

$$\frac{\partial(\varepsilon\rho_g\mathbf{u})}{\partial t} + (\nabla\cdot\varepsilon\rho_g\mathbf{u}\mathbf{u}) = -\varepsilon\nabla p - \beta(\mathbf{u}-\mathbf{v}) - \nabla\cdot(\varepsilon\overline{\boldsymbol{\tau}}_g) + \varepsilon\rho_g\mathbf{g}, \tag{6.2}$$

where ε the void fraction, ρ_g the gas density, $\mathbf{u}$ the gas velocity, p the gas pressure, $\mathbf{v}$ the particle phase velocity, $\bar{\boldsymbol{\tau}}_g$ the gas phase stress tensor, and $\mathbf{g}$ the acceleration due to gravity. The continuity and momentum equations of particle phase are given by

$$\frac{\partial(\varepsilon_s\rho_s)}{\partial t} + (\nabla\cdot\varepsilon_s\rho_s\mathbf{v}) = 0, \tag{6.3}$$

and

$$\frac{\partial(\varepsilon_s\rho_s\mathbf{v})}{\partial t} + (\nabla\cdot\varepsilon_s\rho_s\mathbf{v}\mathbf{v}) = -\varepsilon_s\nabla p + \beta(\mathbf{u}-\mathbf{v}) - \nabla p_s - \nabla\cdot(\varepsilon_s\overline{\boldsymbol{\tau}}_s) + \varepsilon_s\rho_s\mathbf{g}. \tag{6.4}$$

Note that $\varepsilon_s(=1-\varepsilon)$ is the solid fraction, ρ_s is the particle density, p_s is the particle phase pressure, and $\bar{\boldsymbol{\tau}}_s$ is the particle phase stress tensor. The inter-phase momentum transfer coefficient β is used to calculate the drag due to the fluid-particle interaction.

6.2.2 Constitutive equations

Material density

The gas phase density is related to the temperature and the pressure by the ideal gas law:

$$\rho_g = \frac{M_g}{RT} p. \tag{6.5}$$

For the particle phase a constant density is applied, which depends only on the material properties of the particles.

Viscous stress tensor

The gas phase viscous stress tensor $\boldsymbol{\tau}_g$ can be formulated in the following general form for a Newtonian fluid:

$$\bar{\boldsymbol{\tau}}_{\boldsymbol{g}} = -\left[\left(\nu_g - \frac{2}{3}\mu_g\right)(\nabla \cdot \mathbf{u})\mathbf{I} + \mu_g((\nabla \mathbf{u}) + (\nabla \mathbf{u})^T)\right], \tag{6.6}$$

with $\mathbf{I}$ the unit tensor. In Eq.(6.6), ν_g represents the bulk viscosity of the gas phase, which is normally set to zero [11], and μ_g is the gas phase shear viscosity, which is assumed to be constant, and set equal to 1.8×10^{-5} Pa·s.

A similar form is adopted for the viscous stress tensor of the particle phase $\bar{\boldsymbol{\tau}}_s$, which is given by

$$\bar{\boldsymbol{\tau}}_s = -\left[\left(\nu_s - \frac{2}{3}\mu_s\right)(\nabla \cdot \mathbf{v})\mathbf{I} + \mu_s((\nabla \mathbf{v}) + (\nabla \mathbf{v})^T)\right], \tag{6.7}$$

where ν_s and μ_s are respectively the particle phase bulk and shear viscosity. However, the particle phase viscosities cannot be simply treated as constants. From the kinetic theory of granular flows it follows that they depend on the granular temperature, coefficient of restitution, local void fraction, and the radial distribution function.

The inter-phase momentum transfer coefficient

Notwithstanding the great efforts that have been devoted to this topic, a full understanding of gas drag acting on a particle in an assembly is still lacking, and for this reason there is at present no definite consensus on what is the most reliable drag closure. The closures that can be found in literature can typically be divided into two classes: 1) empirical or semi-empirical correlation, and 2) based on data from direct numerical simulation. Typical examples of the first class are the well-known Ergun [12] and Wen and Yu [13] correlations. They obtained their correlations by using experimental bed pressure drop data for stationary homogeneous beds. The drag force expressions were also obtained from the bed expansion measurement by using Richardson-Zaki type of equation [14]. The second class is typified by the

micro-scale simulations, such as DNS [15] and Lattice Boltzmann [16, 17]. The direct numerical simulation method can capture the details of the flow around each particle, and provides an insight into the nature of fluid-solid interaction. One of the advantages is that properties which can be difficult to accurately control in experiments (such as monodispersity, homogeneity, and so on), are well-defined in simulations. Moreover, simulations can provide data that is difficult or impossible to obtain experimentally, for instance the drag force on one particular type of particle in dense bidisperse mixtures. One of the drawbacks is that DNS can only deal with hundreds of particles at present; Furthermore, the Reynolds number that can be studied is typically less than 1000. The use of empirical approaches is much more common at present, especially in industrial applications.

We next present the most widely used drag correlations. To this end, we first write interphase momentum transfer coefficient β in the following general form:

$$\beta = \frac{3}{4} 3\pi\mu_g \varepsilon^2 \, d_p \, (\mathbf{u} - \mathbf{v}) \, f(\varepsilon), \tag{6.8}$$

where $f(\varepsilon)$ is defined as the porosity function. The well-known correlations then correspond to the following expressions for the porosity function $f(\varepsilon)$:

Ergun correlation [12]:

$$f(\varepsilon) = \frac{150(1-\varepsilon)}{18\varepsilon^3} + \frac{1.75}{18} \frac{Re_p}{\varepsilon^3}, \tag{6.9}$$

where Re_p is the particle Reynolds number:

$$Re_p = \frac{\varepsilon \rho_g |\mathbf{u} - \mathbf{v}| d_p}{\mu_g}.$$

Wen-Yu correlation [13]:

$$f(\varepsilon) = \frac{C_d}{24} Re_p \varepsilon^{-4.65}. \tag{6.10}$$

The drag coefficient C_d is a function of the particle Reynolds number and given by ($Re_p < 1000$):

$$C_d = \frac{24}{Re_p}(1 + 0.15 Re_p^{0.687}).$$

LB drag model For Reynolds number smaller than 1 (which is typical valid for Geldart A particles in gas-fluidization suspensions), Hill et al. [16] derived the following relation, based on lattice Boltzmann data:

$$f(\varepsilon) = \frac{10(1-\varepsilon)}{\varepsilon^3} + 0.7 \tag{6.11}$$

Table 6.1: *Exponent n for Geldart A particles.*

Lettieri, Newton and Gates (2002, Powder Technol.) [19]:	gas-fluidization
d_p = 71 μm	n = 9.6
d_p = 57 μm	n = 9.0
d_p = 49 μm	n = 8.2
Massimilla Donsi and Zucchin (1972, Chem. Engng. Sci.) [20]:	gas-fluidization
d_p = 60 μm	n = 7.12
d_p = 53 μm	n = 6.86
d_p = 45 μm	n = 6.1
Lewis and Bowerman (1952, Chem. Engng. Prog.) [21]:	liquid-fluidization
d_p = 86 μm	n = 8.3
Whitmore (1957, J. Inst. Fuel) [22]:	liquid-sedimentation
d_p = 65 μm	n = 9.5

for $\varepsilon < 0.6$ and

$$f(\varepsilon) = \frac{1 + 3\sqrt{0.5(1-\varepsilon)} + (135/64)(1-\varepsilon)\ln(1-\varepsilon) + 17.14(1-\varepsilon)}{1 + 0.681(1-\varepsilon) - 8.48(1-\varepsilon)^2 + 8.16(1-\varepsilon)^3} \tag{6.12}$$

for $\varepsilon \geq 0.6$.

Note that the Wen-Yu correlation can be rewritten in a more general form:

$$f(\varepsilon) = \frac{C_d}{24} Re_p \varepsilon^{-n}. \tag{6.13}$$

The conventional value of the exponent $n = 4.56$ was originally obtained by Richardson and Zaki [14]. For gas-solid systems, the exponent n is extremely scattered [18], however. For Geldart A particles, different values of the exponent n are shown in Table 6.1. These values deviate obviously from the most-commonly used value, 4.65.

Kinetic theory of granular flows

The kinetic theory of granular flows describes the dependence of the rheologic properties of the fluidized particles on local particle concentration and the fluctuating motion of the particles owing to particle-particle collisions [23]. The key quantity used in the kinetic theory of granular flows is the granular temperature, which is analogous to the thermal temperature of the classical kinetic theory of a molecular gas. The granular temperature T is defined as the square velocity fluctuation of particles [24]:

$$T = < v^2 > - < v >^2 \tag{6.14}$$

The variation of the velocity fluctuation of particles is described with a separate conservation equation, the so-called granular temperature equation:

$$\frac{3}{2}\left[\frac{\partial(\varepsilon_s \rho_s T)}{\partial, t} + \nabla \cdot (\varepsilon_s \rho_s T \mathbf{v})\right] = -(p_s \bar{\mathbf{I}} + \varepsilon_s \bar{\boldsymbol{\tau}}_s) : \nabla \mathbf{v} - \nabla \cdot (\varepsilon_s q_s) - 3\beta T - \gamma \tag{6.15}$$

The particle phase pressure p_s is given by [23]

$$p_s = p_s^{(0)}(1+y), \tag{6.16}$$

with

$$p_s^{(0)} = \varepsilon_s \rho_s T,$$

and the excess compressibility [25]

$$y = 2(1+e)\varepsilon_s \chi.$$

where χ is the radial distribution function. In the kinetic theory of granular flows, the bulk viscosity ν_s is given by

$$\nu_s = \frac{5}{3}\mu_0. \tag{6.17}$$

while the shear viscosity μ_s equals

$$\mu_s = 4.064\mu_0\varepsilon_s(\frac{1}{y} + \frac{4}{5} + 0.761y). \tag{6.18}$$

The fluctuating kinetic energy flux q_s is assumed to obey the Fourier's law:

$$q_s = -\kappa_s \nabla T, \tag{6.19}$$

where the thermal conductivity κ_s is

$$\kappa_s = 4.10052\kappa_0\varepsilon_s(\frac{1}{y} + \frac{6}{5} + 0.748y). \tag{6.20}$$

In these expressions,

$$\mu_0 = \frac{5}{64r_p^2}\sqrt{\frac{k_B m T}{\pi}}, \tag{6.21}$$

and

$$\kappa_0 = \frac{75mk_B}{256r_p^2}\sqrt{\frac{mk_B T}{\pi}}. \tag{6.22}$$

There is a term γ to account for the dissipation of fluctuating kinetic energy due to inelastic particle-particle collisions in Eq.(6.15), and is given by

$$\gamma = 3(1-e^2)\varepsilon_s^2\rho_s\chi T\left[\frac{4}{d_p}\sqrt{\frac{T}{\pi}} - (\nabla\cdot\mathbf{v})\right]. \tag{6.23}$$

The radial distribution function χ is presented by Ma and Ahmadi [26]:

$$\chi_0(\varepsilon_s) = \frac{1 + 2.5\varepsilon_s + 4.5904\varepsilon_s^2 + 4.515439\varepsilon_s^3}{\left[1 - (\varepsilon_s/\varepsilon_s^{max})^3\right]^{0.67802}} \tag{6.24}$$

Table 6.2: *Simulation conditions.*

Parameters	value
Gas shear viscosity	1.8×10^{-5} Pa·s
Gas temperature	293 K
Gas pressure	1.01×10^{5} Pa
Gas constant, R	8.314 J/(mol· K)
Coefficient of restitution, e	0.97
CFD cells	$30\times45\times$
Size of the cell	5×5 mm^2
CFD time step,	1.0×10^{-4} s
Particle diameter	75 μm
Particle density	1500 kg/m^3

6.3 Simulation conditions

In this work, we will use a 2D model. Figure 6.1 shows the scheme of the computational mesh and boundary conditions imposed.

The simulation conditions are specified in Table 6.2. The drag model used in this work is based on Eq.(6.13), where the exponent n will be specified in the individual simulations.

The gas flow enters at the bottom through a porous distributor. The initial void volume fraction in each fluid cell is given an average value of 0.4, and with a random variation of $\pm$5%. Also for the boundary condition at the bottom we use an uniform gas-velocity with a superimposed random component (10%), following Goldschmidt et al. [27].

6.4 Simulation results

The particles used in the simulations are mono-disperse, with a diameter of 75 μm and a density $\rho_p = 1500$ kg/m^3. This type of particle has been experimentally investigated by Geldart [5]. Based on their experiments, a minimum fluidization velocity $U_{mf} = 0.22$ cm/s and a minimum bubbling velocity $U_{mb} = 0.68$ cm/s were obtained. The mean void fraction ε at the minimum bubbling point is around 0.635, which corresponds to a bed expansion of $1.31H_0$ (H_0 is the initial packed bed height with a mean porosity of 0.4).

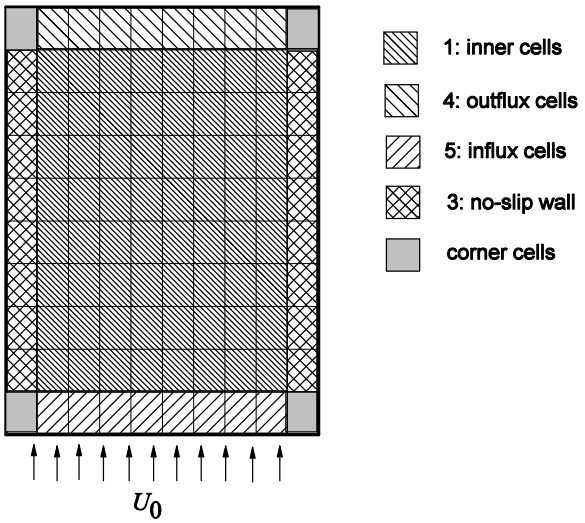

Figure 6.1: *The fluid cells and boundary conditions employed in the two-fluid models.*

6.4.1 Effect of cohesion

As found in the previous chapter, for slightly cohesive particles, a correction for the excess compressibility can be made as following:

$$y_3 = -\sum_{i}^{Nc} C_i \varepsilon_s^i. \tag{6.25}$$

The coefficient C_i depends on the magnitude of the cohesive force. We argue that such a modification, although quite simple, can be used to investigate the influence of the cohesion on the bed hydrodynamics. For simplicity, we only consider the first term in Eq.(6.25), which is given by

$$y_3 = -C_1 \varepsilon_s. \tag{6.26}$$

So the new overall excess compressibility is

$$y = 2(1+e)\varepsilon_s \chi_0 - C_1 \varepsilon_s.. \tag{6.27}$$

which is subsequently used in the expressions for the viscosity and pressure from the kinetic theory of granular flows. We have carried out several sets of simulations with different coefficients C_1.

In Figures 6.2 we show the simulation results for a superficial gas velocity $U_0 = 0.9$ cm/s, which is approximately $1.29U_{mb}$ determined by Geldart [5] in his experiments. Three different coefficients C_1 are used, namely 0.0, 2.0, 10.0. From Figure 6.2, an homogeneous expansion is observed, with an expansion of 12.5% of

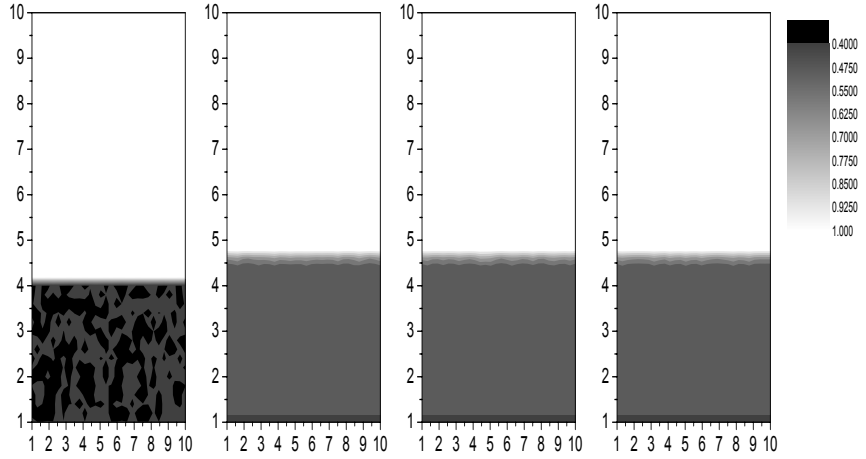

Figure 6.2: *Instantaneous voidage profiles of Geldart A particles. The superficial gas velocity U_0 is set to 0.009 m/s. At the far right is the initial bed used for the simulation. The values for the coefficient C_1 are, from the second to the right to the left, 0.0, 2.0, and 10.0, respectively. The exponent n used in the simulations is 4.65. The results are taken at $t = 5$ s.*

the initial bed regardless of the magnitude of the coefficients C_1. Compared to Geldart's experiments [5], at this point the fluidized bed should bubble, which means that a higher U_{mb} will be obtained from our model. Furthermore, the bed expansion is under-estimated since an expansion of 31% has been found for this type of particles at the minimum bubbling point [5].

We also carried out a set of simulations with a higher superficial gas velocity $U_0 = 0.03$ m/s, as shown in Figure 6.3. The bed should display a bubbling fluidization at this gas velocity. As can be seen, without any cohesive interaction ($C_1 = 0.0$) taken into account, the bed still shows a homogeneous expansion of 50% of the initial bed. However, if we increase the coefficient C_1 to 2.0, the hydrodynamics of the bed becomes quite different. The bed starts to bubble and a bubbling fluidization typical of Geldart A particles can be found. An averaged bed height for this bubbling bed is $\sim$2.0H_0. If an even higher coefficient C_1 is used ($C_1 = 10.0$), the bed still remains in the bubbling regime but a significant decrease of the bed height is observed, which amounts to $1.75H_0$. It can be argued that with a suitable cohesion the bed can transform from a homogeneous regime to a bubbling regime. But an extremely high coefficient C_1 may also lead to a more compact bubbling bed, which is probably due to the strong cohesive interaction.

Clearly, by solely accounting for the cohesion between particles, a realistic bed hydrodynamics cannot be obtained at present. For a lower gas velocity $U_0 = 0.9$ cm/s, an under-estimation of the bed expansion is found. As shown in Table 6.1, for a gas-solid system of Geldart A particles, a large exponent in the voidage dependent part of the drag force is always found. A large exponent means that a high drag force will be calculated for a single particle in an assembly. Thus if a large exponent n is used, we expect a higher bed expansion at a lower gas velocity.

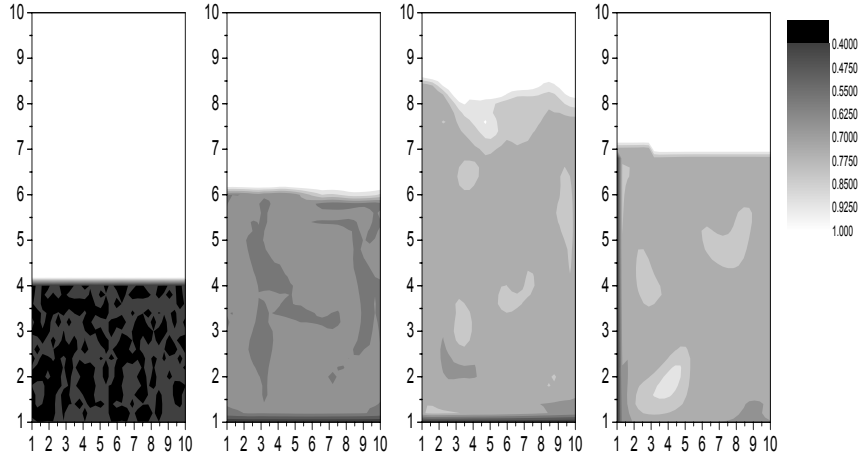

Figure 6.3: *Instantaneous voidage profiles of Geldart A particles. The superficial gas velocity U_0 is set to 0.03 m/s. At the far right is the initial bed used for the simulation. The coefficient C_1 are, from the second to the right to the left, 0.0, 2.0, and 10.0 respectively. The exponent n used in the simulations is 4.65. The results are taken at $t = 5$ s.*

The cohesion clearly has an impact on the bed expansion as shown in Figure 6.3. However, at present we do not know the exact value of the coefficient C_1 for a particular Geldart A particle system. This clearly limits the predictive capability of this model, and an accurate estimate from the DPM simulations is highly desirable. The problem in this is that the value of the Hamaker constant A is not "a priori" known.

It should also be stressed that in this study the cohesive effect has been considered via a very simple approach. A detailed study, in which not only the particle pressure, but other transport coefficients such as particle viscosity are evaluated and carefully tested, is highly desired.

6.4.2 Effect of drag model

Clearly, to product the bed expansion accurately, the influence of not only the cohesion but also the drag models should be considered. Three different models are used: (1) the general form of drag force given by Eq.(6.13) with an exponent $n = 9.6$, which was determined from experiments by Lettieri et al. [19]. (2) the same as (1) but with an standard exponent $n = 4.65$; (3) the lattice Boltzmann drag model given by Eqs.(6.11) and (6.12).

Low gas velocity

In Figure 6.4 we show the results for a gas velocity $U_0 = 0.009$ m/s. For a large exponent (n = 9.6) a higher bed expansion, around 31% of the initial bed height, can be observed. Bubbling behavior is found, which is quite different from the observa-

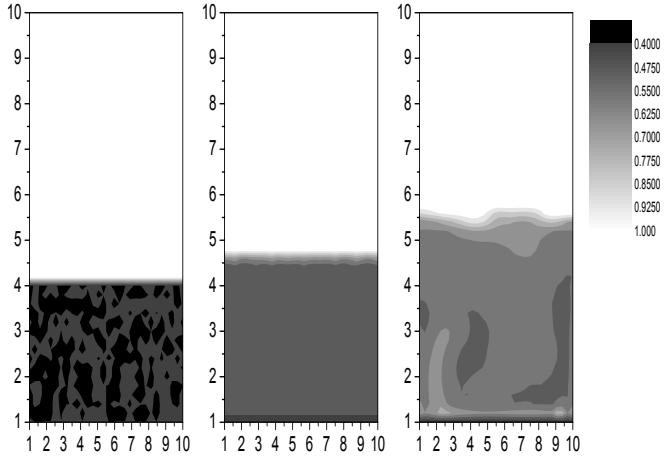

Figure 6.4: *Instantaneous voidage profiles of Geldart A particles. The superficial gas velocity U_0 is set to 0.009 m/s. At the far right is the initial bed used for the simulation. The exponents n are 4.65 (middle) and 9.6 (left). No cohesion is considered here. The results are taken at $t = 5$ s.*

tion with the standard exponent $n = 4.65$. The latter still displays a homogeneous expansion.

Clearly, the commonly-used exponent $n = 4.56$ cannot be used to predict a realistic bed expansion dynamics of Geldart A particles at a low gas velocity, say around U_{mb}. By using a large exponent (n =9.6), which was determined by gas-fluidization of Geldart A particles, we can get a bed expansion much closer to the experimental results [5]. Basically a larger exponent n in Eq.(6.13) will lead to a higher drag at the same gas velocity. It can thus be argued that at the lowe gas velocities the drag force is under-estimated by the commonly-used drag models. This is also evidenced by the large exponents n generally obtained in the fluidization of Geldart A particles (see Table 6.1).

High gas velocity

It has been reported by several researchers [6, 7, 10] that an over-estimated bed expansion was found at a high gas velocity ($\sim$ 0.2 m/s). We also carried out several simulations for a high gas velocity, $U_0 = 0.2$ m/s. We still use the drag model given by Eq.(6.13) with an exponent $n = 4.65$. The simulation domain, however, is enlarged so that a high bed expansion can be accommodated. The computational domain is composed of 30×70 cells, and the size of each cell still remains as 5×5 mm^2. With such a high gas velocity the bed in fact is in the turbulent fluidization regime. In Figure 6.5, we show the results obtained at different points in time when the bed reaches a dynamical equilibrium. Clearly the particle phase displays a turbulence-like flow pattern. Also an over-estimation of bed height is found in the simulations, which is around 100% of the initial bed height.

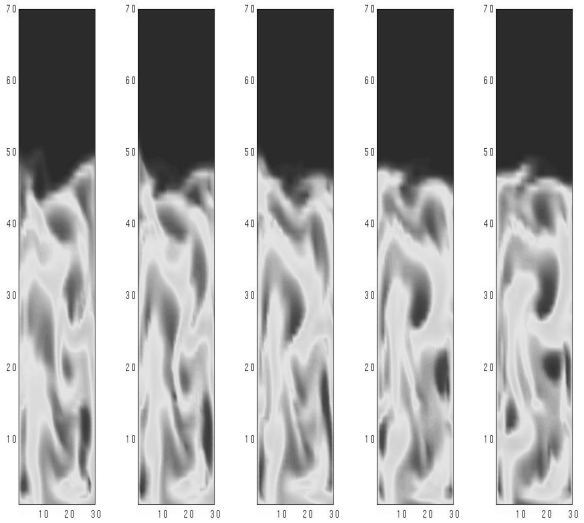

Figure 6.5: *The bed expansion dynamics of Geldart A particles from the two-fluid model. The superficial gas velocity U_0 is set to 0.2 m/s. The exponent n is 4.65. No cohesion is considered here. The results are, from the right to left, taken at $t = 9.6, 9.7, 9.8, 9.9$ and 10.0 s.*

Since the LB drag model given by Eqs.(6.11) and (6.12) is obtained essentially at low Reynolds number, we also carried out a set of simulations for this drag model. The results are shown in Figure 6.6. As can be seen, no big differences can be observed compared to the results from the drag model given by Eq.(6.13) with an exponent $n = 4.65$.

A similar simulation was also carried out by McKeen and Pugsley [10]. They also found an over-estimation of the bed height, compared to their experimental results. They argued that a factor should be used to scale down the drag force in this regime, in order to obtain a better aggreement with the experiments. In Figure 6.7 we show the results of our simulations with a drag force ($n = 4.65$) scaled down by a factor 0.15. A significantly decrease of the bed height is found, which is around 16% of the initial bed height. This value is quite close to that observed in the experiments by McKeen and Pugsley [10].

6.5 Discussion and conclusions

In this chapter we have investigated the effect of cohesion and drag models on the bed hydrodynamics of Geldart A particles. For a low gas velocity $U_0 = 0.009$ m/s, the effect of coefficient C_1, which is introduced to account for the presence of cohesion, on the bed expansion is a quite small. For a higher gas velocity $U_0 = 0.03$ m/s, we found a transition from the homogeneous fluidization to bubbling fluidization with an increase of the coefficient C_1. It is thus argued that the cohesion plays a

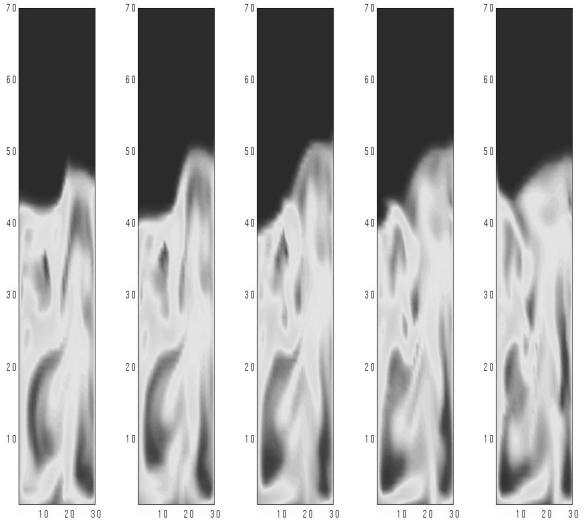

Figure 6.6: *The same as in Figure 6.5, but here used is the LB drag model.*

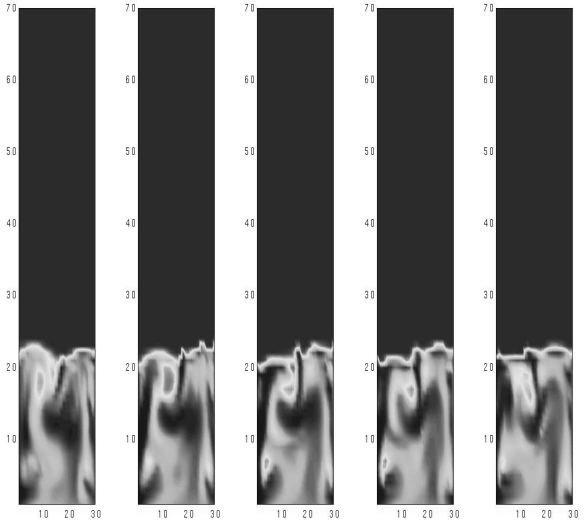

Figure 6.7: *The same as in Figure 6.5, but the drag force is scaled by a factor of 0.15.*

role in the bed expansion of Geldart A particles. However, it is difficult at present to derive an exact value of the coefficient C_1 for a particular Geldart A particle system. An accurate procedure to measure the effect of cohesion on viscosity and pressure in DPM model is highly required. Furthermore, the consideration of cohesion, although important, is still not sufficient to obtain a realistic bed expansion dynamics.

In order to arrive at a better prediction of the bed expansion, the influence of the drag models should be considered as well. We have tested the commonly-used drag model which is given by Eq.(6.13) with an exponent $n = 4.65$. It has been found that at the low gas velocity, this drag model gives under-prediction of the bed expansion. Alternatively, we used a large exponent $n = 9.6$ as well, which was shown to given a better prediction of the bed expansion. Essentially, a large exponent means a higher drag force acting on a single particle in an assembly. This suggests that at a low gas velocity, a scale up of the standard drag model is required.

On the other hand, however, a scale down of the standard drag model is necessary at high gas velocity, for example at $U_0 = 0.2$ m/s. This was also found in previous studies [6, 7, 10]. Clearly, the effect of the drag model on the bed expansion of Geldart A particles is far more complicated. A simple scaling-up or -down cannot be generally adopted. A detailed study on gas-particle drag for Geldart A particles is definitely required.

References

[1] Kuipers J.A.M., van Duin K.J., van Beckum F.P.H., and van Swaaij W.P.M., 1992. A numerical model of gas-fluidized beds. *Chem. Engng. Sci.*, **47**: 1913.

[2] Patil D.J., van Sint Annaland M., and Kuipers J.A.M., 2005. Critical comparison of hydrodynamic models for gas-solid fluidized beds-Part I : bubbling gas-solid fluidized beds operated with a jet. *Chem. Engng. Sci.*, **60**: 57.

[3] Patil D.J., van Sint Annaland M., and Kuipers J.A.M., 2005. Critical comparison of hydrodynamic models for gas-solid fluidized beds-Part II: freely bubbling gas-solid fluidized beds. *Chem. Engng. Sci.*, **60**: 73.

[4] Kuipers J.A.M., and van Swaaij W.P.M., 1998. Computational fluid dynamics applied to chemical reaction engineering. *Adv. Chem. Engng.*, **24**: 227.

[5] D. Geldart, 1973. Types of gas fluidization. *Powder Technol.*, **7**: 285.

[6] Ferschneider G., and Mege P., 1996. Eulerian simulation of dense phase fluidized bed. *Revue de l' Institut français du pétrole*, **51**: 301.

[7] Bayle J., Mege P., and Gauthier T., 2001. Dispersion of bubble flow properties in a turbulent FCC fluidized bed. In: *Fluidization X*, Kwauk M., Li J., and Yang W.-C., (eds.), Engineering Foundation, New York, USA. p.125.

[8] Lettieri P., Cammarata L., Micale G.D.M., and Yates J., 2003. CFD simulations of gas fluidized beds using alternative Eulerian-Eulerian modelling approaches. *Int. J. Chem. Reactor Engng.*, **1**: A5.

[9] Chen Z., Gibilaro L.G., and Foscolo P.U., 1999. Two-dimensional voidage waves in fluidized beds. *Ind. Eng. Chem. Res.*, **38**: 610.

[10] McKeen T.R., and Pugsley T.S., 2003. Simulation and experimental validation of a freely bubbling bed of FCC catalyst. *Powder Technol.*, **129**: 139.

[11] Bird R.B., Stewart W.E., and Lightfood E.N., 1960. *Transport Phenomena.* John Wiley & Sons, New York, USA.

[12] Ergun S., 1952. Fluid flow through packed columns. *Chem. Engng. Progs.*, **48**: 89.

[13] Wen C.Y., and Yu Y.H., 1966. Mechanics of fluidization. C*hem. Engng. Prog. Symp. Ser.*, **62**: 100.

[14] Richardson J.F., and Zaki W.N., 1954. Sedimentation and Fluidisation: Part I. *Trans. Instn. Chem. Engrs.*, **32**: 35.

[15] Pan T.W., Joseph D.D., Bai R., Glowinski R., and Sarin V., 2002. Fluidization of 1204 spheres: simulation and experiment. *J. Fluid Mech.*, **451**: 169.

[16] Hill R.J., Koch D.L., and Ladd J.C., 2001. Moderate-Reynolds-numbers flows in ordered and random arrays of spheres. *J. Fluid. Mech.*, **448**: 315.

[17] Van der Hoef M.A., Beetstra R., and Kuipers J.A.M., 2005. Lattice Boltzmann simulations of the low Reynolds number flow past mono and bidisperse arrays of spheres: results for the permeability and drag force. *J. Fluid Mech.* In press.

[18] Morgan J.P., Taylor R.W., and Booth F.L. 1971. The value of the exponent n in the Richard and Zaki equation, for fine solid fluidized with gases under pressure. *Powder Technol.*, **4**: 286.

[19] Lettieri P., Newton D., and Yates J.G., 2002. Homogeneous bed expansion of FCC catalysts, influence of temperature on the parameters of the Richardson-Zaki equatio. *Powder Technol.*, **123**: 221.

[20] Massimilla L., Dons G., and Zucchini C., 1972. The structure of bubble-free gas fluidized beds of fine fluid cracking catalyst particles. *Chem. Engng. Sci.*, **27**: 2005.

[21] Lewis E.W., and Bowerman E.W., 1952. Fluidisation of solid particles in liquids. *Chem. Engng. Prog.*, **48**: 603.

[22] Whitmore R.L., 1957. *J. Inst. Fuel*, **30**: 328.

[23] Lun C.K.K., Savage S.B., Jeffrey D.J., and Chepurniy N., 1984. Kinetic theories for granular flow: inelastic particles in Couette flow and slightly inelastic particles in a general flow field. *J. Fluid Mech.*, **140**: 223.

[24] Nieuwland J.J., van Sint Annaland M., Kuipers J.A.M. and van Swaaij W.P.M., 1996, Hydrodynamic modeling of gas/particle flows in riser reactors. *AIChE J.*, **42**: 1569.

[25] Chapman S., and Cowling T.G., 1970. *The Mathematical theory of nonuniform gases* (3rd Edn). Cambridge University Press, Cambridge, uk.

[26] Ma D., and Ahmadi G., 1986. An equation of state for dense rigid sphere gases. *J. Chem. Phys.*, **84**: 3449.

[27] Goldschmidt M.J.V., Beetstra R., and Kuipers J.A.M., 2004. Hydrodynamic modelling of dense gas-fluidised beds: comparison and validation of 3D discrete particle and continuum models. *Powder Technol.*, **142**: 23.

Summary

The most widespread industrial application of dense gas-solid flows is encountered in the domain of gas-fluidized beds. If operated with well-matched gas and particle parameters, fluidized beds can provide many advantages such as uniform temperature distribution, high mass transfer rates, continuous operation, and relative simplicity in geometric configuration. For this reason, gas-fluidized beds have been widely applied to petroleum, metallurgical, chemical, energy, environmental, and food industries in the past decades. However, the understanding of the hydrodynamics of the complex gas-solid two-phase flows in gas-fluidized beds is not complete. The design and scale up of a fluidized bed reactor still depends mostly on the measurement techniques and preliminary tests on pilot-scale model reactor. This is a very expensive and time-consuming activity.

The development of the computational fluid dynamics (CFD) techniques in recent years provides a valuable tool in the design and scale up of fluidized bed reactors. However, the establishment of a general modeling approach, if not impossible, is quite difficult, since for the varying operation conditions a number of different fluidization regimes can be encountered. A great challenge in CFD modeling of gas-solid two-phase flows is to obtain realistic predictions of the fluidization behavior of small particles ($< 100\ \mu$m) such as group A particles according to Geldart's classification. This type of particles are found to display a unique homogeneous expansion in gas-fluidized bed reactors within a certain range of gas velocities, where the solid fraction is normally very high (in the range of $0.5 \sim 0.6$). Despite many detailed phenomenological investigations in the past years, a realistic prediction of fluidization behavior of Geldart A powders is still difficult with current CFD models.

This work aims at studying the fluidization behavior of Geldart A particles with a multi-level modeling approach. At the microscopic-scale the most fundamental lattice Boltzmann model will be used to investigate the gas-particle interaction. The starting point of the work reported in this study, however, is the mesoscale discrete particle model. This model allows one to study the effect of the particle-particle interactions on the fluidization behavior in great detail. By taking a volume-averaged gas flow field into account, the effects of the gas flow on the fluidization of Geldart A particles can also be investigated. At the macroscopic-scale the two-fluid model is used, in which the constitutive closures are developed from the kinetic theory of granular flows. The information obtained from the discrete particle model can be used to improve this two-fluid model, which offers a

potential tool to support the design and scale-up of engineering scale equipment.

Discrete particle modeling

A 2D simulation study revealed some typical features of fluidization behavior of Geldart A particles including the gross circulation of particles in the absence of bubbles, the formation of cavities and channels in homogeneous fluidization, and fast bubbles. The structure of the forces acting on the particles is also studied, and the homogeneous fluidization regime is shown to be a quasi-equilibrium state where a force balance only exists at the macroscopic-level but not at the level of individual particles. The drag forces and van der Waals forces are two important sources of the local force fluctuations, and thus of the velocity fluctuation of the particles.

An analysis of the velocity fluctuation of particles has then been carried out. It is shown that an anisotropy of the velocity fluctuation of particles exists in both the homogeneous fluidization regime and the bubbling regime. At least three basic interactions, i.e. the fluid-particle interaction, the particle-particle collisions (and the particle-wall collisions), and the interparticle van der Waals forces, can be identified as the main sources of velocity fluctuations of particles. The homogeneous fluidization is actually a transition phase resulting from the competition of these three interactions. In the bubbling regime, however, the effect of the interparticle van der Waals forces vanishes and the fluid-particle interaction becomes the dominant factor determining the fluidization behavior of Geldart A particles. Additionally, we find that the velocity fluctuation of the particles obeys an exponential function of the squared superficial gas velocity in the homogeneous fluidization regime, and not a linear function as found by Cody et al. (Powder Technol. 1996).

The comparison of the particulate pressure obtained from our simulations with the theoretical prediction by Koch and Sangani (J. Fluid Mech., 1999) suggests that the difference of particulate pressure is more pronounced in the homogeneous fluidization regime than that in the bubbling regime. This further indicates that the fluid-particle interaction is a dominant factor responsible for the bubbling regime but not for the homogeneous fluidization. Our results for the bubbling regime are also found to be in a good agreement with the experimental results by Rahman and Campbell (J. Fluid Mech., 2003).

The simulations have also been carried out in a 3D fluidized bed, by which we study the effects of the gas and particle properties on the fluidization behavior of Geldart A particles. We first find that the generation of the overshoot of the pressure drop near the minimum fluidization point is affected by both the particle-wall friction and the interparticle van der Waals forces, which confirm the experimental results by Loezos et al. (Powder Technol. 2002) and Rietema et al. (Chem. Engng. Sci., 1990).

In all the cases we studied in this research, the predicted U_{mf} was in a good agreement with the correlation by Abrahamsen and Geldart (Powder Technol., 1980). The minimum bubbling velocity U_{mb}, in general, shows a qualitative agree-

ment with this correlation. The interparticle van der Waals force is found to delay the onset of bubbles and extend the interval of homogeneous fluidization. The higher the granular Bond number, the higher U_{mb}, until a transition to Geldart C behavior is encountered, where no U_{mb} can be discerned. Also the particle density and gas density are shown to have a weak effect on U_{mb}. For heavy particles, the window of homogeneous fluidization is decreased mainly due to the increase in U_{mf}. By contrast, it has been found that the particle size has a strong effect on U_{mb}. The predicted U_{mb} for different particle diameter agrees with the correlation except for fine particles with a diameter $d_p < 40\mu$m. This may be due to the fact that we turned off the interparticle van der Waals forces in these particular simulations. It can be argued that for larger particles with a diameter $d_p > 40\mu$m the interparticle van der Waals forces may have a negligible effect on the formation of homogeneous fluidization. For fine particles, however, a proper incorporation of interparticle van der Waals forces is highly desired. Finally, the effect of the gas viscosity has been examined. We found that the minimum bubbling velocities from our simulations for different gas viscosity show a systematic deviation from the empirical correlation by Abrahamsen and Geldart. In particular, we found that with an increasing gas shear viscosity the U_{mb} experiences a minimum point near $2.0 \times 10^{-5}\mathrm{Pa}\cdot\mathrm{s}$, while in the correlation by Abrahamsen and Geldart the minimum bubbling velocity decreases monotonously for increasing μ_g. Interestingly, if we fit the data up to $2.0\times10^{-5}\mathrm{Pa}\cdot\mathrm{s}$, a slope of -0.267 has been obtained, which is not very different from the value -0.347 in the correlation by Abrahamsen and Geldart.

Kinetic theory of granular flows

A soft-sphere discrete particle model is used to test the kinetic theory of granular flows (KTGF), with emphasis on the prediction of excess compressibility as it is the key quantity in KTGF for calculating the particle pressure and other transport coefficients. To this end, it is first essential to find a suitable method to continuously "heat" the granular system, since the dissipation in collisions will have the effect that continuously loose their kinetic energy. A simple rescaling procedure is found to be insufficient to keep the system running for a long time in an equilibrium state in particular for dense systems. This is because in this procedure, the fast particles will gain more energy while the slower particles will gain less energy. By accelerating each particle with a random acceleration, the granular system is found to stay in the equilibrium state. However, it is not as computationally efficient as the rescaling procedure. A random accelerating procedure is thus used for higher solid fractions and rescaling procedure is only used for dilute systems, where the system is found to stay in the equilibrium state for an appreciably long time.

For slightly cohesive particles, only a very small deviation has been found from the classical kinetic theory of granular flows, which suggests that with the Hamaker constants tested in the range used in this research the cohesion only has a weak influence on the excess compressibility. It is expected that in the presence of a strong cohesive force, particles will form complicated agglomerates. In this case, an equi-

librium state may not exist, so that the validity of kinetic theory of granular flows is questionable. However, the quantification of the cohesive force is not straightforward, since there is no reference force (such as gravitational force) in these systems. Note also that the absolute value of the force is not precisely known, since it is extremely difficult to directly measure the cohesive forces between Geldart A particles, and a theoretical estimate based on the (bulk) particle properties is also unreliable since these forces strongly depend on the surface properties.

A correction of the KTGF is made by using a modified excess compressibility that accounts for the effects of cohesion between particles. The excess compressibility due to cohesion, y_3, depends on the magnitude of the cohesive force and the solids volume fractions. For a weak cohesive force, y_3 can be well represented by $y_3 = -C_1\varepsilon_s^3 - C_2\varepsilon_s^4$, while for a strong cohesive force tested as well in this study, $y_3 = -C_3\varepsilon_s - C_4\varepsilon_s^2$.

Two-fluid model

We have investigated the effect of cohesion and drag models on the bed hydrodynamics of Geldart A particles based on the two-fluid model. For a high gas velocity $U_0 = 0.03$ m/s, we found a transition from the homogeneous fluidization to bubbling fluidization with an increase of the coefficient C_1, which is used to account for the contribution of cohesion to the excess compressibility. Thus cohesion can play a role in the bed expansion hydrodynamics of Geldart A particles. However, in order to get a better prediction of bed expansion, the influence of the drag models should be considered as well. We test the commonly-used drag model which is given by the Wen and Yu correlation with an exponent $n = 4.65$. It has been found at low gas velocity, that this drag model gives under-prediction of the bed expansion. Alternatively, we used a large exponent $n = 9.6$ reported in experimental gas-fluidization studies, which was shown to given a better prediction of the bed expansion. These findings suggest that for a low gas velocity, a scale-down of the commonly-used drag model is required. On the other hand, however, a scale-up of the commonly-used drag model is necessary for high gas velocity, for example $U_0 = 0.2$ m/s. Therefore a simple "ad-hoc" scaling-up or -down of the drag force, which has been suggested by some researchers, cannot be generally adopted. A more detailed study of drag model for Geldart A particles is also desired.

Samenvatting

De meest voorkomende industriële toepassing van verdichte gas-deeltjes stromingen zijn gas-gefluïdiseerde bedden. Als de juiste waarden voor gas en deeltjes parameters worden gekozen, dan hebben gefluïdiseerde bedden een aantal waardevolle eigenschappen, zoals een uniforme temperatuurverdeling, hoge massa-overdrachtssnelheden, en eenvoudige continue operatie. Vanwege deze eigenschappen worden gas-gefluïdiseerde bedden veel toegepast in de petroleum, metallurgische, en chemische industrieën, alswel de levensmiddelen en milieu gerelateerde industrieën. Echter, ons begrip van de complexe gas-vast stromingen in gas-gefluïdiseerde bedden is verre van compleet. Het gevolg is dat het ontwerpen en opschalen van gefluïdiseerde bed reactoren veelal moet gebeuren aan de hand van schaalmodel reactoren en uitgebreide experimentele metingen, hetgeen een langdurig en dus ook kostbaar proces is.

De recente ontwikkeling van "computational fluid dynamics" (CFD) technieken biedt een belangrijk hulpmiddel voor het ontwerpen en opschalen van gefluïdiseerde bed reactoren. Echter, aangezien de stromingsregimes zeer verschillend kunnen zijn, is het erg moeilijk om een algemeen toepasbaar numeriek model te ontwikkelen, dat alle soorten van fluïdisatie goed kan beschrijven. Een van de grote uitdagingen voor CFD modellen is het om het juiste fluïdisatie gedrag te voorspellen van zeer klein deeltjes ($< 100\ \mu$m), zoals de A deeltjes in de Geldart classificatie. Uniek voor dit type deeltjes is dat ze bij bepaalde gassnelheden een fluïdisatieregime van homogene expansie vertonen, waar de deeltjesdichtheid zeer hoog is (50-60 volume procent). Het is tot nu toe nog niet gelukt om deze homogene expansie met CFD modellen nauwkeurig te beschrijven, ondanks het feit dat er in de afgelopen jaren enorm veel onderzoek naar verricht is.

Het onderzoek dat beschreven is in dit proefschrift houdt zich bezig met het bestuderen van het fluïdisatie gedrag van Geldart A deeltjes met behulp van een numeriek model dat gas-vast systemen beschrijft op een meer gedetailleerd niveau dan de traditionele CFD modellen: het discrete deeltjes model. De vaste fase is hier niet continu, maar wordt gemodelleerd met bolvormige deeltjes, wat het mogelijk maakt om de invloed van deeltjes-deeltjes interacties op het fluïdisatie gedrag te bestuderen. De gasfase wordt beschreven met CFD modellen, waarbij er een "two-way" koppeling is tussen de dynamica van de beide fasen. Dit maakt het mogelijk om ook het effect van de gas dynamica op het fluïdisatiegedrag te bestuderen. Behalve het bestuderen van de invloed van de diverse interacties op de fluïdisatie, wordt het discrete deeltjes model ook gebruikt om de effectieve deeltjes druk te

bepalen, wat een belangrijke parameter is de hogere schaal CFD modellen. Dit geeft dus een directe mogelijkheid om de CFD modellen te verbeteren, en op deze manier kan het discrete deeltjes model een belangrijke bijdrage leveren aan de ontwikkeling en opschaling van chemische reactoren. In de volgende secties beschrijven we de belangrijkste uitkomsten van het onderzoek.

Discrete deeltjes modellering

De 2D discrete deeltjes simulatie vertoonde het typische fluïdisatie gedrag van Geldart A deeltjes, zoals het op grote schaal circuleren van deeltjes in afwezigheid van bellen, en de vorming van holtes en kanalen bij homogene fluïdisatie. De structuur van de krachten op de deeltjes is ook bestudeerd, waaruit bleek dat het regime van homogene fluïdisatie een quasi-evenwichts toestand is, waar een balans van krachten bestaat op het macroscopische niveau, maar niet op het niveau van de individuele deeltjes. De snelheidsfluctuaties van de deeltjes blijkt anisotroop te zijn in zowel het homogene fluïdisatie regime als in het heterogene ("bubbling") regime. Er kunnen 3 krachten bijdragen aan de snelheidsfluctuaties: de deeltjes-deeltjes krachten, de gas-deeltjes krachten, en de cohesieve van der Waals krachten. De homogene fluïdisatie blijkt een overgangsfase te zijn welke het gevolg is van de competitie van de drie krachten. Voor het "bubbling" regime blijkt dat de van der Waals krachten relatief onbelangrijk worden: het zijn dan voornamelijk de gas-deeltjes krachten die het fluïdisatie gedrag bepalen. Ook blijkt dat in het regime van homogene fluïdisatie de snelheidsfluctuatie van de deeltjes een exponentiële functie van de kwadratische superficiële snelheid te zijn, waar Cody et al. (Powder Techn. 1996) een lineair verband vonden. Een vergelijking van de deeltjesdruk in de simulatie met de theoretische voorspelling van Koch en Sangani (J. Fluid Mech., 1999) suggereert dat het verschil extremer is in het regime van homogene fluïdisatie, vergeleken met het "bubbling" regime. Dit is een andere belangrijke aanwijzing dat de vloeistof-deeltjes interacties de dominante factor zijn in het "bubbling" regime, maar niet in het regime van homogene fluïdisatie. Onze resultaten voor het "bubbling" regime blijken in goede overeenstemming te zijn met de experimentele resultaten van Rahman en Campbell (J. Fluid Mech., 2003).

Hiernaast zijn er ook simulaties uitgevoerd voor 3-D gefluïdiseerde bedden, met het doel om de effecten van gas en deeltjeseigenschappen op het fluïdisatie gedrag van A-deeltjes te bestuderen. Allereerst vinden we dat de drukval doorschiet vlakbij het punt van minimum fluïdisatie, hetgeen ook gemeld word in de experimenten van Loezos et al. (Powder Technol. 2002) and Rietema et al. (Chem. Engng. Sci., 1990). Ook voor de waarde van U_{mf} vonden we in alle gevallen een goede overeenstemming tussen de simulatie resultaten en de correlatie van Abrahamsen en Geldart (Powder Technol., 1980) welke gebaseerd is op experimentele data. Voor de minimum "bubbling" snelheid U_{mb} vonden we een kwalitatieve overeenstemming tussen de simulatie data en de Abrahamsen en Geldart correlatie. De cohesive van der Waals krachten blijken U_{mb} te verhogen, en maken dus het interval van homogene fluïdisatie groter. Hoe hoger het granulaire bindingsgetal, hoe hoger U_{mb}, totdat er een overgang naar C-deeltjes bereikt is, en geen U_{mb} meer kan worden

waargenomen. Verder blijkt, dat zowel de gas- en deeltjesdichtheid nauwelijks invloed hebben op U_{mb}. Voor zware deeltjes wordt het interval van homogene fluïdisatie echter wel kleiner omdat U_{mf} toeneemt. De deeltjesgrootte blijkt wel een grote invloed op U_{mb} te hebben. De simulatiewaarden voor U_{mb} bij verschillende diameters komen goed overeen met de correlatie, behalve voor hele fijne deeltjes met een diameter $d_p < 40\ \mu$m. Dit zou verklaard kunnen worden door het feit dat in deze simulaties de cohesive krachten uitgeschakeld zijn. Voor relatief grote deeltjes ($d_p > 40\ \mu$m) is te verwachten dat deze krachten naar verhouding weinig effect hebben, maar voor kleinere deeltjes zouden ze zeker meegenomen moeten worden. Tenslotte is ook nog onderzocht wat het effect is van de viscositeit van het gas. We vonden dat de U_{mb} in de simulaties bij verschillende viscositeiten systematisch afwijkt van de Abrahamsen-Geldart correlatie. In het bijzonder vonden we dat bij oplopende viscositeit, de U_{mb} in de simulaties een minimum vertoont bij ongeveer 2×10^{-5}Pa·s, waar de correlatie een monotome afname van U_{mb} voorspelt. Intressant is dat een lineaire fit van de simulatie data tot 2×10^{-5}Pa · s een helling van -0.267 oplevert, wat redelijk dicht bij de waarde -0.347 ligt, welke volgt uit de Abrahamsen-Geldart correlatie.

Kinetische theorie van granulaire stroming

In dit onderdeel van het proefschrift is het “soft-sphere” model gebruikt voor het testen van de kinetische theorie van granulaire stroming (KTGS), en in het bijzonder de voorspelling voor de excess compressibiliteit, aangezien dit binnen de KTGS de centrale grootheid is voor het bepalen van de deeltjesdruk en viscositeit. Hiervoor is het essentieel om eerst een geschikte methode te vinden om het systeem “op te warmen”, aangezien de energiedissipatie tijdens botsingen er voor zorgt dat de deeltjes voortdurend kinetische energie verliezen. De meest simpele methode, het voortdurend schalen van de deeltjessnelheid naar de juiste temperatuur, blijkt niet altijd tot een evenwichssituatie te leiden die stabiel is over een voldoende lange tijd, in het bijzonder niet bij hoge deeltjesdichtheden, omdat de snelle deeltjes meer energie opnemen dan de langzame deeltjes. Door de deeltjes een random versnelling te geven, in plaats van te schalen, blijkt dat wel een langdurige stabiele evenwichtssituatie bereikt kan worden. Het nadeel is echter dat deze procedure minder efficiënt is; daarom is de random versnelling methode gebruikt voor dichte systemen, en de schalingsmethode alleen voor verdunde systemen, waarvoor blijkt dat het system lang genoeg in de evenwichtstoestand kan blijven.

Voor licht cohesieve deeltjes wordt een kleine afwijking van de klassieke kinetische theorie gevonden, waaruit we kunnen concluderen dat voor deze deeltjes de invloed van cohesie op de excess compressibiliteit klein is. Voor sterke cohesieve krachten is te verwachten dat de deeltjes complexe aglomeraten vormen. In dat geval zou er zelfs geen evenwichtstoestand kunnen bestaan, waarmee de hele kinetische theorie op losse schroeven komt te staan. Een probleem is dat het in onze systemen lastig is om de grootte van van de cohesive kracht aan te geven, omdat er geen directe referentiekracht, zoals de zwaartekracht, is. Maar ook de ab-

solute waarde van de kracht is niet precies bekend, aangezien het zeer lastig is om de cohesieve kracht direct te meten, en een theoretische voorspelling op grond van de "bulk" deeltjeseigenschappen (bijv. de polariseerbaarheid) onbetrouwbaar is omdat de kracht erg afhankelijk is van de oppervlakte-eigenschappen van de deeltjes.

De KTGS kan gecorrigeerd worden door een excess compressibiliteit te gebruiken die aangepast is voor het effect van de cohesive krachten. Het deel van de excess compressibiliteit dat van deze krachten afhangt, y_3, blijkt goed beschreven te kunnen worden met de functie $y_3 = -C_1\epsilon_s^3 - C_2\epsilon^4$ voor cohesive krachten die relatief zwak zijn, en $y_3 = -C_3\epsilon_s - C_4\epsilon^2$ voor relatief sterke cohesive krachten.

Two-fluid model

In het laatste deel van dit onderzoek is het effect van cohesie en wrijvingskracht op het fluïdisatie gedrag van A deeltjes onderzocht in het two-fluid model. Voor hoge gassnelheden ($U_o = 0.03$ m/s) werd een overgang gevonden van homogene naar "bubbling" fluïdisatie door de coëfficiënt C_1 te verhogen, welke een mate was voor de bijdrage van de cohesieve krachten in de excess compressibiliteit. Het blijkt dus dat deze krachten wel degelijk een invloed kunnen hebben op het fluïdisatie gedrag. De invloed van de gas-deeltjes wrijvingskracht op de bed expansie is ook onderzocht aan de hand van de bekende Wen-Yu correlatie. Voor een exponent $n = 4.65$ vinden we dat voor lage gassnelheden deze correlatie een te lage bed expansie geeft. Een exponent $n = 9.6$, welke resulteerde uit experimentele gas-fluïdisatie studies, blijkt een veel realistischere bed expansie te geven. Dit geeft aan dat voor een lage gassnelheid een lagere wrijvingskracht nodig zou zijn om overeenstemming met de experimentele waarneming te krijgen. Aan de andere kant, voor hoge gassnelheden blijkt juist dat een hogere wrijvingskracht vereist is. Een ad-hoc schaling van de wrijvingskracht, zoals gehanteerd door enkele onderzoekers, blijkt dus geen zinvolle methode te leveren om een betere overeenstemming tussen simulatie en experiment te verkrijgen. Een meer gedetailleerde studie van de gast-vast interactie voor Geldart A deeltjes is duidelijk vereist.

List of Publications

1. In-situ measurement of droplet size distribution by light scattering method. In: *Proceeding of the Second International Symposium on Measuring Techniques for Multiphase Flow*, August 30-September 1, 1998, Beijing, China. (with Y. Lu, T. Hu, S. Wang and Y. Xu)

2. Inverse technique devised from modification of annealing-evolution algorithm for particle sizing by light scattering. *Powder Technology*. 1999, **104**: pp80-83. (with S. Wang and Y. Xu)

3. Inversion of particle-size distribution from angular light-scattering data with genetic algorithms. *Applied Optics*. 1999, **38**: pp2677-2686. (with S. Wang, Y. Lu, T. Hu, Z. Zhu, and Y. Xu)

4. A novel PIV technique using one frame of image. In: *Proceedings of the European Conference on Lasers and Electro-Optics and the International Quantum Electronics Conference*, September 10-15, 2000, Nice Acropolis, Nice, France. (with S. Wang and Y. Xu)

5. A numerical study of fluidization behavior of Geldart A particles using discrete particle model. *Powder Technology*. 2004, **139**: pp129-139. (with M. A. van der Hoef and J. A. M. Kuipers)

6. Discrete particle simulation of the homogeneous fluidization of Geldart A particles. In: *Proceedings of the 11th International Conference on Fluidization: Present and Future for Fluidization Engineering*, May 9-14, 2004, Ischia, (Naples), Italy. (with M. A. van der Hoef and J. A. M. Kuipers)

7. On-line measurement of dust concentration in the exhaust duct by laser scattering integration method. In: *Proceedings of the 3rd International Symposium on Two-Phase Flow Modeling and Experimentation*, September 22-25, 2004, Pisa, Italy. (with S. Wang, Y. Wu, and Y. Zhao)

8. The effects of particle and gas properties on the fluidization of Geldart A particles. *Chemical Engineering Science*, (accepted). (with M. A. van der Hoef and J. A. M. Kuipers)

9. Longitudinal and transverse mixing in rotary kilns: a discrete element method approach. *Chemical Engineering Science*, (accepted). (with G. J. Finnie, N. P. Kruyt, C. Zeilstra, and J. A. M. Kuipers)

10. Fluidization of supercritical water in micro reactor. *Chemical Engineering Science*, (accepted). (with B. Potic, S.R.A. Kersten, M.A. van der Hoef, J.A.M. Kuipers, and W.P.M. van Swaaij)

11. From discrete particle model to a continuous model of Geldart A particles. *Chemical Engineering Research and Design*, (accepted). (with M.A. van der Hoef and J.A.M. Kuipers)

12. Modelling of chemical vapor deposition in a fluidized bed reactor based on discrete particle simulation. *International Journal of Chemical Reactor Engineering*, (In preparing). (with G. Czok, J.A.M. Kuipers, and J. Werther)

13. Discrete particle model for gas-solid two-phase flows. (In preparing). (with C. Zeilstra, M.A. van der Hoef, and J.A.M. Kuipers)

14. Kinetic theory of granular flows for cohesive particles: based on the discrete element model. (In preparing). (with M.A. van der Hoef and J.A.M. Kuipers)

15. Two-fluid modeling for gas fluidization of Geldart A particles. (In preparing). (with M.A. van der Hoef and J.A.M. Kuipers)

About the author

Mao Ye was born on February 14th, 1973 in Chongyang County, Hubei, China. After completing his secondary education at E'nan High School in 1990, he attended East China Shipbuilding Institute (ECSI), where he received a B.Sc. degree of Power Engineering in July 1994. Subsequently he joined Thermal Energy Engineering Research Institute at Southeast University in Nanjing as a graduate student. Working on several projects with focus on optical particle characterization in solid-gas two-phase flows, he obtained a M.Sc. and a Ph.D. degree in April 1997 and June 2000, respectively. The Ph.D. thesis "The light scattering methods for particle characterization in solid-gas two-phase flows" was awarded the Best Ph.D. Thesis in Jiangsu Province in 2002 and nominated as the candidates of the Best 100 Ph.D. Theses by Ministry of Education, P.R. China in 2003.

In December 2000, he moved to the group of Fundamentals of Chemical Reaction Engineering (FAP) at Universiteit Twente as a research fellow, where he started to work on computational fluid dynamics (CFD) of multi-phase flows. From March 2001, he has been employed by Foundation for Fundamental Research on Matter (FOM) as an OIO with a project titled "Multi-level modeling of dense solid-gas two-phase flows".

He is author and co-author of more than 20 papers in peer-reviewed journals and conference proceedings. He has delivered varied technical presentations in more than 10 institutes and academic conferences. He is a member of scientific panel of the 7th World Congress of Chemical Engineering in Glasgow, Scotland, July 10-14 2005.

From May 2005, he will join the Department of Mechanical Engineering at Technische Universiteit Eindhoven (TU/e) as a postdoctoral researcher with a project on direct numerical simulation (DNS) of solid-gas two-phase flows.